GdR ISIS

15ème école d'été de PEYRESQ (04)
21 au 25 juin 2021
« *Traitement du Signal et des Images pour la co-conception de systèmes imageurs innovants* »

Retour d'expérience de la mission spatiale SMOS au service de la *co-conception* de la future mission SMOS*hr*

Éric ANTERRIEU
IR CNRS calcul scientifique

Centre d'Études Spatiales de la BIOsphère
CNRS / UMR 5126
18 av. Edouard Belin, 31401 TOULOUSE cedex 9, FRANCE
Eric.Anterrieu@cesbio.cnes.fr

Retour d'expérience de la mission spatiale SMOS au service de la *co-conception* de la future mission SMOS*hr*

1ère partie: SMOS

The SMOS space mission

❖ *The context*

ESA's Soil Moisture and Ocean Salinity (SMOS) mission has been designed to observe both soil moisture over the Earth's landmasses and salinity over the oceans from space.

SM data are urgently required for hydrological studies and data on OS are vital for improving our understanding of ocean circulation patterns. *SMOS was a direct response to the current lack of global observations of SM and OS.*

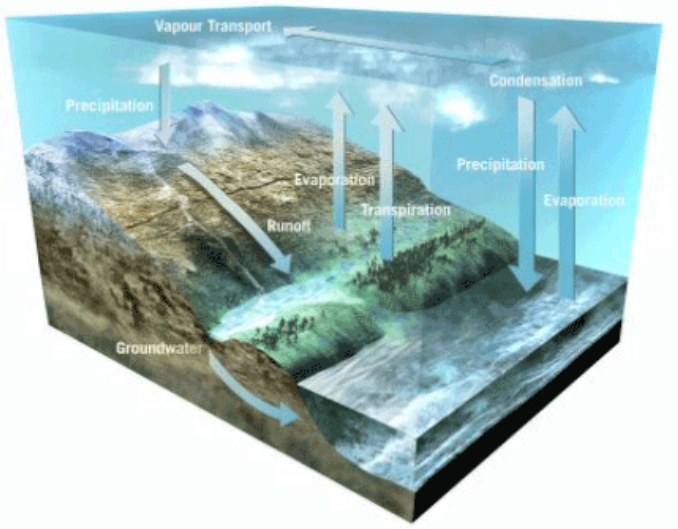

The SMOS space mission

❖ *The concept*

A novel instrument has been especially developed with the objective to demonstrate the use of a Microwave Imaging Radiometer by Aperture Synthesis for imaging SM and OS by "capturing" images of emitted micro-wave radiation T_b in the "protected" L-band (1400–1427 MHz).

SMOS was the first attempt to apply to Earth remote sensing the concept of aperture synthesis initially developed by radio astronomers.

VLA *(1970's)*

The SMOS space mission

❖ *The concept*

A novel instrument has been especially developed with the objective to demonstrate the use of a Microwave Imaging Radiometer by Aperture Synthesis for imaging SM and OS by "capturing" images of emitted micro-wave radiation T_b in the "protected" L-band (1400–1427 MHz).

SMOS was the first attempt to apply to Earth remote sensing the concept of aperture synthesis initially developed by radio astronomers.

CBI *(1990's)*

The SMOS space mission

❖ *The concept*

A novel instrument has been especially developed with the objective to demonstrate the use of a Microwave Imaging Radiometer by Aperture Synthesis for imaging SM and OS by "capturing" images of emitted micro-wave radiation T_b in the "protected" L-band (1400–1427 MHz).

SMOS was launched on 2nd November 2009 and although designed for a five-year mission, it is still operational after more than 12 years in orbit.

SMOS *(2000's)*

The SMOS space mission

❖ *The instrument*

The idea of aperture synthesis is to obtain a high-resolution image by using the interferometric information corresponding to spatial frequencies distributed over a wide virtual pupil.

The single payload of SMOS is the Microwave Imaging Radiometer by Aperture Synthesis MIRAS, operating in full-pol mode in the “protected” L-band.

The SMOS space mission

❖ *The instrument*

The idea of aperture synthesis is to obtain a high-resolution image by using the interferometric information corresponding to spatial frequencies distributed over a wide virtual pupil.

MIRAS: a Y-shaped array equipped with 69 antennas provide interfero-metric measurements, 3 (of them) operating also as reference radiometers to provide measurements of the average brightness temperature of the scene under observation.

The SMOS space mission

❖ *The instrument*

The idea of aperture synthesis is to obtain a high-resolution image by using the interferometric information corresponding to spatial frequencies distributed over a wide virtual pupil.

A demonstrator has been successfully ground tested and has flown onboard an Hercule C130 of the Royal Danish Air Force under the control of the Technical University of Denmark.

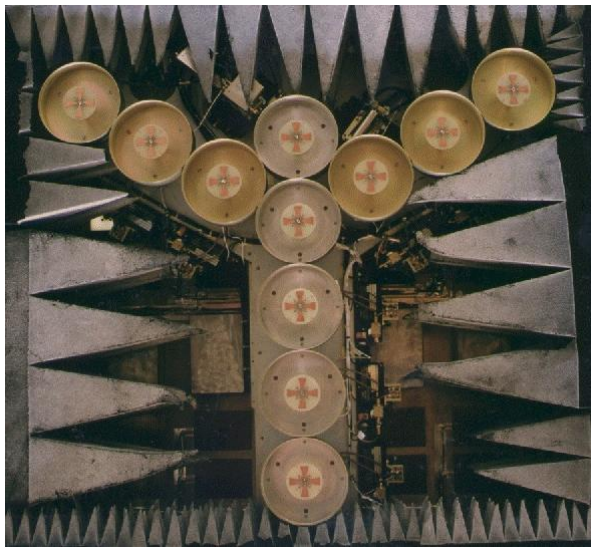

Aperture synthesis imaging

❖ *Arrays with connected antennas*

The radio signals received by the two antennas are sampled and directly transmitted via links to the correlation unit which combines them to produce interference fringes in real time.

Cosmic Background Imager

Very Large Array

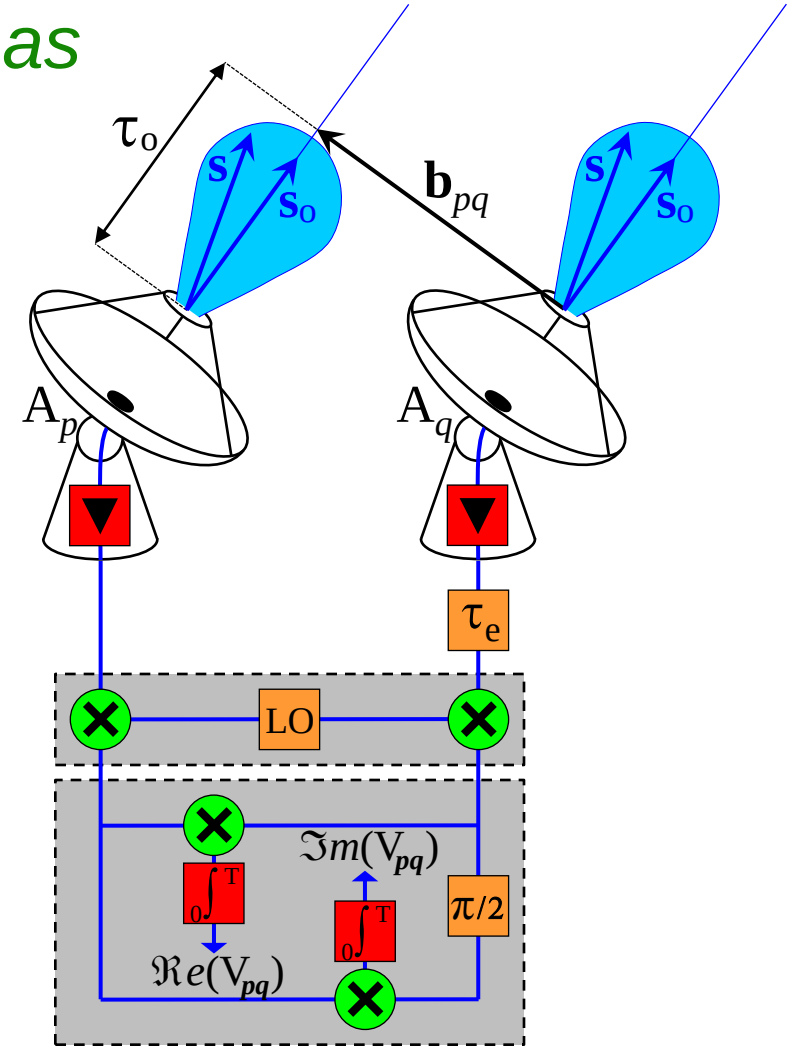

Aperture synthesis imaging

❖ *Arrays with unconnected antennas*

1) The radio signals received by the two antennas are sampled, recorded alongside together with an accurate time base and then stored on a media…

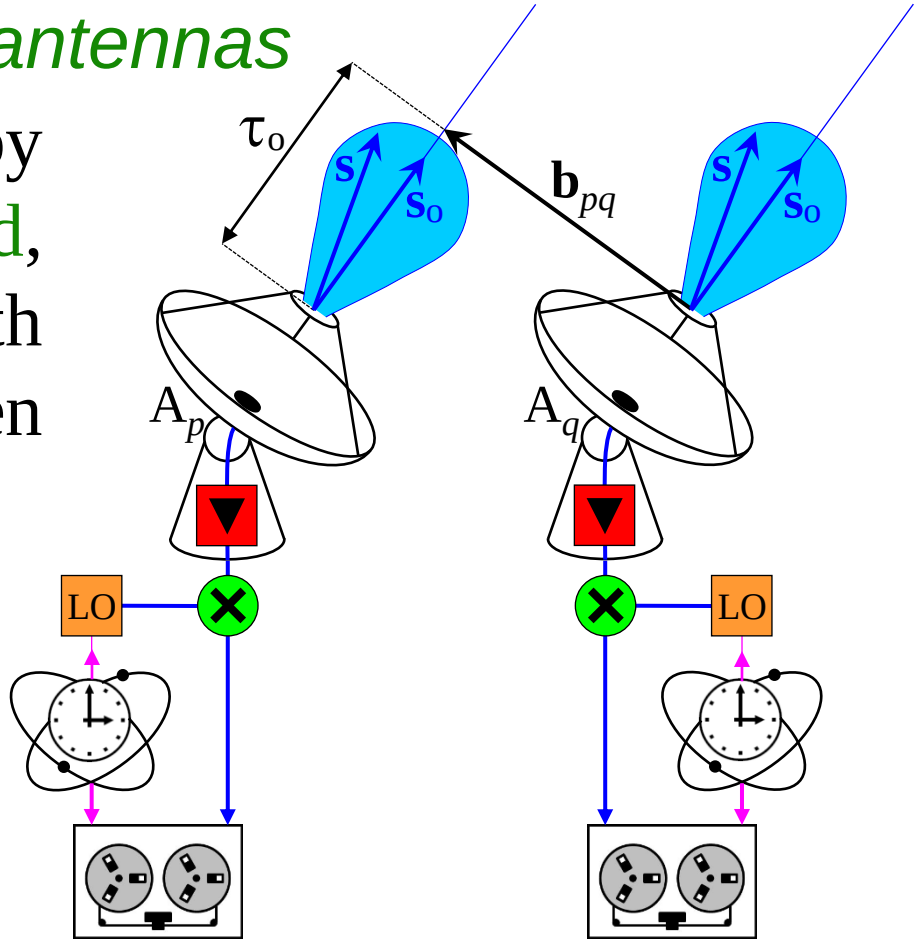

Very Long Baseline Array

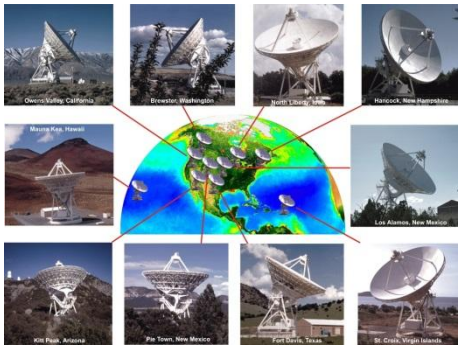

Very Long Baseline Interferometry

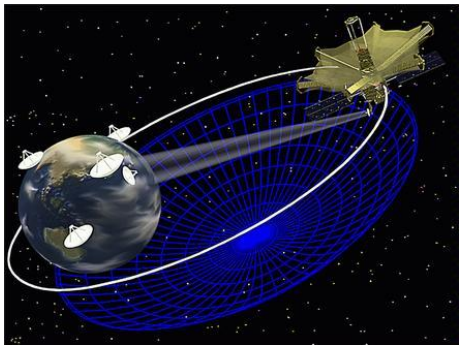

Aperture synthesis imaging

❖ *Arrays with unconnected antennas*

1) The radio signals received by the two antennas are sampled, recorded alongside together with an accurate time base and then stored on a media.

2) At a later time, at the location of a correlation unit, the data are synchronized, then played back together and combined just like if they were coming in real time from the two antennas.

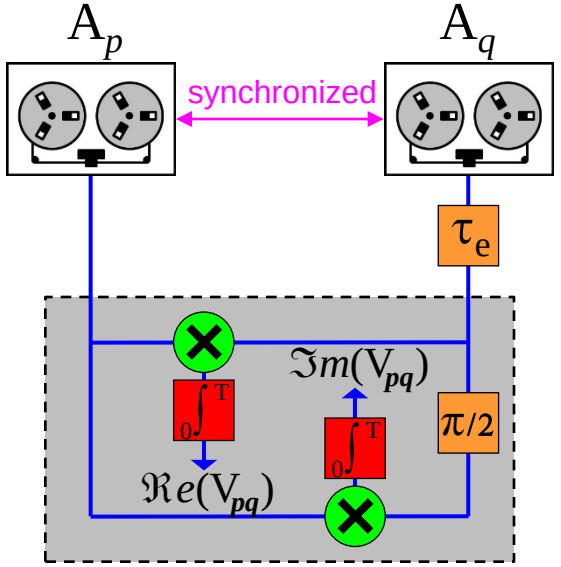

VLBI correlation unit hosted by the Max Planck Institute for Radio Astronomy

Aperture synthesis imaging

❖ *Complex visibilities*

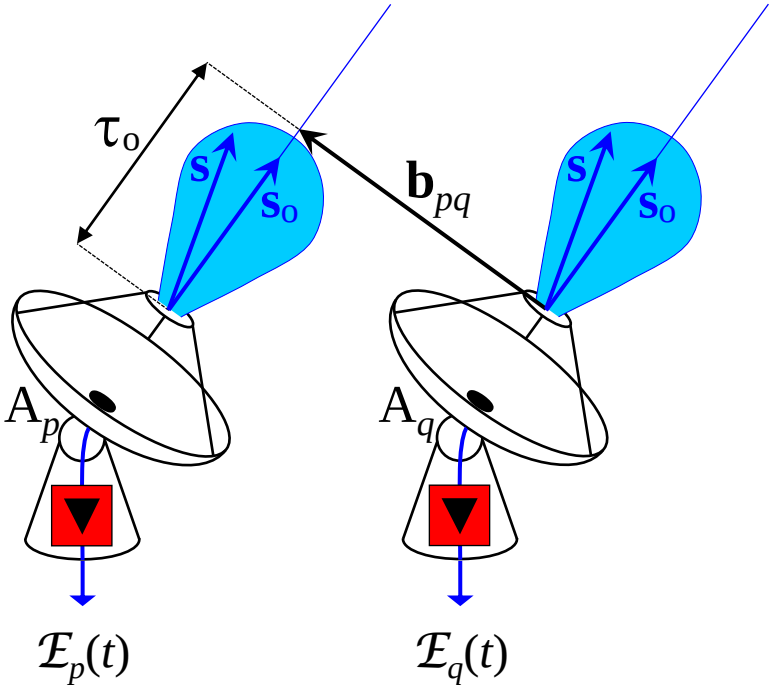

Whether the antennas are connected or not, interferometer measurements are obtained by cross-correlating the signals $\mathcal{E}_p(t)$ and $\mathcal{E}_q(t)$ collected by pairs of spatially separated antennas A_p and A_q which have overlapping fields of view, yielding samples of the spatial coherence function V_{pq} (also termed complex visibilities) of the brightness temperature distribution T_b of the scene under observation for the angular frequency $\mathbf{u}_{pq} = \mathbf{b}_{pq}/\lambda_o$.

Aperture synthesis imaging

❖ *Key parameters of an array*

1) Field of view: the extent of the observed scene that is synthesized by the instrument (with the aid of the computer).

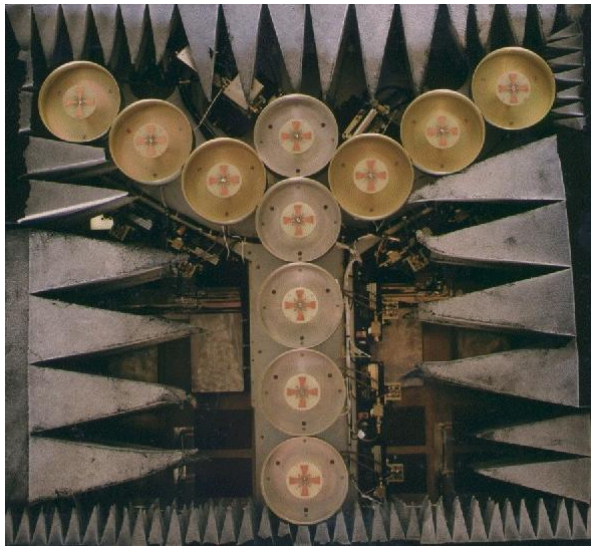

MIRAS demonstrator

2) Angular resolution: the ability to distinguish small details of the observed scene (estimated with Rayleigh / Schuster / Sparrow criterions of PSF, not of PSF^2 !).

3) Radiometric sensitivity: the smallest temperature deviation that can be discerned by the instrument.

Aperture synthesis imaging

❖ *Key parameters of an array*

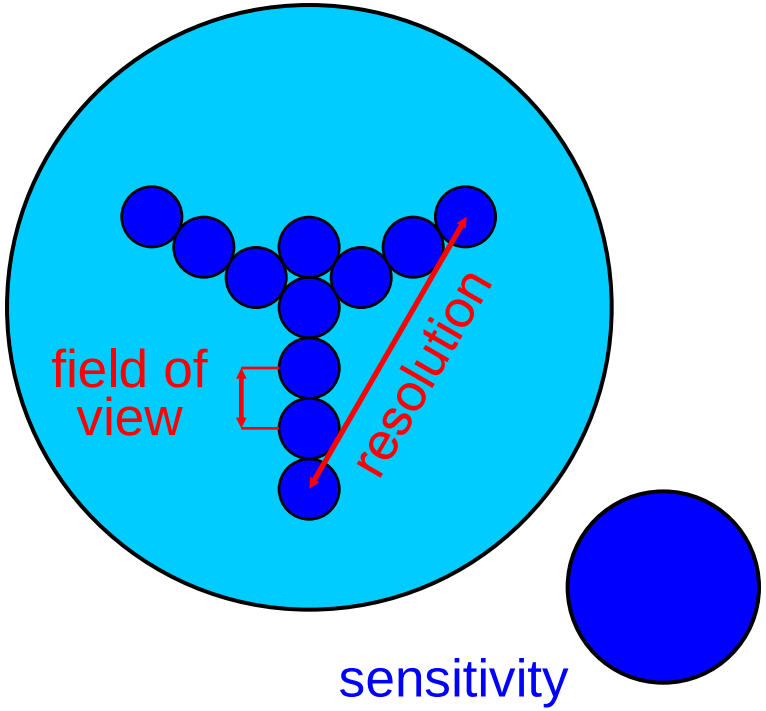

1) Field of view: the extent of the observed scene that is synthesized by the instrument (with the aid of the computer).

2) Angular resolution: the ability to distinguish small details of the observed scene (estimated with Rayleigh / Schuster / Sparrow criterions of PSF, not of PSF^2 !).

3) Radiometric sensitivity: the smallest temperature deviation that can be discerned by the instrument.

Aperture synthesis imaging

❖ *Van Cittert – Zernike theorem*

The VCZ theorem rests on a number of assumptions:

- incoherence of the source;
- distance to the source;
- angular size of the source;
- quasi-monochromatic source;
- two-dimensional source;
- homogeneous medium;

…

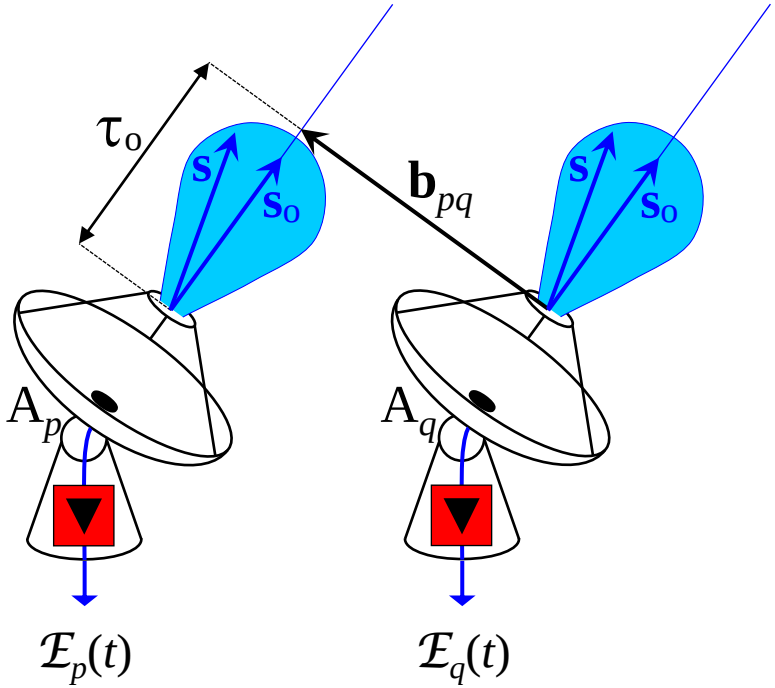

$$V_{pq} \propto \langle \mathcal{E}_p \, \mathcal{E}_q^* \rangle = \frac{1}{T_i} \int \mathcal{E}_p(t) \, \mathcal{E}_q^*(t) \, dt$$

$$V_{pq} \propto \int \mathcal{F}_p(\boldsymbol{\sigma}) \, \mathcal{F}_q^*(\boldsymbol{\sigma}) \, T(\boldsymbol{\sigma}) \, e^{-2j\pi \, \mathbf{b}_{pq} \cdot \boldsymbol{\sigma}} \, d\Omega \text{ with } \boldsymbol{\sigma} = \mathbf{s} - \mathbf{s}_o$$

Aperture synthesis imaging

❖ *Van Cittert – Zernike theorem*

The VCZ theorem does not account for space-time-frequency dependent perturbations of the incident electromagnetic wave from emission to detection:

- spurious emission (RFI);
- Doppler effect;
- coupling/crosstalk effects;

…

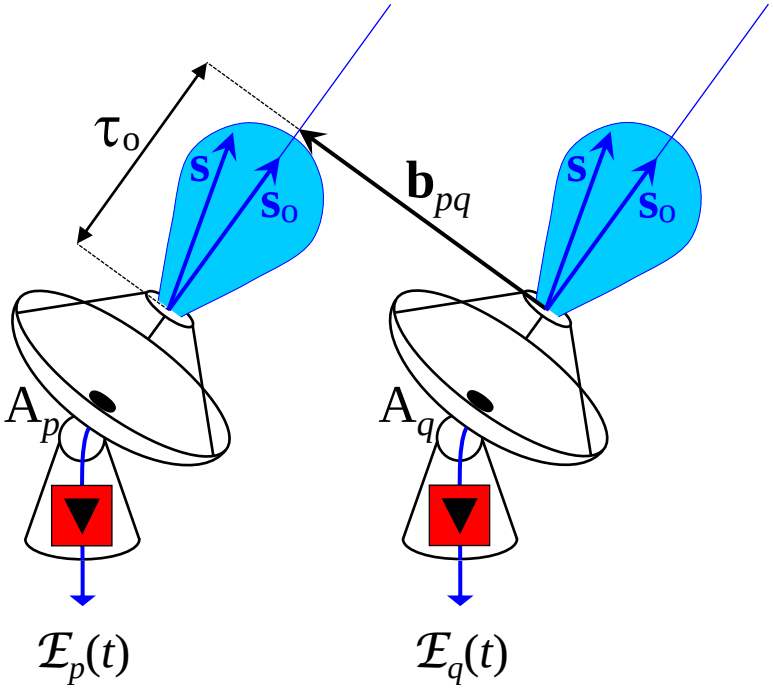

$$V_{pq} \propto \langle \mathcal{E}_p \, \mathcal{E}_q^* \rangle = \frac{1}{T_i} \int \mathcal{E}_p(t) \, \mathcal{E}_q^*(t) \, dt$$

$$V_{pq} \propto \int \mathcal{F}_p(\boldsymbol{\sigma}) \, \mathcal{F}_q^*(\boldsymbol{\sigma}) \, T(\boldsymbol{\sigma}) \, e^{-2j\pi \, \mathbf{b}_{pq} \cdot \boldsymbol{\sigma}} \, d\Omega \text{ with } \boldsymbol{\sigma} = \mathbf{s} - \mathbf{s}_o$$

Instrument modeling

❖ *Van Cittert – Zernike revisited*

$$\mathbf{V}_{pq} \propto \frac{1}{\sqrt{\Omega_p \Omega_q}} \iint_{\|\xi\| \le 1} \mathcal{F}_p(\xi)\, \mathcal{F}_q^*(\xi)\, [\mathbf{T}_b(\xi) - \mathbf{T}_{rec}]\, \tilde{\mathbf{r}}_{pq}(t)\, \frac{e^{-2j\pi \mathbf{u}_{pq}\cdot\xi}}{\sqrt{1-\|\xi\|^2}}\, d\xi$$

$$\mathbf{V} = \mathbf{G}\,\mathbf{T}$$

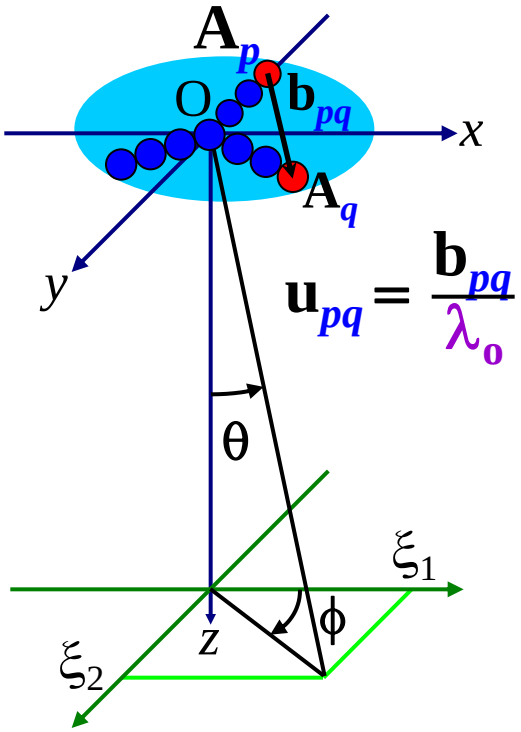

F : antenna voltage pattern

$\mathbf{T}_{rec}$: receivers temperature

$\tilde{\mathbf{r}}$: fringe washing function ($t = \mathbf{u}_{kl}\cdot\xi / f_o$)

V : complex visibilities

$\mathbf{T}_b$: brightness temperature ($\mathbf{T}(\xi) = \mathbf{T}_b(\xi) - \mathbf{T}_{rec}$)

Instrument modeling

- *Van Cittert – Zernike revisited*

$$\mathbf{V}_{pq} \propto \frac{1}{\sqrt{\Omega_p \Omega_q}} \iint_{\|\xi\| \le 1} \mathcal{F}_p(\xi)\, \mathcal{F}_q^*(\xi)\, [\mathbf{T}_b(\xi) - \mathbf{T}_{rec}]\, \tilde{\mathbf{r}}_{pq}(t)\, \frac{e^{-2j\pi \mathbf{u}_{pq}\cdot\xi}}{\sqrt{1-\|\xi\|^2}}\, d\xi$$

$$\mathbf{V} = \mathbf{G}\,\mathbf{T}$$

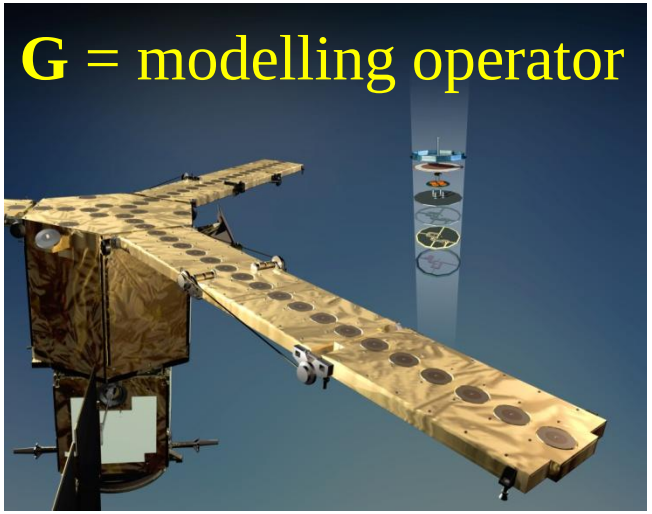

Instrument modeling

❖ ***G** is not a Fourier transform…*

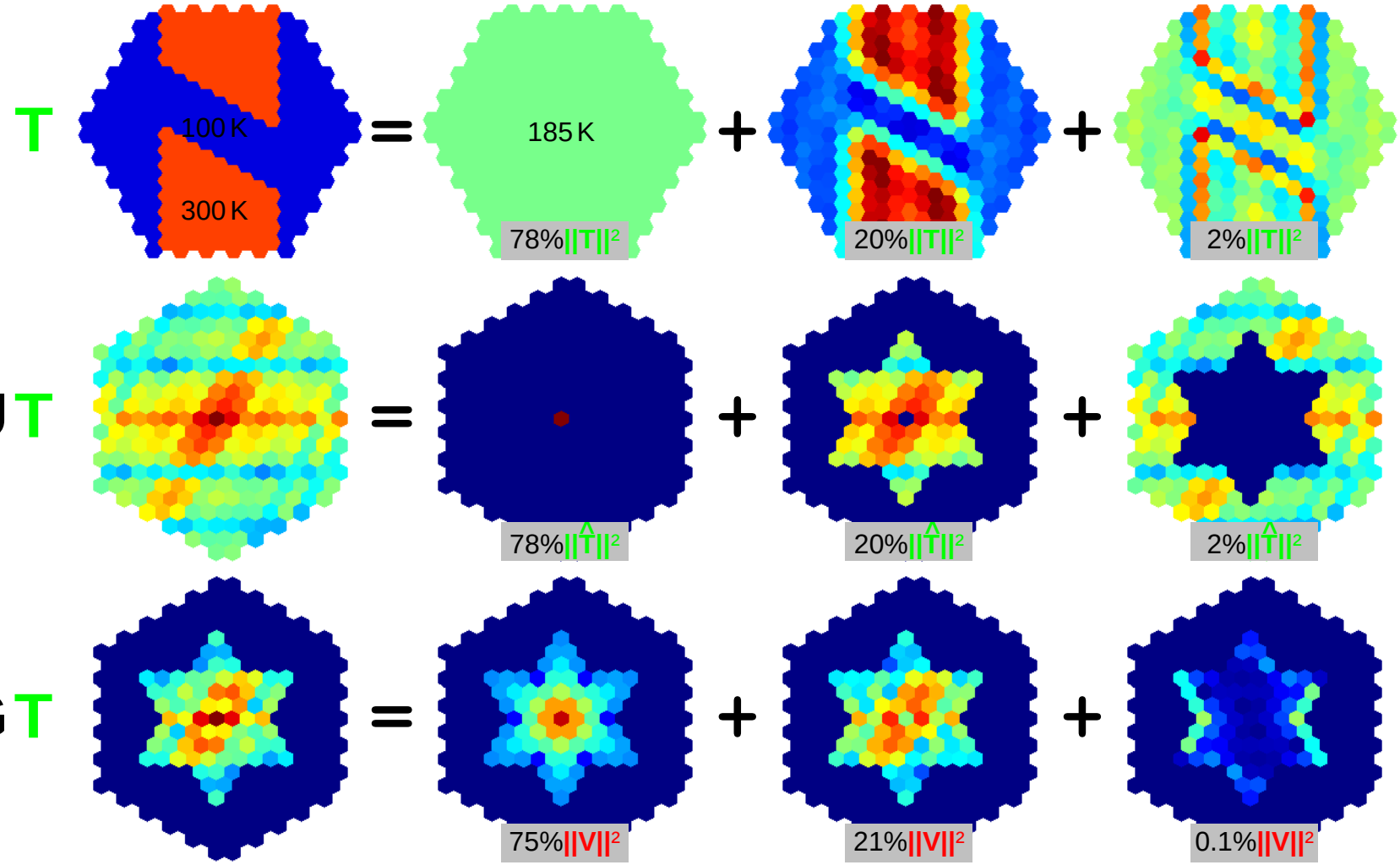

Instrument modeling

❖ *What is an inverse problem ?*

$T \rightarrow \mathbf{G}\ T = V$ direct problem

inverse problem $T = \mathbf{G}^{-1}\ V \leftarrow V$

❖ *What is an ill-posed problem ?*

J. Hadamard (1902), R. Courant (1962):

"A problem satisfying the requirements of existence, uniqueness and continuity is said to be well-posed."

❖ *How to regularize an ill-posed problem ?*

The general principle of regularization methods is to introduce *a priori* information in order to compensate for the lack/loss of information in the imaging process.

Instrument modeling

❖ *What is an ill-conditioned problem ?*

The discretization of a linear inverse problem leads to a linear algebraic system: a rather simple mathematical problem with many numerical methods for solving it.

S. Twomey (1977):

"The crux of the difficulty was that the numerical inversions were producing results which were physically unacceptable but were mathematically acceptable."

One says that the corresponding linear algebraic system is ill-conditioned. (even if the solution exists and is unique, it is completely corrupted by small perturbations on the data.)

Instrument modeling

❖ *An ill-posed problem*

$$\mathbf{V}_{pq} \propto \frac{1}{\sqrt{\Omega_p \Omega_q}} \iint_{\|\xi\| \le 1} \mathcal{F}_p(\xi)\, \mathcal{F}_q^*(\xi)\, [\mathbf{T}_b(\xi) - \mathbf{T}_{rec}]\, \tilde{\mathbf{r}}_{pq}(t)\, \frac{e^{-2j\pi \mathbf{u}_{pq} \cdot \xi}}{\sqrt{1-\|\xi\|^2}}\, d\xi$$

$$\mathbf{V} = \mathbf{G}\,\mathbf{T}$$

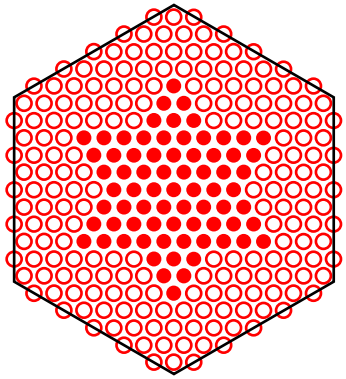

45 visibilities

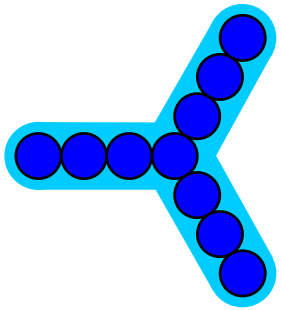

10 antennas

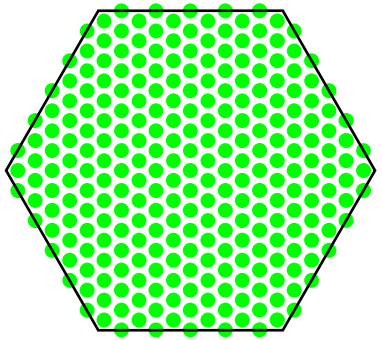

256 pixels

number of data < number of unknowns

Sampling grids

❖ *From array to grids*

Instrument

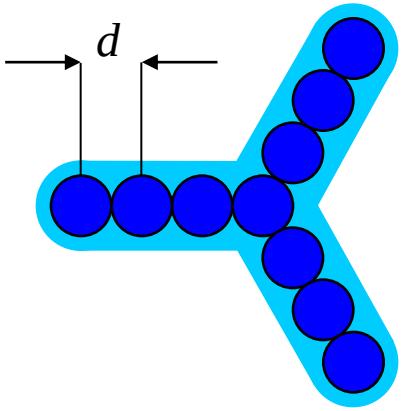

Fourier domain

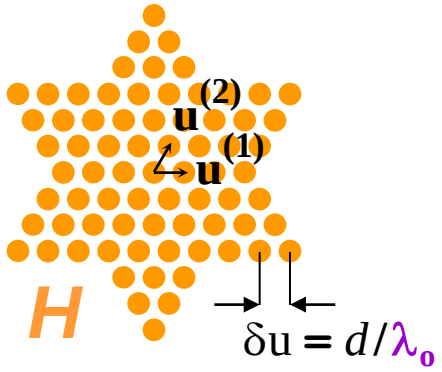

Sampling grids

❖ *From array to grids*

Instrument

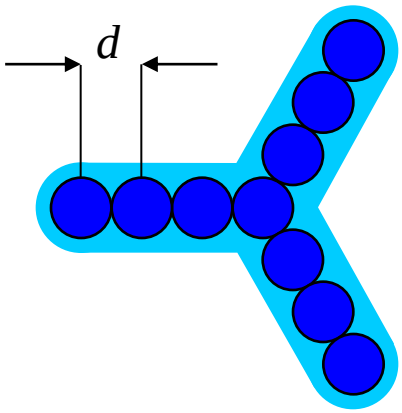

Fourier domain

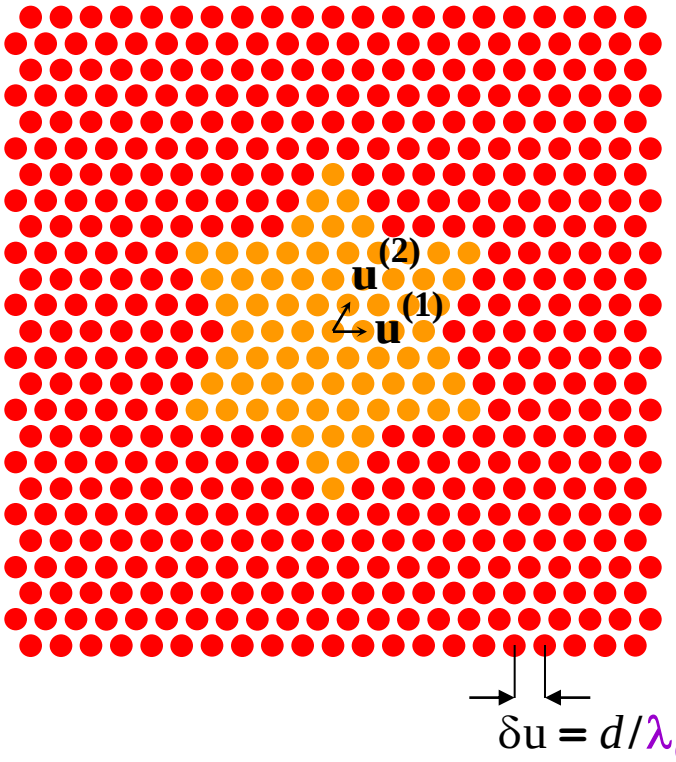

Sampling grids

❖ *From array to grids*

Instrument

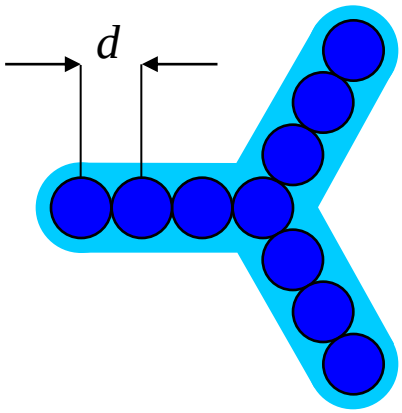

Fourier domain

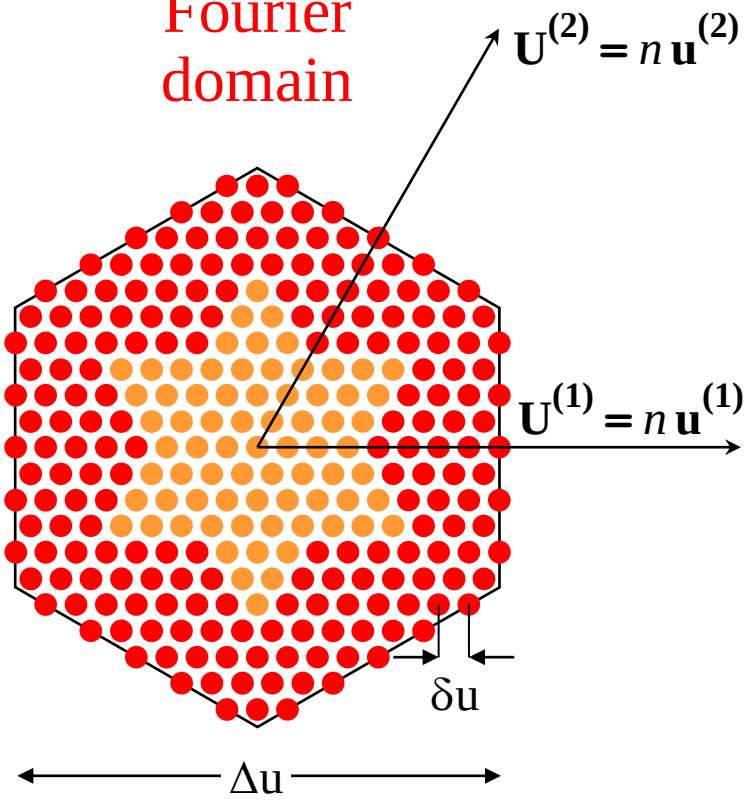

Sampling grids

- *Dual grids*

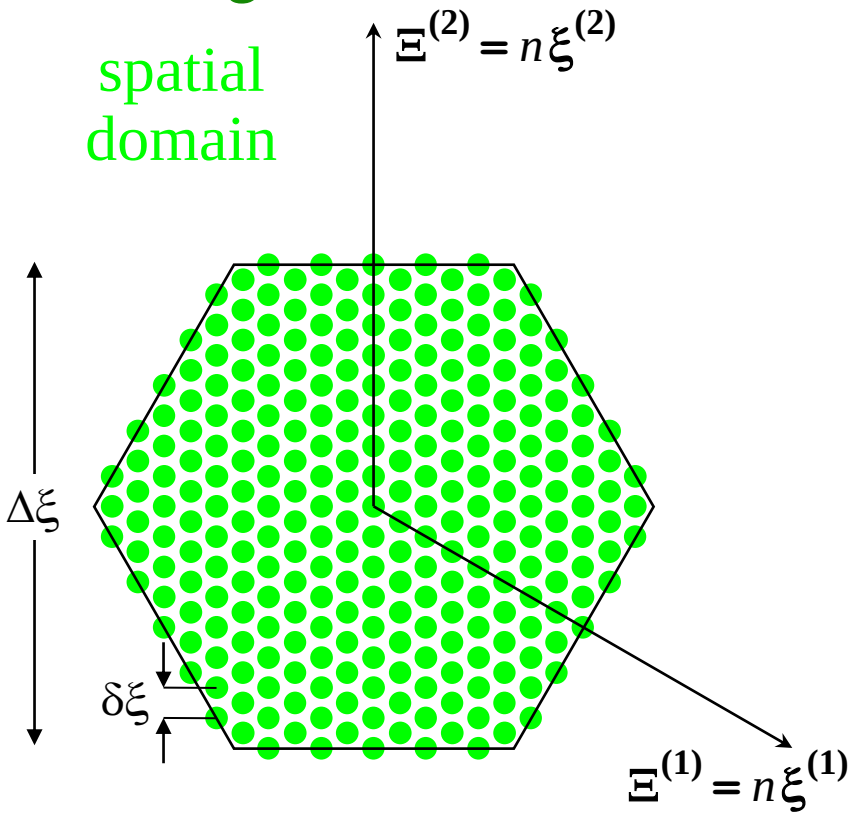

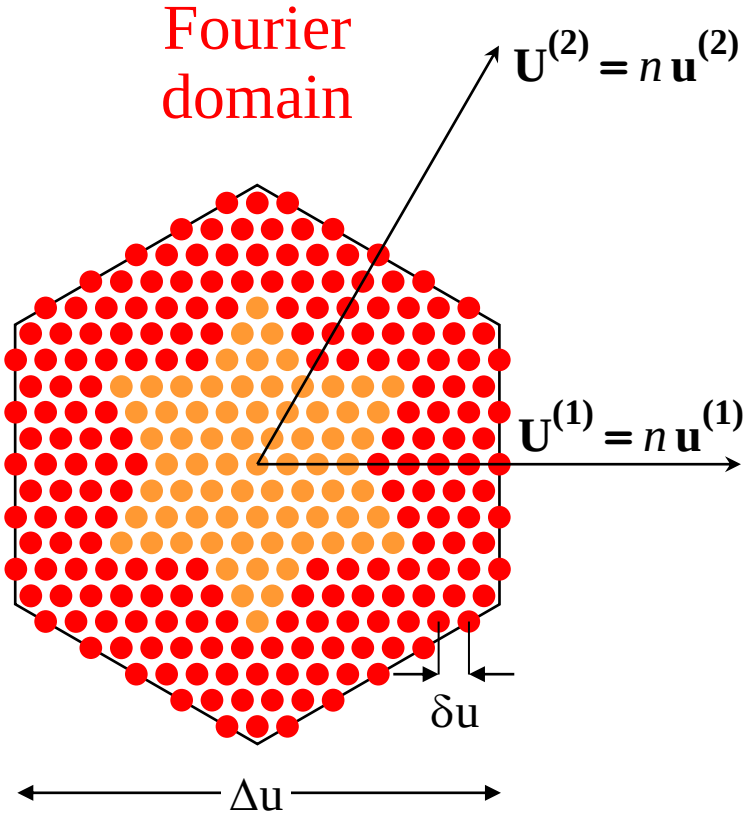

reciprocal lattices: $\boldsymbol{\xi}^{(i)} \cdot \mathbf{U}^{(j)} = \boldsymbol{\Xi}^{(i)} \cdot \mathbf{u}^{(j)} = \delta_{i,j}$

$\Delta\xi\,\delta u = \Delta u\,\delta\xi = 2/\sqrt{3}$ with $\Delta u = n\,\delta u$ and $\Delta\xi = n\,\delta\xi$

Sampling grids

❖ *Dual grids*

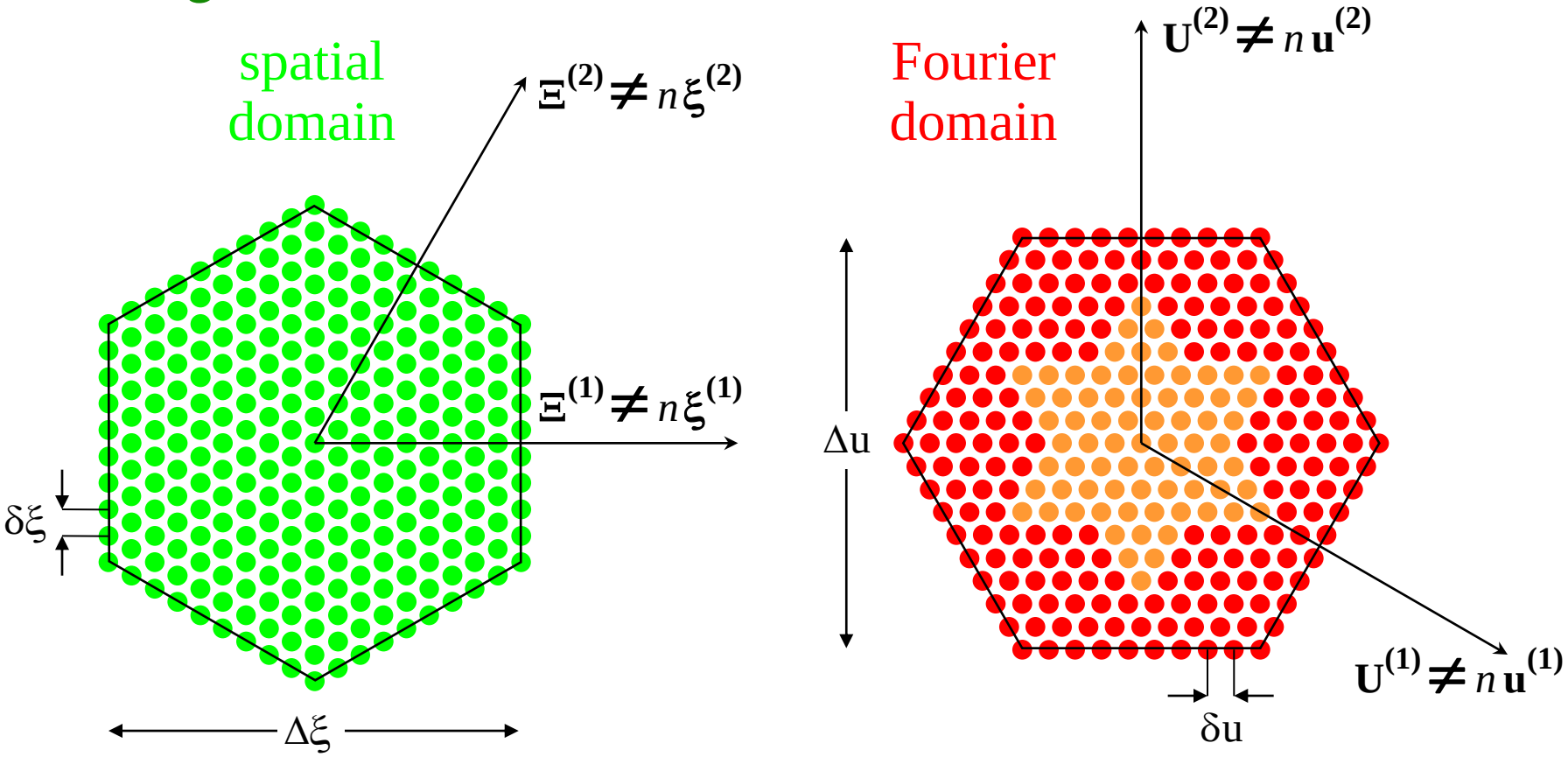

not reciprocal lattices: $\boldsymbol{\xi}^{(i)} \cdot \mathbf{U}^{(j)} \neq \delta_{i,j}$ and $\boldsymbol{\Xi}^{(i)} \cdot \mathbf{u}^{(j)} \neq \delta_{i,j}$

Sampling grids

❖ *Hexagonal processing*

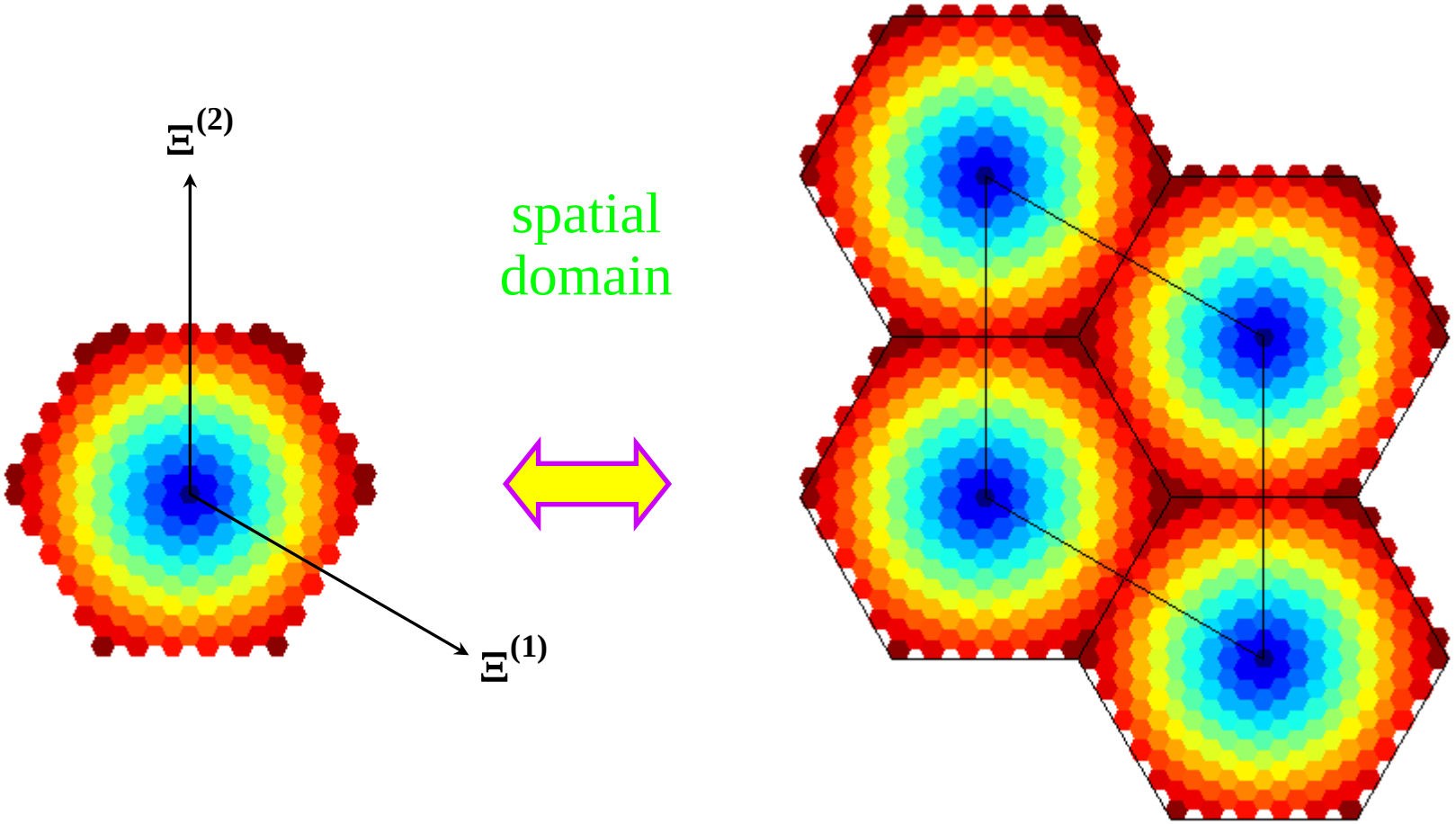

Sampling grids

❖ *Hexagonal processing*

n^2 pixels hexagonal grid ⇔ n^2 pixels cartesian grid

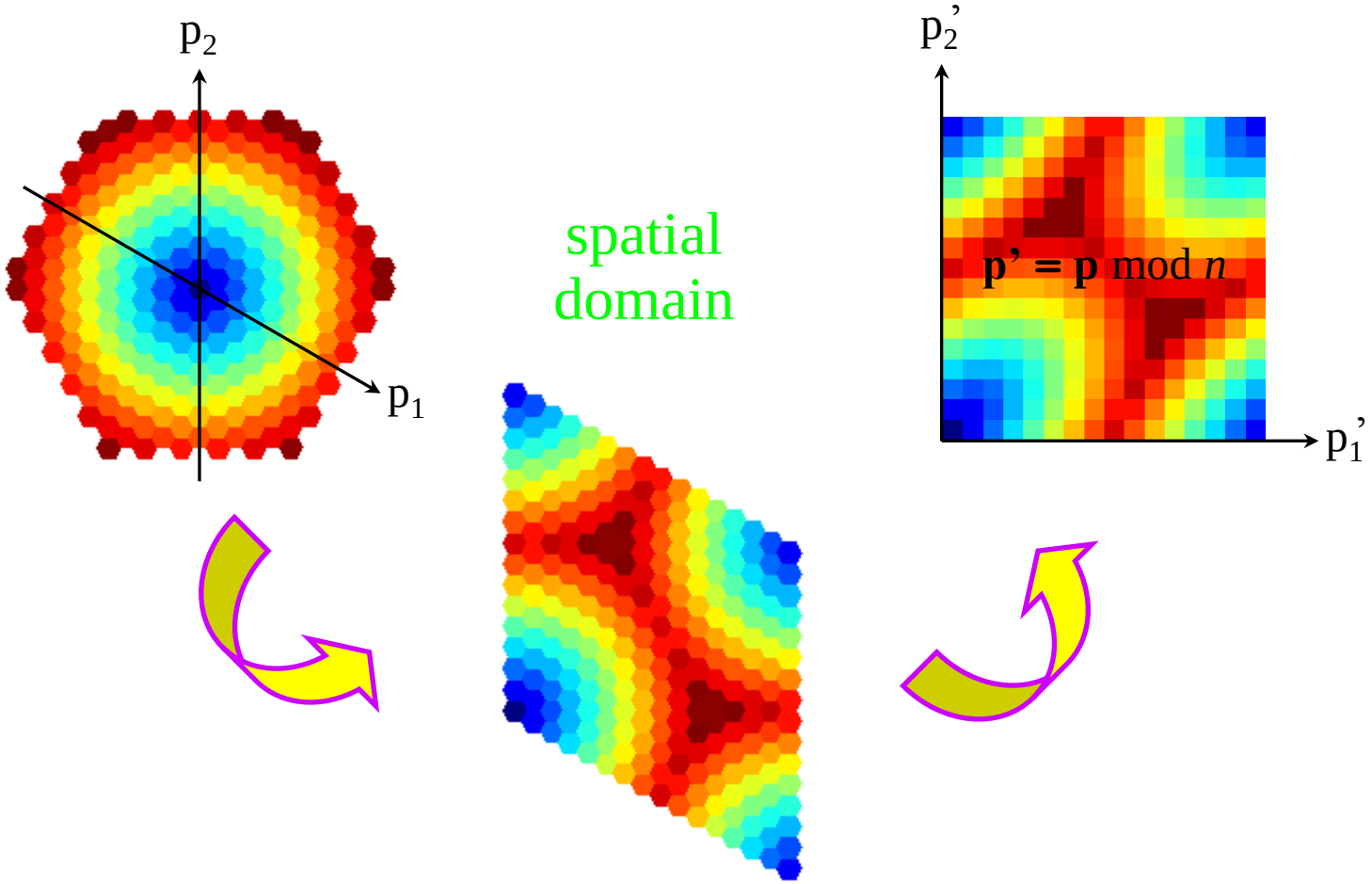

Sampling grids

❖ *Hexagonal processing*

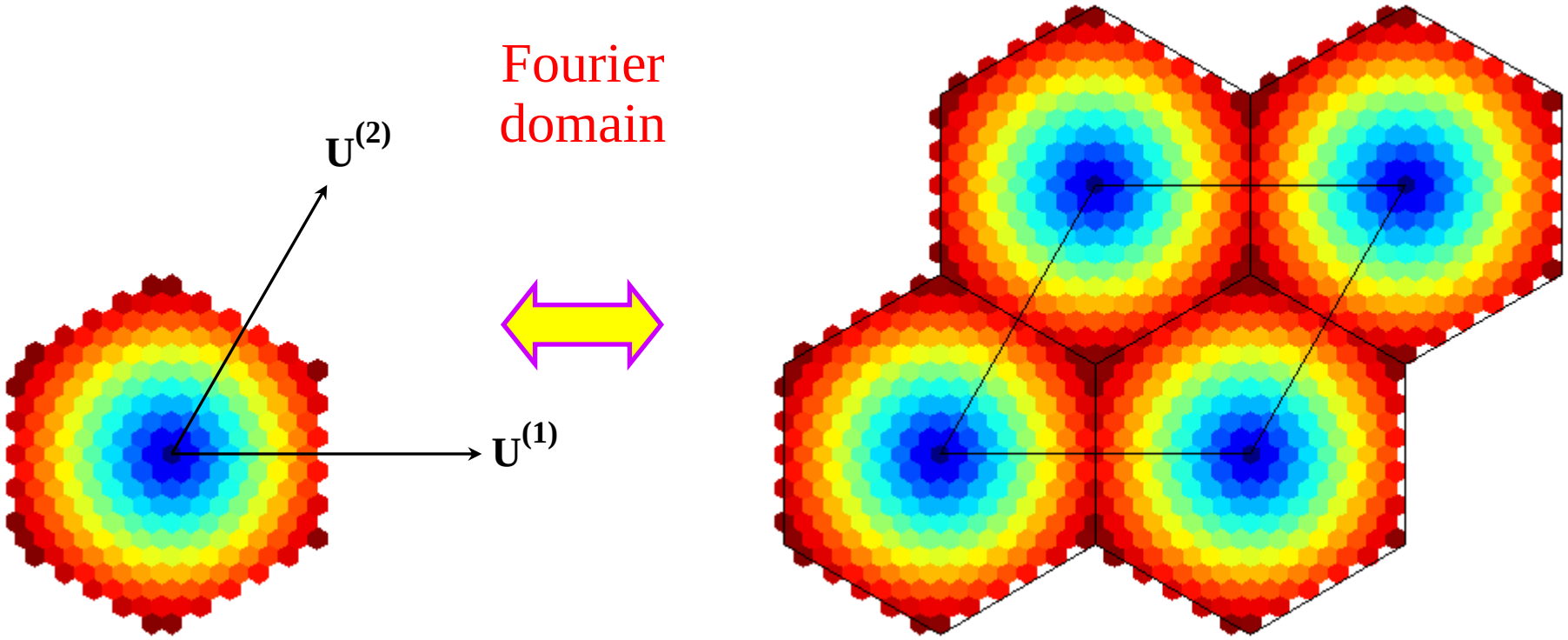

Sampling grids

❖ *Hexagonal processing*

n^2 pixels hexagonal grid ⇔ n^2 pixels cartesian grid

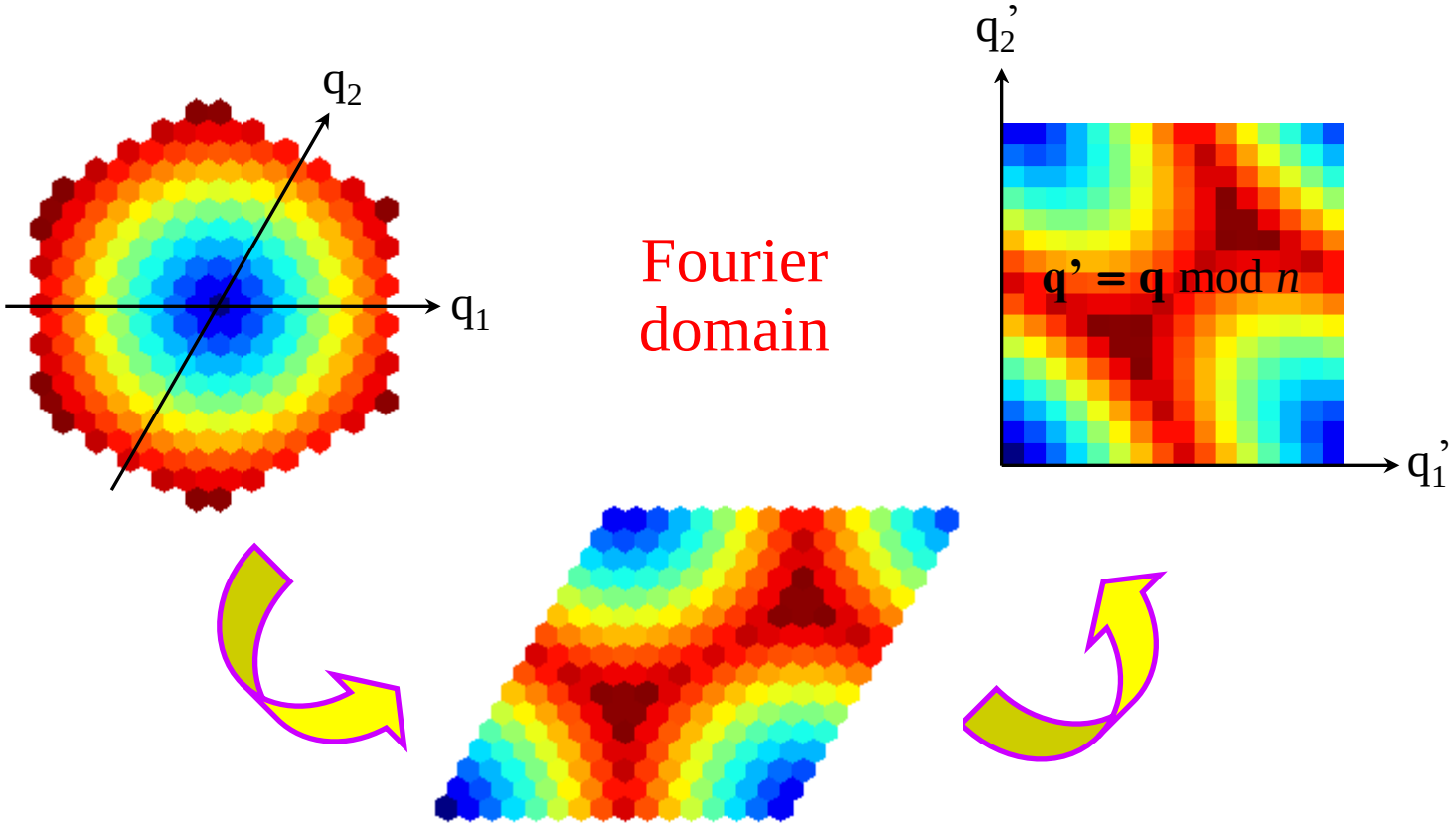

Sampling grids

- *Hexagonal processing*

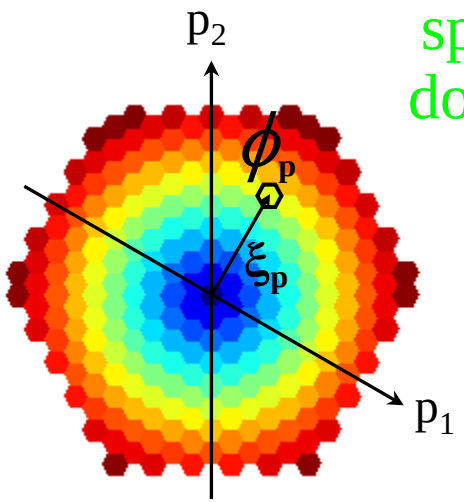

spatial domain

$$\xi_{\mathbf{q}} = p_1 \xi^{(1)} + p_2 \xi^{(2)}$$

$$\hat{\phi}_{\mathbf{q}} = \sum_{\mathbf{p}} \phi_{\mathbf{p}} \, e^{-2j\pi \xi_{\mathbf{p}} \cdot \mathbf{u}_{\mathbf{q}}}$$

reciprocal lattices:

$$\xi^{(i)} \cdot \mathbf{U}^{(j)} = \Xi^{(i)} \cdot \mathbf{u}^{(j)} = \delta_{i,j}$$

$$\hat{\phi}_{\mathbf{q}} = \sum_{\mathbf{p}} \phi_{\mathbf{p}} \, e^{-2j\pi \frac{\mathbf{p} \cdot \mathbf{q}}{n}}$$

Fourier domain

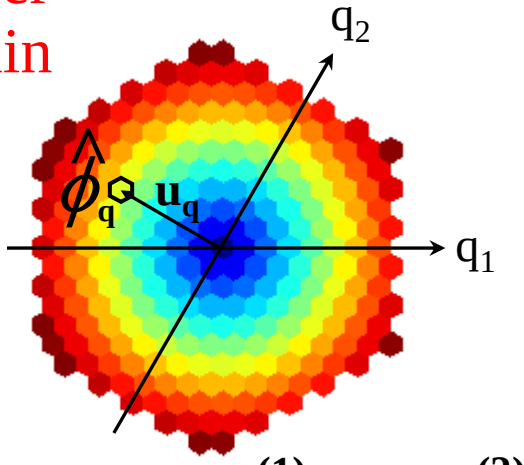

$$\mathbf{u}_{\mathbf{p}} = q_1 \mathbf{u}^{(1)} + q_2 \mathbf{u}^{(2)}$$

Sampling grids

❖ *Hexagonal processing*

n^2 pixels hexagonal grid ⇔ n^2 pixels cartesian grid

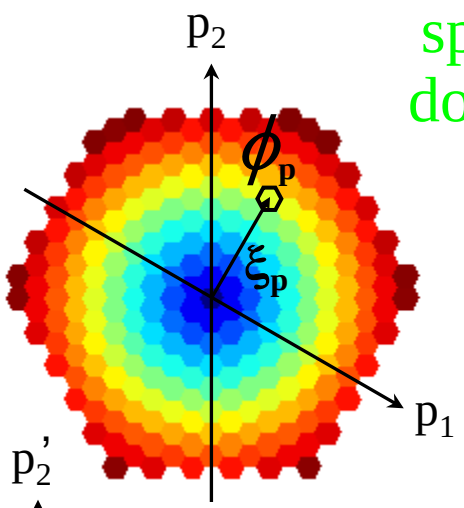

spatial domain

Fourier domain

$$\hat{\phi}_{\mathbf{q}} = \sum_{\mathbf{p}} \phi_{\mathbf{p}} \, e^{-2j\pi \frac{\mathbf{p}\cdot\mathbf{q}}{n}}$$

$$\hat{\phi}_{\mathbf{q}} = \sum_{\mathbf{p}} \phi_{\mathbf{p}} \, e^{-2j\pi \frac{\mathbf{p'}\cdot\mathbf{q'}}{n}}$$

FFT

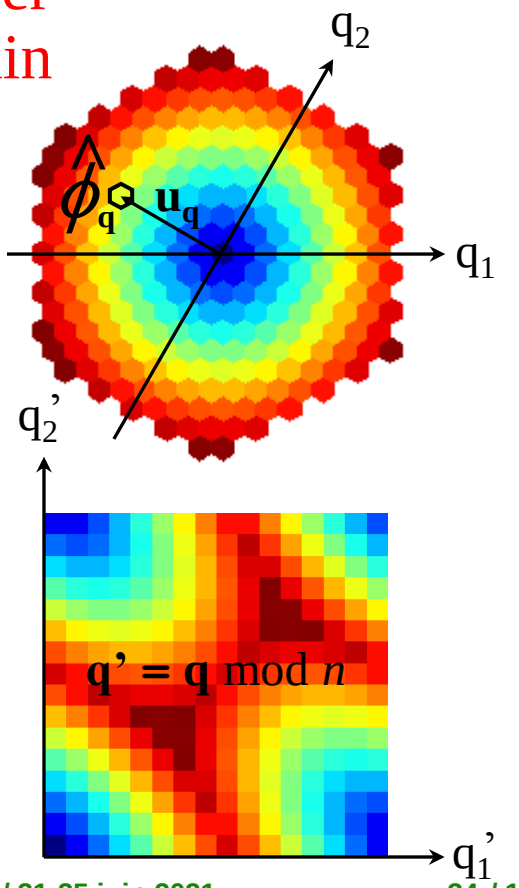

Sampling grids

❖ *Resampling at ground level*

Reconstructed brightness temperature maps are obtained in the direction cosines domain of the reference frame attached to the instrument. These hexagonally sampled images have to be projected onto the Earth surface.

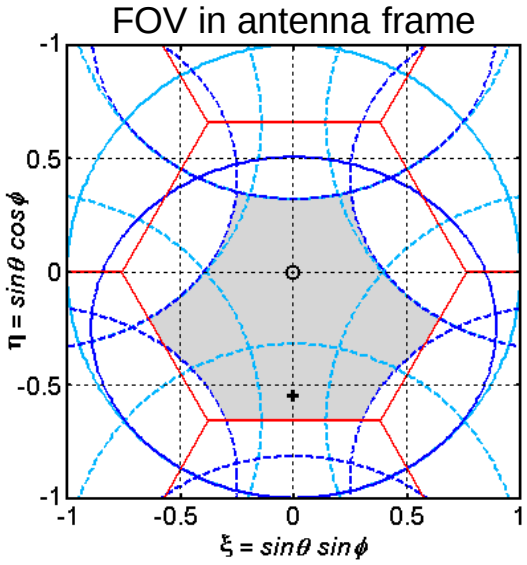

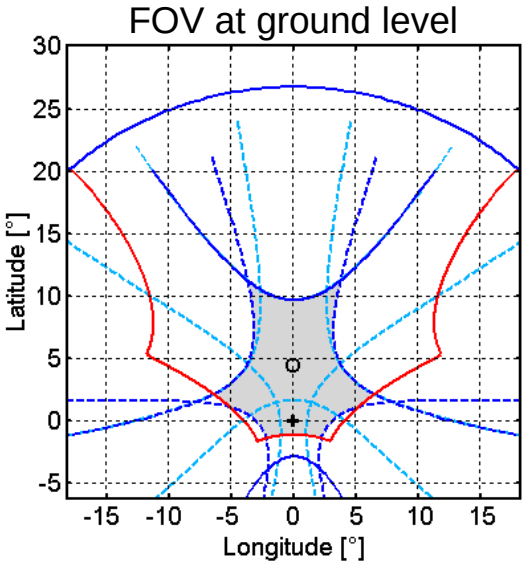

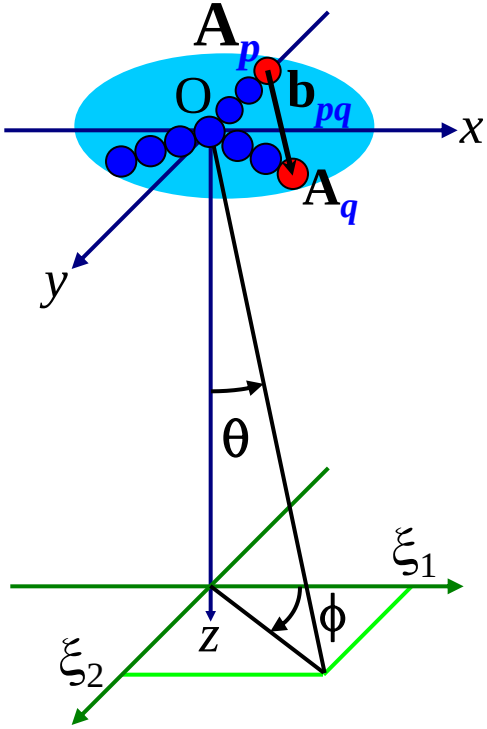

Sampling grids

❖ *Resampling at ground level*

Reconstructed brightness temperature maps are obtained in the direction cosines domain of the reference frame attached to the instrument. These hexagonally sampled images have to be projected onto the Earth surface.

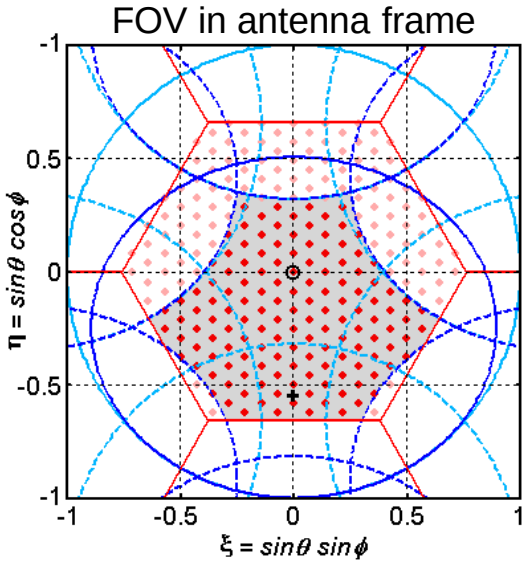

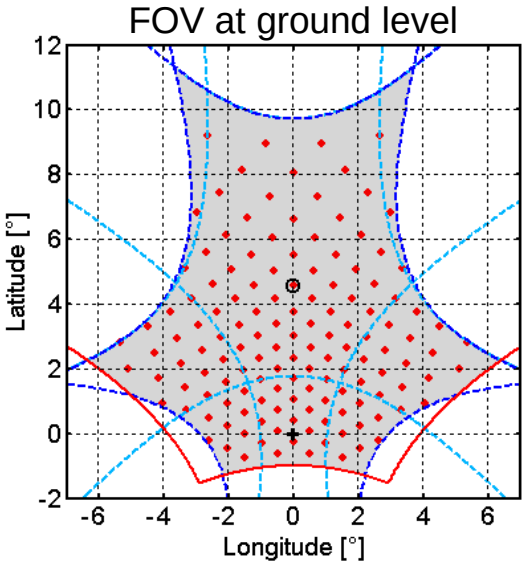

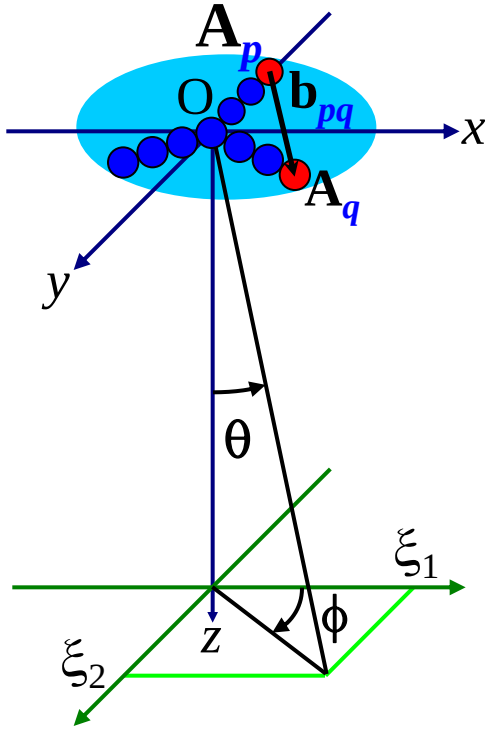

Sampling grids

❖ *Resampling at ground level*

Reconstructed brightness temperature maps are obtained in the direction cosines domain of the reference frame attached to the instrument. These hexagonally sampled images have to be projected onto the Earth surface.

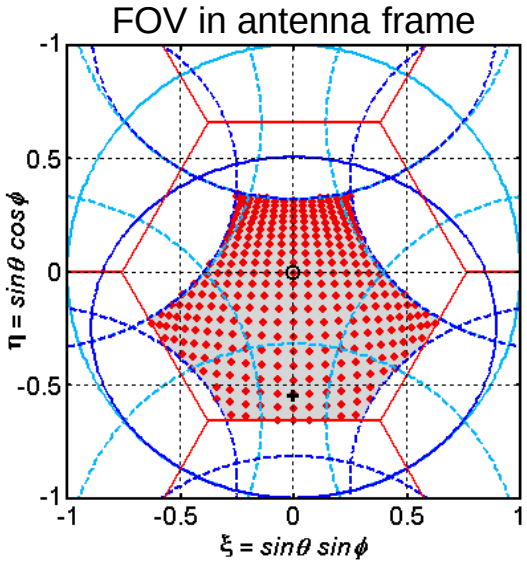

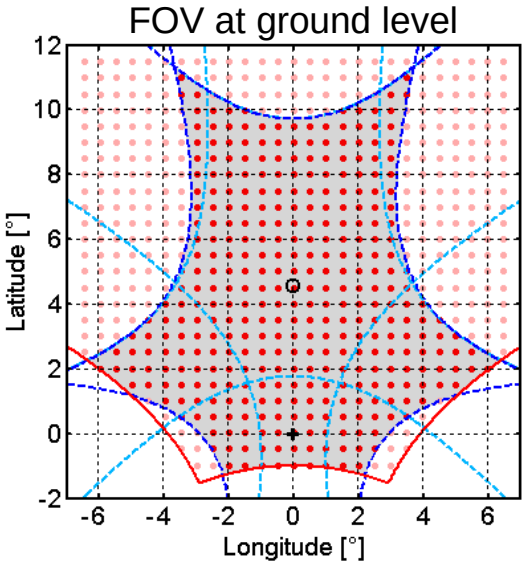

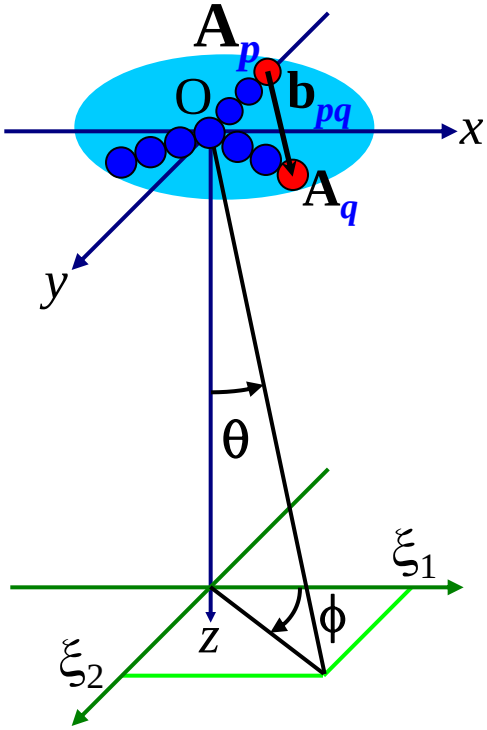

Instrument modeling

❖ *An ill-posed problem*

$$\mathbf{V}_{pq} \propto \frac{1}{\sqrt{\Omega_p \Omega_q}} \iint_{\|\xi\| \le 1} \mathcal{F}_p(\xi)\, \mathcal{F}_q^*(\xi)\, [\mathbf{T}_b(\xi) - \mathbf{T}_{rec}]\, \tilde{\mathbf{r}}_{pq}(t)\, \frac{e^{-2j\pi \mathbf{u}_{pq}\cdot\xi}}{\sqrt{1-\|\xi\|^2}}\, d\xi$$

$$\mathbf{V} = \mathbf{G}\,\mathbf{T}$$

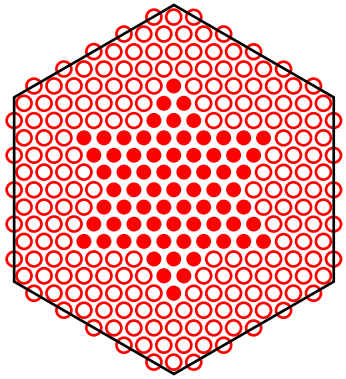

45 visibilities

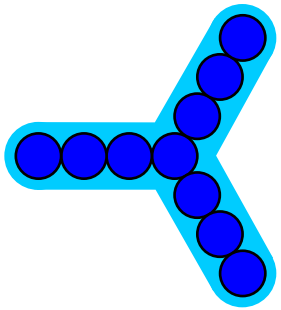

10 antennas

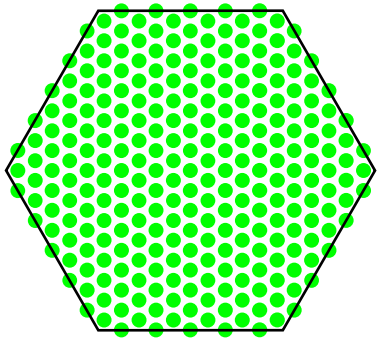

256 pixels

number of data < number of unknowns

Regularized inversion

- *Least-squares…*

$$\min_{\mathbf{T}\in\mathbb{R}^{n^2}} \|\mathbf{V}-\mathbf{G}\mathbf{T}\|^2$$

$$\mathbf{G}^*\mathbf{G}\,\mathbf{T}=\mathbf{G}^*\mathbf{V}$$

$$\mathbf{T}_r=\mathbf{G}^+\mathbf{V} \text{ with } \mathbf{G}^+=(\mathbf{G}^*\mathbf{G})^{-1}\mathbf{G}^*$$

Regularized inversion

- *Least-squares…*

$$\min_{\mathbf{T}\in\mathbb{R}^{n^2}} \|\mathbf{V}-\mathbf{G}\mathbf{T}\|^2$$

$$\mathbf{G}^*\mathbf{G}\,\mathbf{T}=\mathbf{G}^*\mathbf{V}$$

eigenvalues of $\mathbf{G}^*\mathbf{G}$

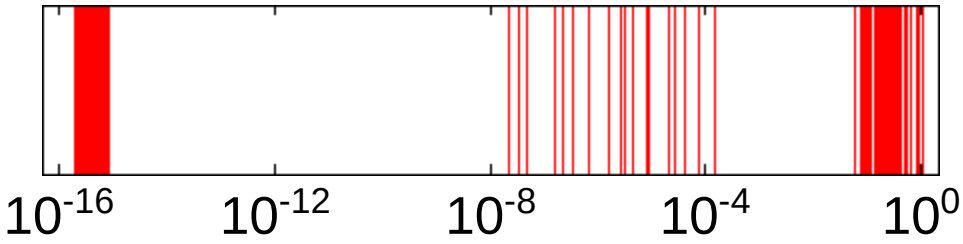

$$\mathbf{T}_r=\mathbf{G}^+\mathbf{V} \text{ with } \mathbf{G}^+=(\mathbf{G}^*\mathbf{G})^{-1}\mathbf{G}^*$$

$\mathbf{G}^*\mathbf{G}$ is singular

Regularized inversion

- *Tikhonov regularization*

$$\min \; \|\mathbf{V} - \mathbf{G}\mathbf{T}\|^2 + \mu \|\mathbf{T}\|^2$$

$\mathbf{T} \in \mathbb{R}^{n^2}$

$\mu \in \mathbb{R}$

$$(\mathbf{G}^*\mathbf{G} + \mu \mathbf{I})\,\mathbf{T} = \mathbf{G}^*\mathbf{V}$$

eigenvalues of $\mathbf{G}^*\mathbf{G} + \mu \mathbf{I}$

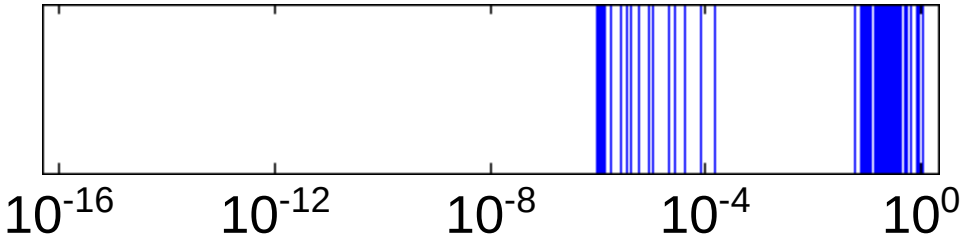

$$\mathbf{T}_r = \mathbf{G}_\mu^+ \mathbf{V} \quad \text{with} \quad \mathbf{G}_\mu^+ = (\mathbf{G}^*\mathbf{G} + \mu \mathbf{I})^{-1}\mathbf{G}^*$$

μ is the Lagrange regularization parameter

Regularized inversion

❖ *Minimum norm regularization*

$$\begin{cases} \min_{\mathbf{T}\in\mathbb{R}^{n^2}} \|\mathbf{T}\|^2 \\ \mathbf{V} = \mathbf{G}\mathbf{T} \end{cases}$$

singular values of $\mathbf{G}$

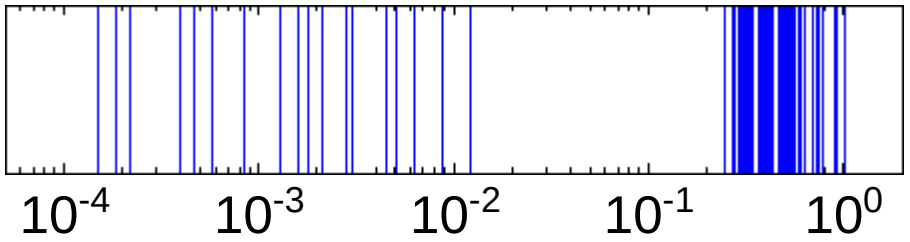

$$\mathbf{T_r} = \mathbf{G}^{+}\mathbf{V} \text{ with } \mathbf{G}^{+} = \underbrace{\sum_{i\geq 1} \frac{1}{\sigma_i} \boldsymbol{v_i}\boldsymbol{u_i}^{T}}_{\mathbf{G}^{*}(\mathbf{G}\mathbf{G}^{*})^{-1}} \Leftarrow \mathbf{G} = \sum_{i\geq 1} \sigma_i \boldsymbol{u_i}\boldsymbol{v_i}^{T} \text{ (SVD)}$$

Regularized inversion

❖ *Minimum norm regularization*

$$\begin{cases} \min_{\mathbf{T}\in\mathbb{R}^{n^2}} \|\mathbf{T}\|^2 \\ \mathbf{V} = \mathbf{G}\mathbf{T} \end{cases}$$

singular values of **G**

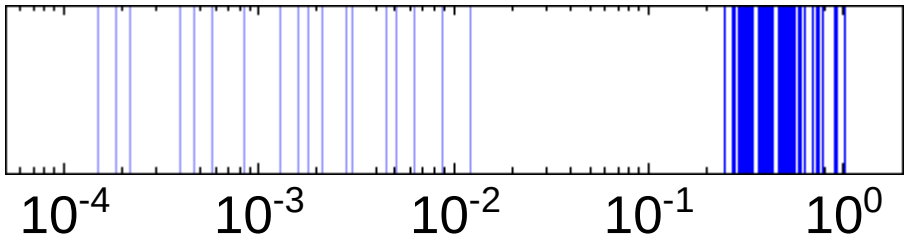

$$\mathbf{T_r} = \mathbf{G}_m^+ \mathbf{V} \text{ with } \mathbf{G}_m^+ = \sum_{i\geq m} \frac{1}{\sigma_i} \boldsymbol{v_i} \boldsymbol{u_i}^T \Leftarrow \underset{m\geq 1}{\mathbf{G}_m = \sum_{i\geq m} \sigma_i \boldsymbol{u_i} \boldsymbol{v_i}^T} \text{ (TSVD)}$$

m plays the role of a regularization parameter

Regularized inversion

❖ *Band-limited regularization*

$$\mathbf{V}_{pq} \propto \frac{1}{\sqrt{\Omega_p \Omega_q}} \iint_{\|\xi\| \le 1} \mathcal{F}_p(\xi)\, \mathcal{F}_q^*(\xi)\, [\mathbf{T}_b(\xi) - \mathbf{T}_{rec}]\, \tilde{\mathbf{r}}_{pq}(t)\, \frac{e^{-2j\pi \mathbf{u}_{pq}\cdot\xi}}{\sqrt{1-\|\xi\|^2}}\, d\xi$$

$$\mathbf{V} = \mathbf{G}\,\mathbf{T}$$

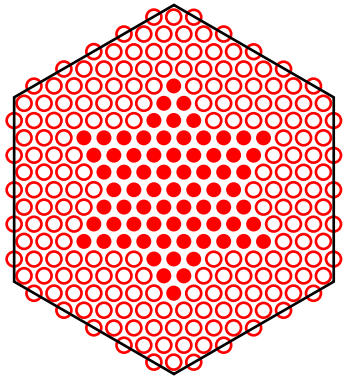

45 visibilities

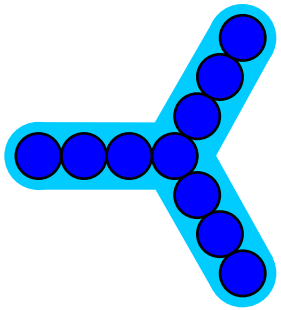

10 antennas

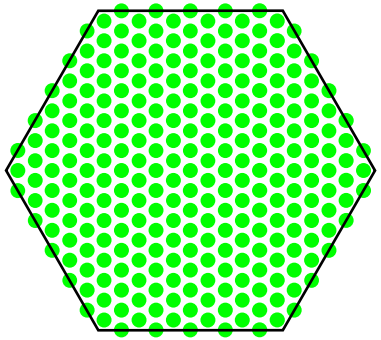

256 pixels

number of data < number of unknowns

Regularized inversion

❖ *Band-limited regularization*

$$\mathbf{V}_{pq} \propto \frac{1}{\sqrt{\Omega_p \Omega_q}} \iint_{\|\xi\| \le 1} \mathcal{F}_p(\xi)\, \mathcal{F}_q^*(\xi)\, [\mathbf{T}_b(\xi) - \mathbf{T}_{rec}]\, \tilde{\mathbf{r}}_{pq}(t)\, \frac{e^{-2j\pi \mathbf{u}_{pq}\cdot\xi}}{\sqrt{1-\|\xi\|^2}}\, d\xi$$

$$\mathbf{V} = \mathbf{G}\,\mathbf{T}$$

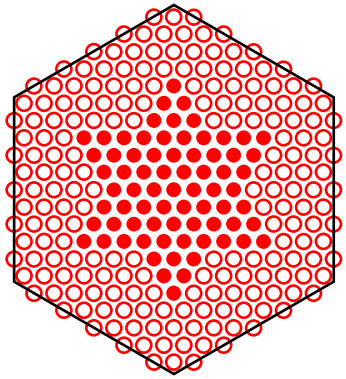

45 visibilities

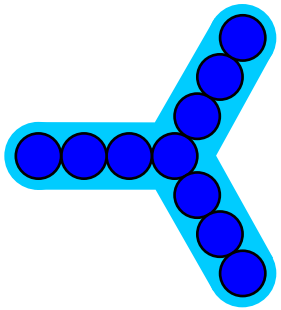

10 antennas

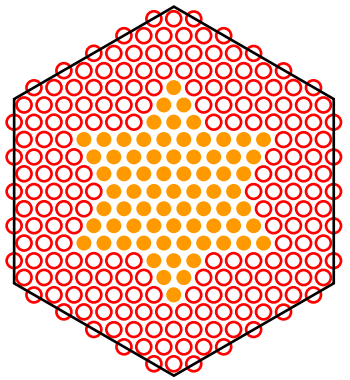

36 frequencies

number of data > number of unknowns

Regularized inversion

- *Band-limited regularization*

$$\mathbf{V}_{pq} \propto \frac{1}{\sqrt{\Omega_p \Omega_q}} \iint_{\|\xi\| \le 1} \mathcal{F}_p(\xi)\, \mathcal{F}_q^*(\xi)\, [\mathbf{T}_b(\xi) - \mathbf{T}_{rec}]\, \tilde{\mathbf{r}}_{pq}(t)\, \frac{e^{-2j\pi \mathbf{u}_{pq}\cdot\xi}}{\sqrt{1-\|\xi\|^2}}\, d\xi$$

$$\mathbf{V} = \mathbf{G}\,\mathbf{T}$$

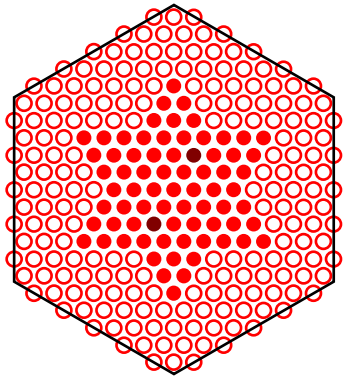

45 visibilities

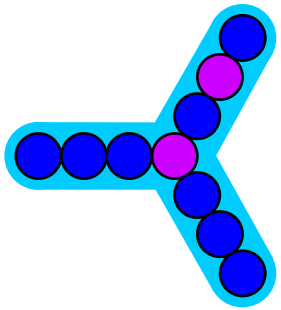

10 antennas

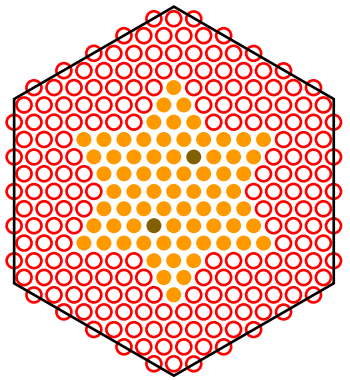

36 frequencies

number of data > number of unknowns

Regularized inversion

❖ *Band-limited regularization*

$$\mathbf{V}_{pq} \propto \frac{1}{\sqrt{\Omega_p \Omega_q}} \iint_{\|\xi\| \le 1} \mathcal{F}_p(\xi)\, \mathcal{F}_q^*(\xi)\, [\mathbf{T}_b(\xi) - \mathbf{T}_{rec}]\, \tilde{\mathbf{r}}_{pq}(t)\, \frac{e^{-2j\pi \mathbf{u}_{pq}\cdot\xi}}{\sqrt{1-\|\xi\|^2}}\, d\xi$$

$$\mathbf{V} = \mathbf{G}\,\mathbf{T}$$

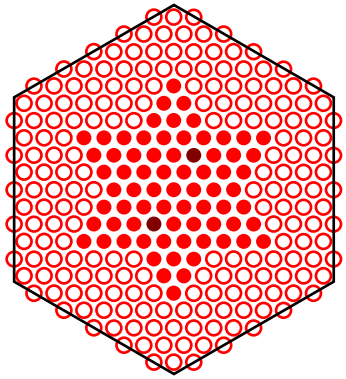

45 visibilities

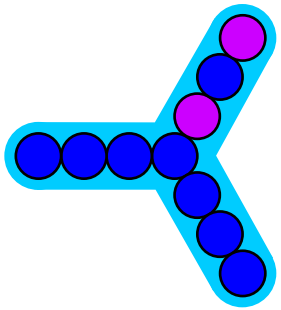

10 antennas

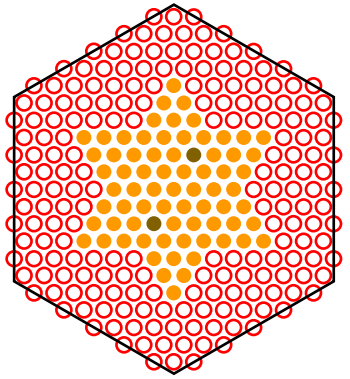

36 frequencies

number of data > number of unknowns

Regularized inversion

❖ *Band-limited regularization*

$$\begin{cases} \underset{\mathbf{T}\in\mathbb{R}^{n^2}}{\min} \left\| \mathbf{V} - \mathbf{G}\mathbf{T} \right\|^2 \\ (\mathbf{I} - \mathbf{P}_H)\,\mathbf{T} = \mathbf{0} \end{cases}$$

singular values of $\mathbf{J}$

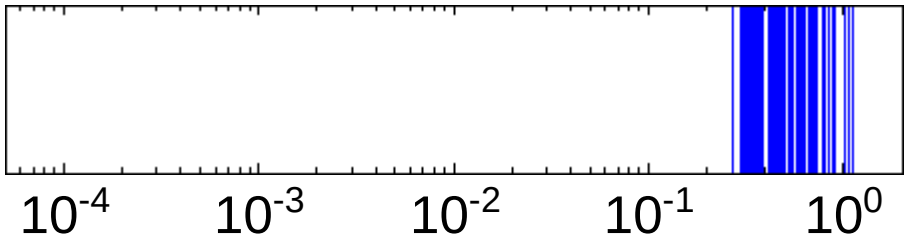

$$\mathbf{J}^*\mathbf{J}\,\hat{\mathbf{T}}_H = \mathbf{J}^*\mathbf{V} \quad \text{with} \quad \mathbf{J} = \mathbf{G}\,\mathbf{U}^*\mathbf{Z}$$

$$\mathbf{T}_r = \mathbf{U}^*\mathbf{Z}\,\mathbf{J}^+\,\mathbf{V} \quad \text{with} \quad \mathbf{J}^+ = \left(\mathbf{J}^*\mathbf{J}\right)^{-1}\mathbf{J}^*$$

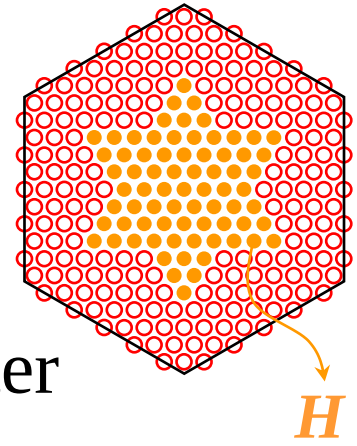

$\mathbf{P}_H$ plays the role of a regularization parameter

Regularized inversion

- *The L-curve…*

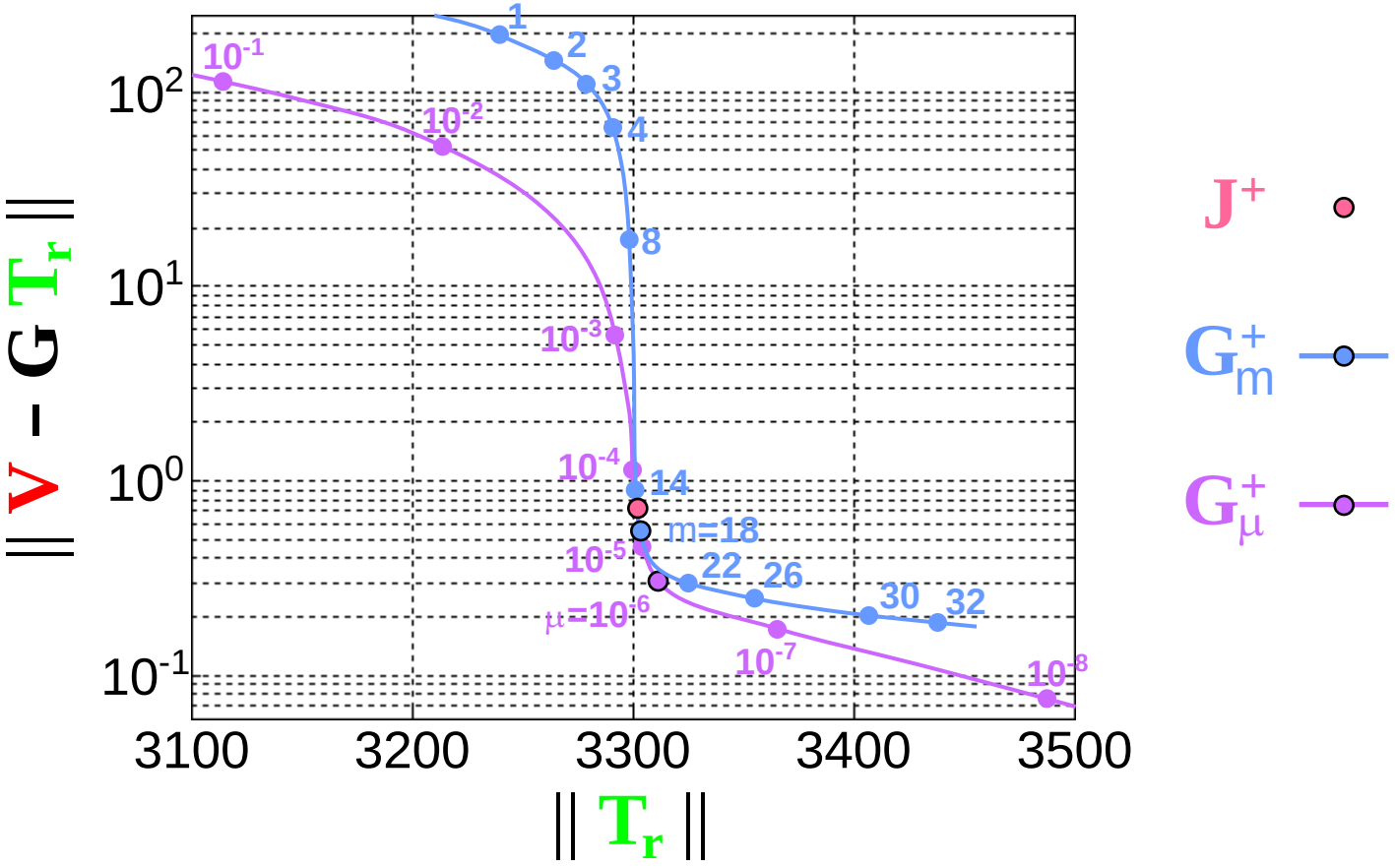

Regularized inversion

❖ *Error analysis*

Whatever the reconstruction operator $\mathbf{R}^+$, the propagation of random errors from complex visibilities $\mathbf{V}$ to the reconstructed map $\mathbf{T_r}$ is governed by the equality:

$$\frac{\sqrt{\mathbf{E}[\|\Delta \mathbf{T_r}\|^2]}}{\|\mathbf{T_r}\|} = \frac{\|\mathbf{V}\|}{\|\mathbf{T_r}\|} \|\mathbf{R}^+\|_f \frac{\sqrt{\mathbf{E}[\|\Delta \mathbf{V}\|^2]}}{\|\mathbf{V}\|}$$

Reconstruction artifacts can be identified within a complete error analysis involving the singular vectors $\mathbf{T_k}$ of $\mathbf{R}$ (and specially those associated to the smallest singular values):

$$\mathbf{T_r} = \sum_{\mathbf{k}} (\mathbf{T_k}|\mathbf{T_r})\, \mathbf{T_k}$$

Regularized inversion

❖ *Error analysis*

Reconstruction artifacts can be identified within a complete error analysis involving the singular vectors $\mathbf{T_k}$ of $\mathbf{R}$ (and specially those associated to the smallest singular values):

$$\mathbf{T_r} = \sum_{\mathbf{k}} (\mathbf{T_k} | \mathbf{T_r}) \, \mathbf{T_k}$$

The (cosine of the) separation angle φ_k between $\mathbf{T_k}$ and $\mathbf{T_r}$ is an indicator of the level of excitation of the singular vector in the reconstructed map:

$$cos\, \varphi_k = \frac{(\mathbf{T_k} | \mathbf{T_r})}{\sqrt{\sum_{\mathbf{k}} (\mathbf{T_k} | \mathbf{T_r})^2}}$$

Regularized inversion

❖ *Pros & cons*

	regularization parameter	number of unknowns	complexity of inversion	stability of inversion	apodization	resampling
Tikhonov						
minimum-norm						
band-limited						

Regularized inversion

❖ *Differential reconstruction*

$$\begin{cases} \min_{\delta T \in \mathbb{R}^{n^2}} \left\| \delta V - G \delta T \right\|^2 \\ (I - P_H)\, \delta T = 0 \end{cases}$$

where

$$\delta T = T - \tilde{T}$$

$$\delta V = V - G\tilde{T}$$

$$T_r = U^* Z J^+ (V - G\tilde{T}) + \tilde{T}$$

$$\tau_r = U^* \hat{W} U T_r + T_{rec}$$

$$\tau_w = U^* \hat{W} U T_b$$

to be compared:

$$\Delta\tau_r = \tau_r - \tau_w$$

Instrument modeling

❖ *Dual polarization mode*

$$\mathbf{V}_{pq}^{x} \propto \frac{1}{\sqrt{\Omega_p \Omega_q}} \iint_{\|\xi\| \le 1} \left[\mathbf{C}_p^{x}(\xi)\, \mathbf{C}_q^{*x}(\xi)\, [\mathbf{T}_b^{x}(\xi) - \mathbf{T}_{rec}] + \mathbf{X}_p^{x}(\xi)\, \mathbf{X}_q^{*x}(\xi)\, [\mathbf{T}_b^{y}(\xi) - \mathbf{T}_{rec}] \right] \tilde{\mathbf{r}}_{pq}(t)\, \frac{e^{-2j\pi \mathbf{u}_{pq} \cdot \xi}}{\sqrt{1 - \|\xi\|^2}}\, d\xi$$

$$\mathbf{V}_{pq}^{y} \propto \frac{1}{\sqrt{\Omega_p \Omega_q}} \iint_{\|\xi\| \le 1} \left[\mathbf{X}_p^{y}(\xi)\, \mathbf{X}_q^{*y}(\xi)\, [\mathbf{T}_b^{x}(\xi) - \mathbf{T}_{rec}] + \mathbf{C}_p^{y}(\xi)\, \mathbf{C}_q^{*y}(\xi)\, [\mathbf{T}_b^{y}(\xi) - \mathbf{T}_{rec}] \right] \tilde{\mathbf{r}}_{pq}(t)\, \frac{e^{-2j\pi \mathbf{u}_{pq} \cdot \xi}}{\sqrt{1 - \|\xi\|^2}}\, d\xi$$

C : co-polar antenna gain pattern

X : cross-polar antenna gain pattern

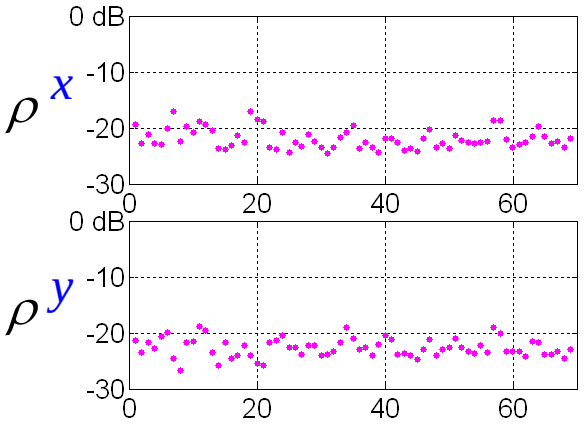

coupling ρ

Instrument modeling

❖ *Dual polarization mode*

$$\mathbf{V}_{pq}^{x} \propto \frac{1}{\sqrt{\Omega_p \Omega_q}} \iint_{\|\xi\| \le 1} \left[\mathbf{C}_p^{x}(\xi)\, \mathbf{C}_q^{*x}(\xi)\, [\mathbf{T}_b^{x}(\xi) - \mathbf{T}_{rec}] + \mathbf{X}_p^{x}(\xi)\, \mathbf{X}_q^{*x}(\xi)\, [\mathbf{T}_b^{y}(\xi) - \mathbf{T}_{rec}] \right] \tilde{\mathbf{r}}_{pq}(t)\, \frac{e^{-2j\pi \mathbf{u}_{pq} \cdot \xi}}{\sqrt{1 - \|\xi\|^2}}\, d\xi$$

$$\mathbf{V}_{pq}^{y} \propto \frac{1}{\sqrt{\Omega_p \Omega_q}} \iint_{\|\xi\| \le 1} \left[\mathbf{X}_p^{y}(\xi)\, \mathbf{X}_q^{*y}(\xi)\, [\mathbf{T}_b^{x}(\xi) - \mathbf{T}_{rec}] + \mathbf{C}_p^{y}(\xi)\, \mathbf{C}_q^{*y}(\xi)\, [\mathbf{T}_b^{y}(\xi) - \mathbf{T}_{rec}] \right] \tilde{\mathbf{r}}_{pq}(t)\, \frac{e^{-2j\pi \mathbf{u}_{pq} \cdot \xi}}{\sqrt{1 - \|\xi\|^2}}\, d\xi$$

$$\mathbf{V} = \mathbf{G}\,\mathbf{T}$$

$$\mathbf{V} = \begin{bmatrix} \mathbf{V}^{x} \\ \mathbf{V}^{y} \end{bmatrix} \qquad \mathbf{G} = \begin{bmatrix} \mathbf{G}^{xx} & \mathbf{G}^{xy} \\ \mathbf{G}^{yx} & \mathbf{G}^{yy} \end{bmatrix} \qquad \mathbf{T} = \begin{bmatrix} \mathbf{T}^{x}(\xi) \\ \mathbf{T}^{y}(\xi) \end{bmatrix} = \begin{bmatrix} \mathbf{T}_b^{x}(\xi) - \mathbf{T}_{rec} \\ \mathbf{T}_b^{y}(\xi) - \mathbf{T}_{rec} \end{bmatrix}$$

Regularized inversion

❖ *Dual polarization mode*

$$\begin{pmatrix} T_r^x \\ T_r^y \end{pmatrix} = \begin{pmatrix} U^* Z & 0 \\ 0 & U^* Z \end{pmatrix} \begin{pmatrix} J^{xx} & J^{xy} \\ J^{yx} & J^{yy} \end{pmatrix}^+ \begin{pmatrix} V^x \\ V^y \end{pmatrix}$$

numerical implementation in ground segment

69 antennas
dual polarisation
(**J** ~ 400 Mbytes)

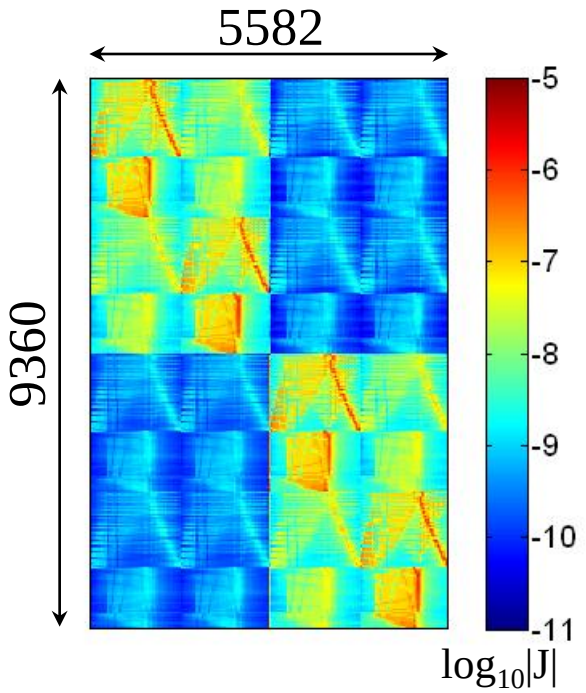

Regularized inversion

❖ *Dual polarization mode*

$$\begin{pmatrix} T_r^x \\ T_r^y \end{pmatrix} = \begin{pmatrix} U^* Z & 0 \\ 0 & U^* Z \end{pmatrix} \begin{pmatrix} J^{xx} & J^{xy} \\ J^{yx} & J^{yy} \end{pmatrix}^{+} \left[\begin{pmatrix} V^x \\ V^y \end{pmatrix} - \begin{pmatrix} G^{xx} & G^{xy} \\ G^{yx} & G^{yy} \end{pmatrix} \begin{pmatrix} \tilde{T}^x \\ \tilde{T}^y \end{pmatrix} \right] + \begin{pmatrix} \tilde{T}^x \\ \tilde{T}^y \end{pmatrix}$$

numerical implementation in ground segment

69 antennas
dual polarisation
(**J** ~ 400 Mbytes)

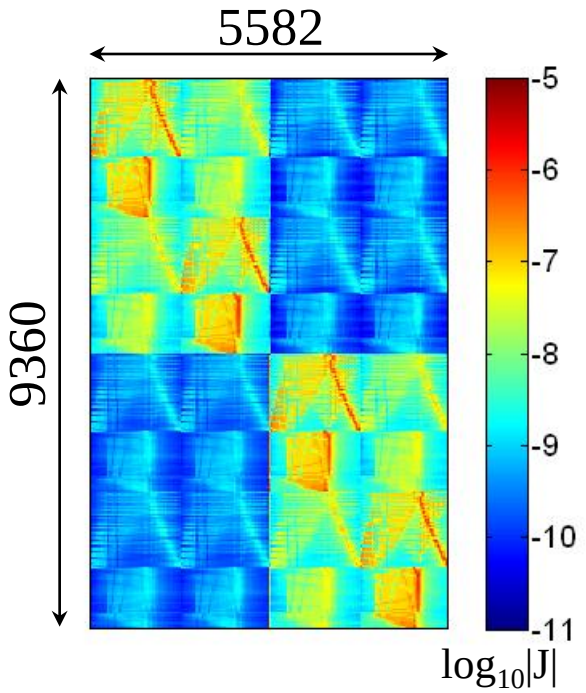

Regularized inversion

- *Full polarization mode*

$$\begin{pmatrix} T_r^{\,x} \\ T_r^{\,y} \\ T_r^{\,3} \\ T_r^{\,4} \end{pmatrix} = \cdot \cdot \cdot \begin{pmatrix} V^{\,x} \\ V^{\,y} \\ V^{\,xy} \end{pmatrix}$$

numerical implementation in ground segment

69 antennas
full polarisation
(**J** ~ 1.3 Gbytes)

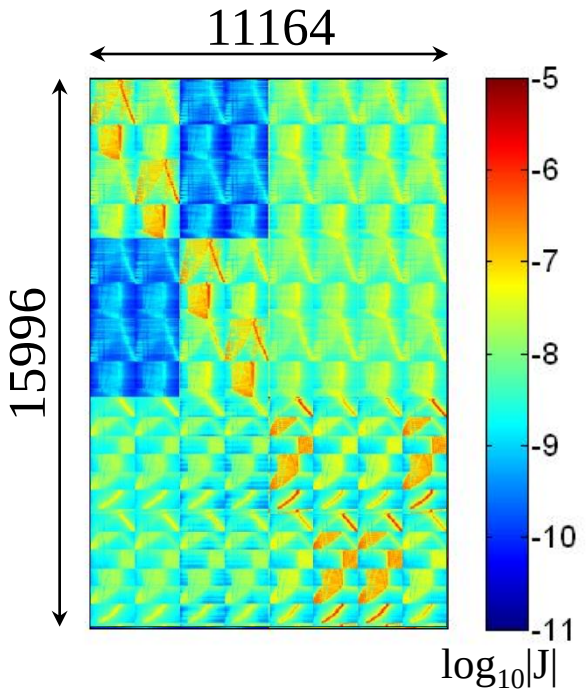

Illustrations & performances

❖ *Instrument modeling matrix:* ***G***

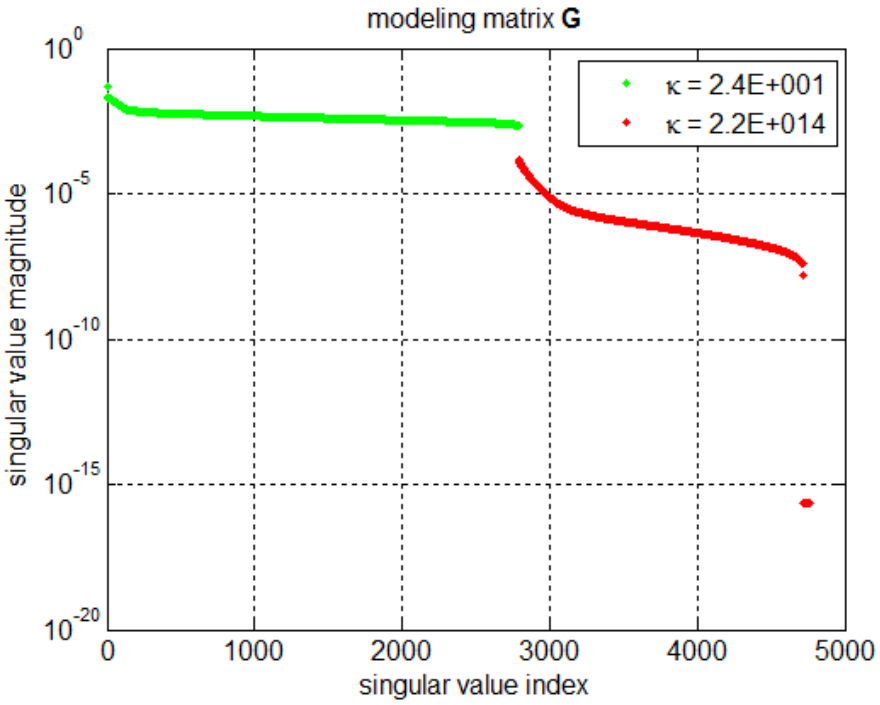

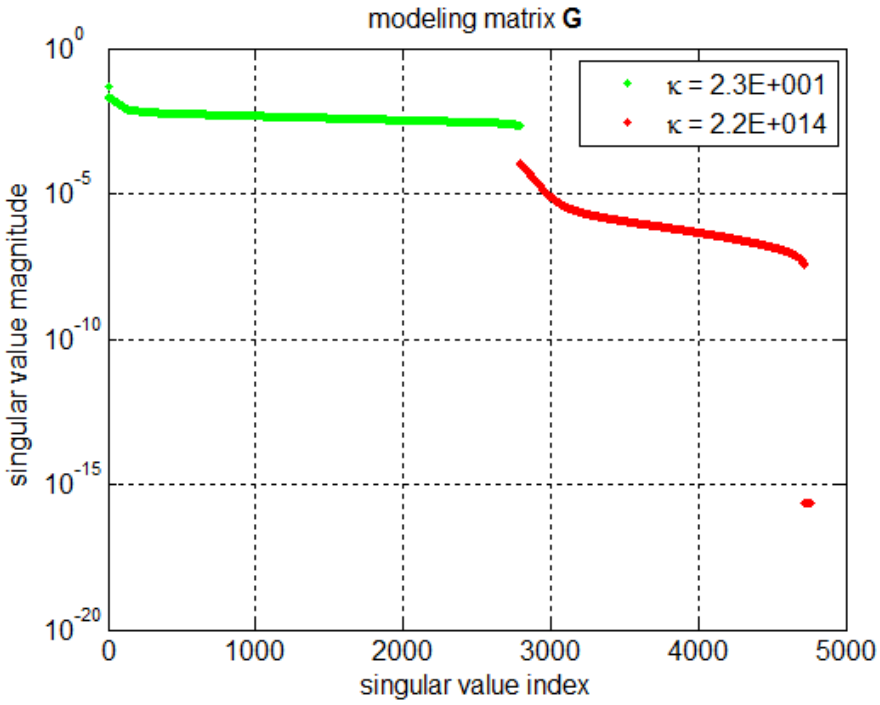

Illustrations & performances

❖ *Regularized modeling matrix: **J***

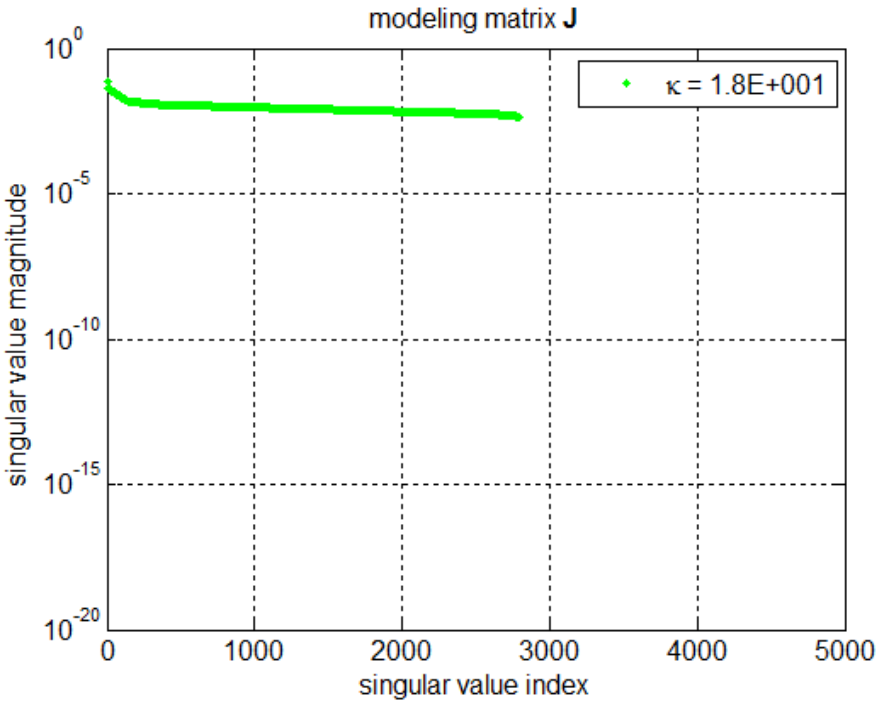

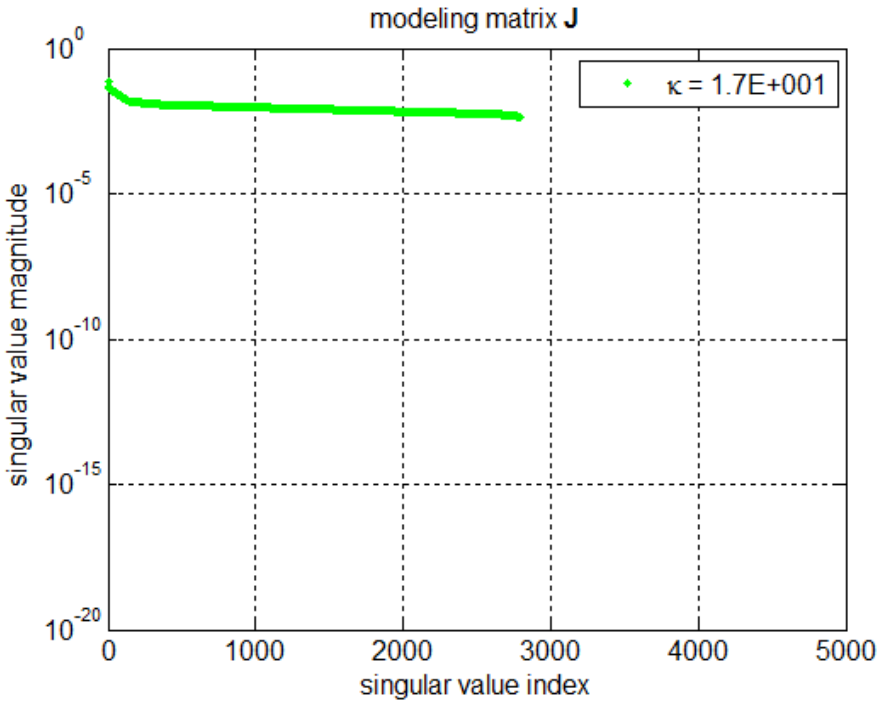

Illustrations & performances

❖ *Noise propagation: $\Delta V = N(0,\sigma^2)$ with $\sigma = 0.01$ K*

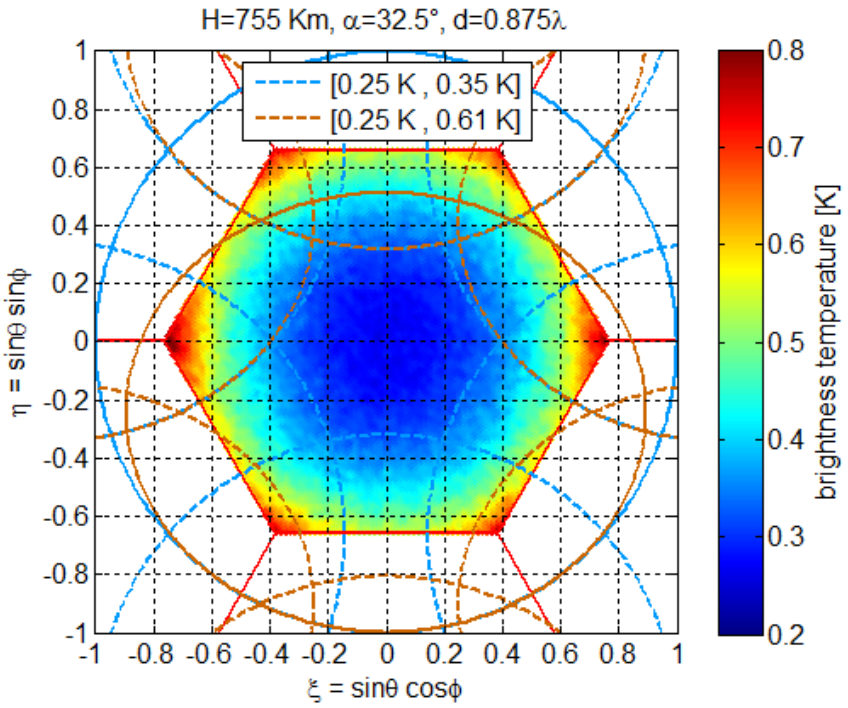

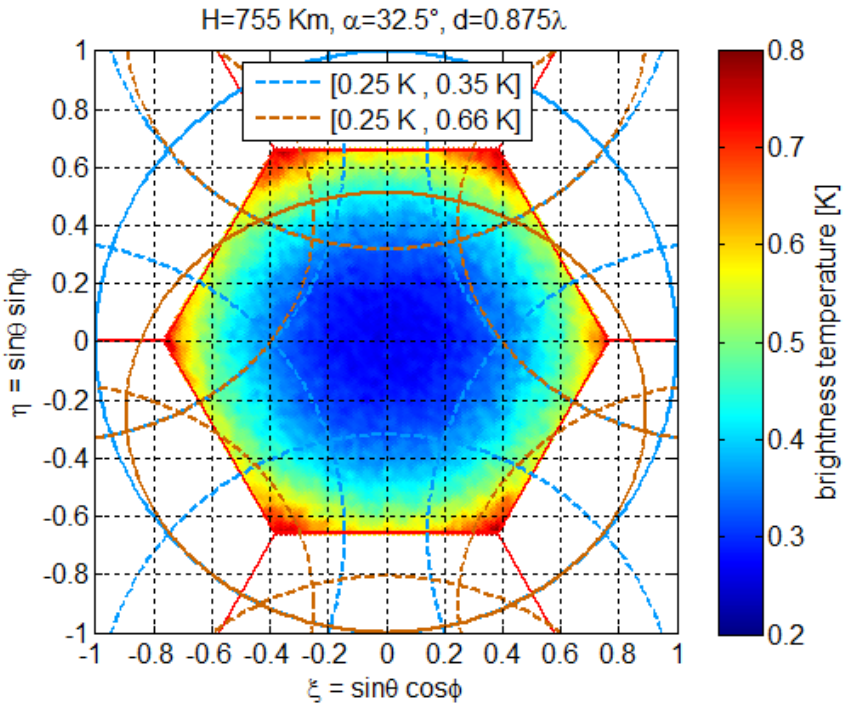

Amplification factor: ×25 (num. simul.)
(boresight) ×25 (radio. theory)

Illustrations & performances

❖ *Noise propagation: $\Delta V = N(0,\sigma^2)$ with $\sigma = 0.01$ K*

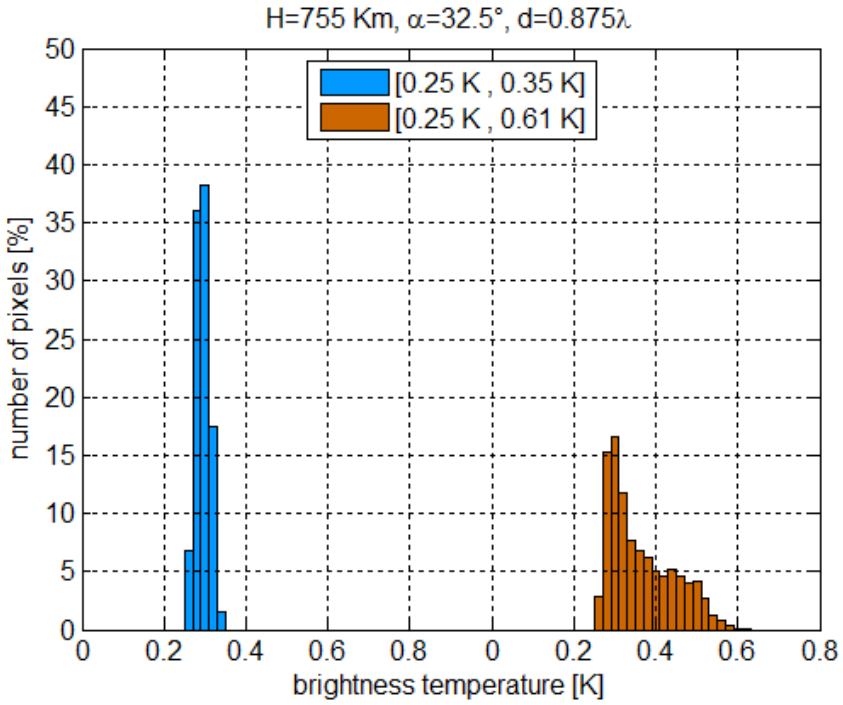

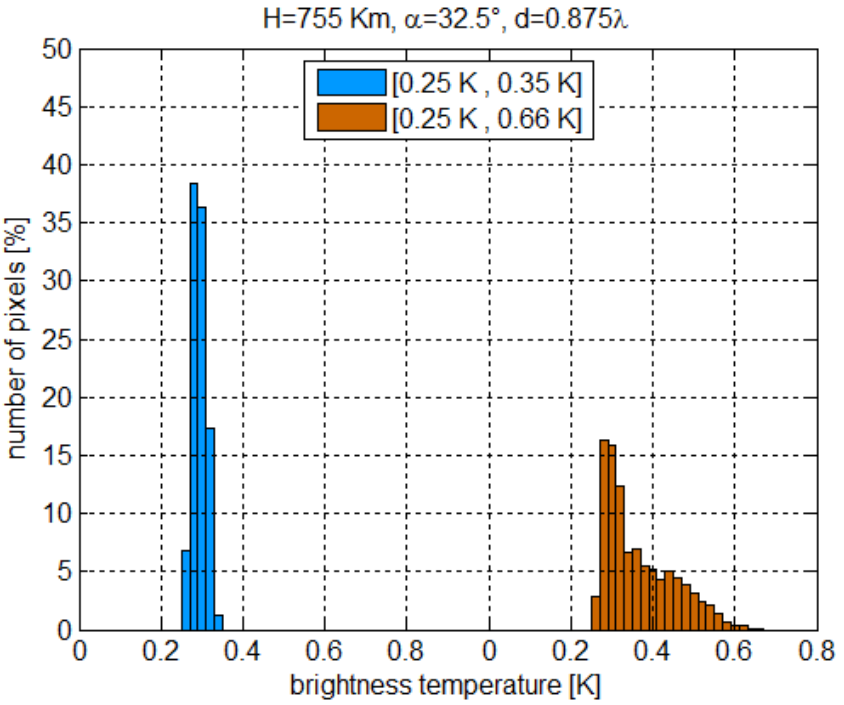

Amplification factor: ×25 (num. simul.)
(boresight) ×25 (radio. theory)

Illustrations & performances

- *Observed scene: H & V*

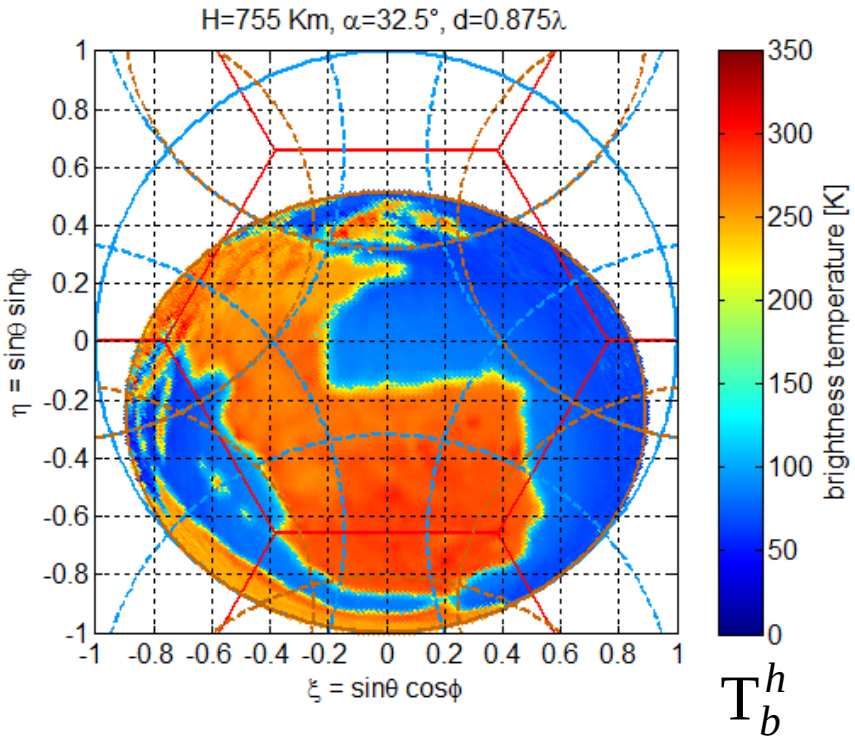

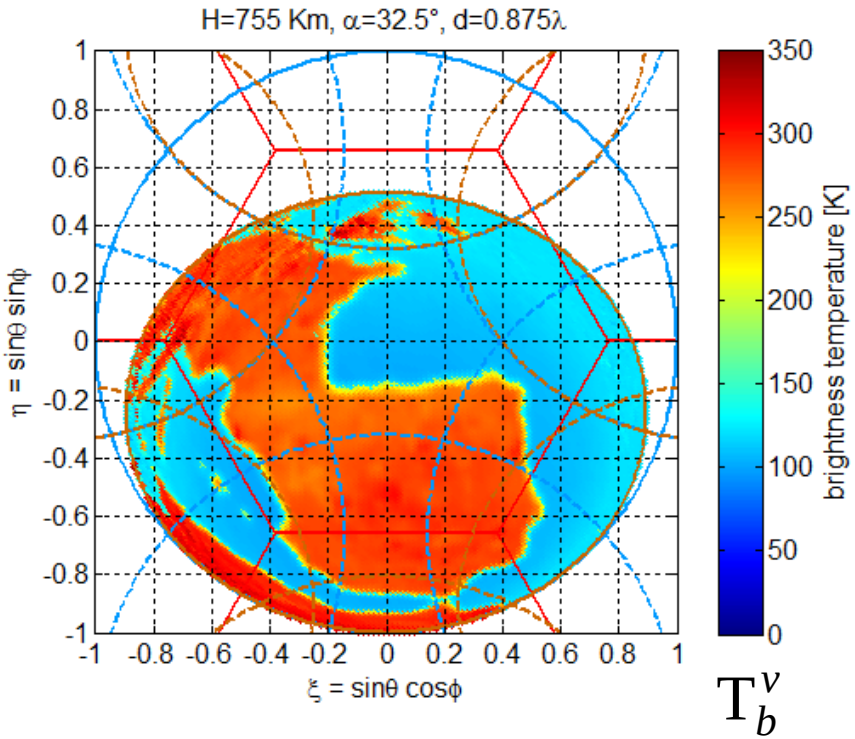

Illustrations & performances

- *Observed scene: X & Y*

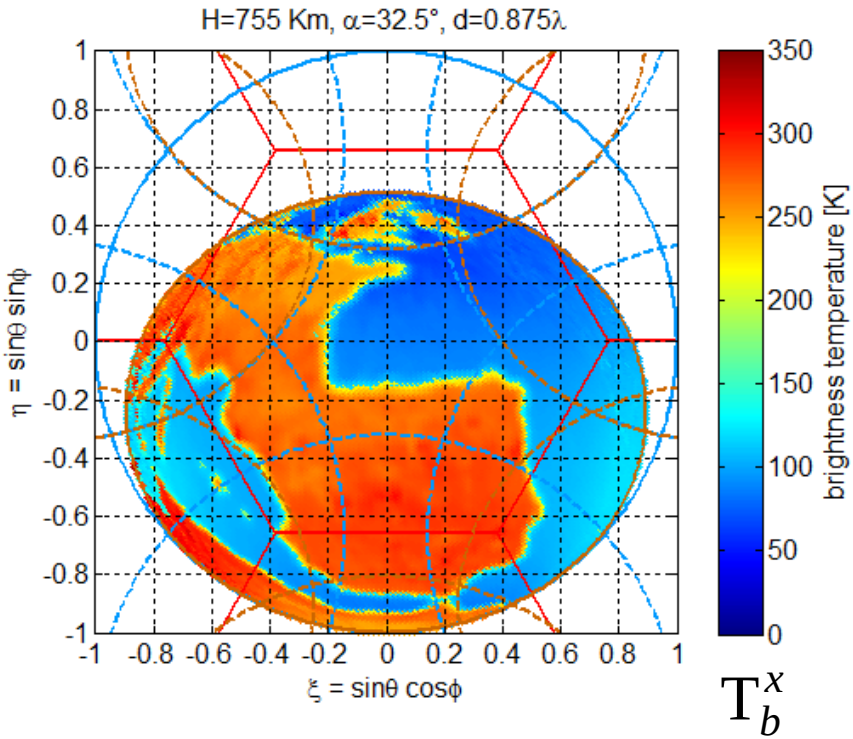

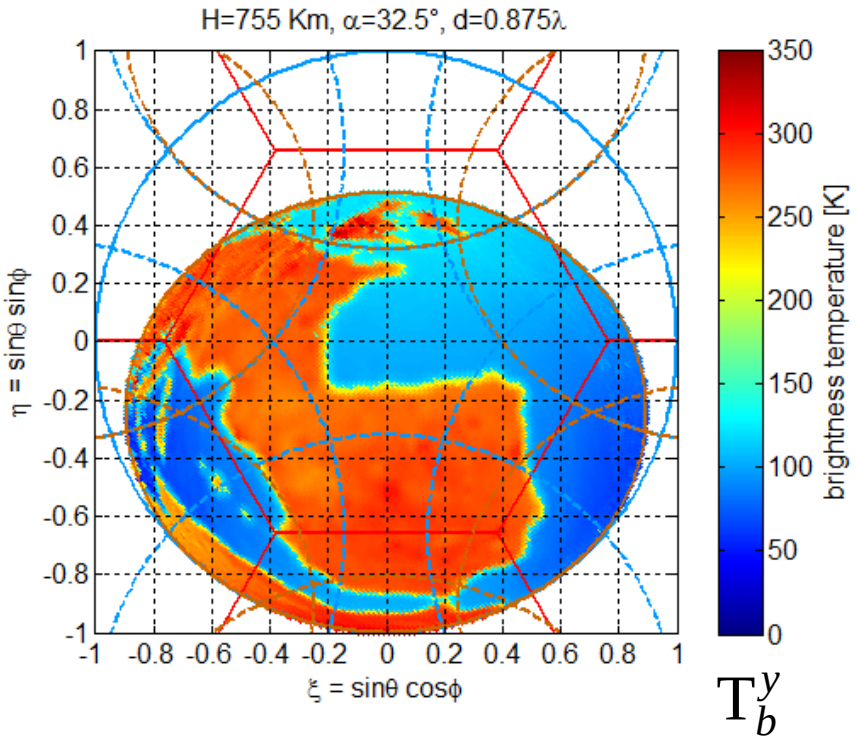

Illustrations & performances

❖ *Standard inversion*

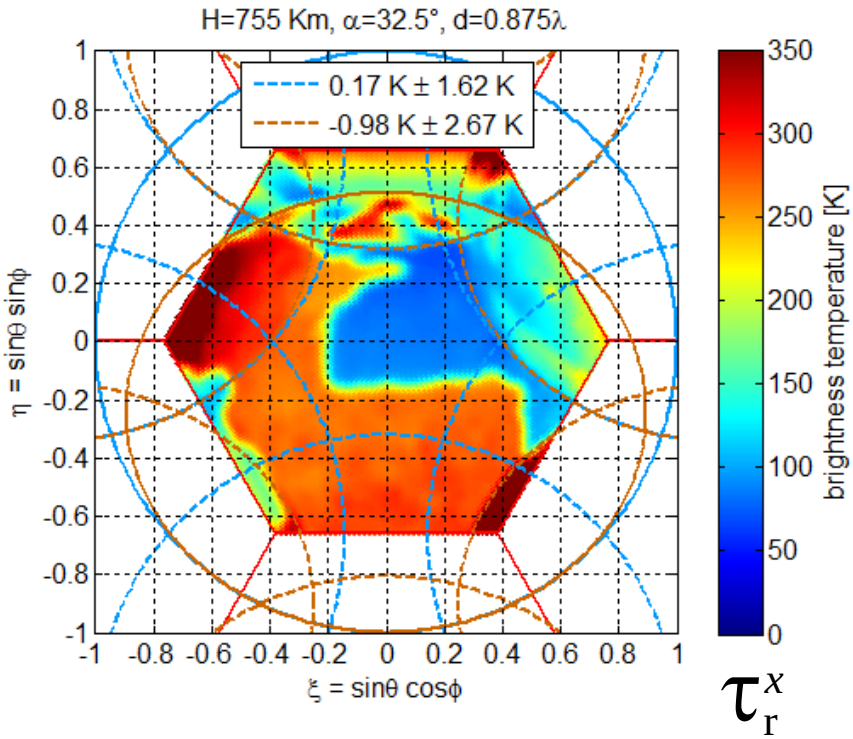

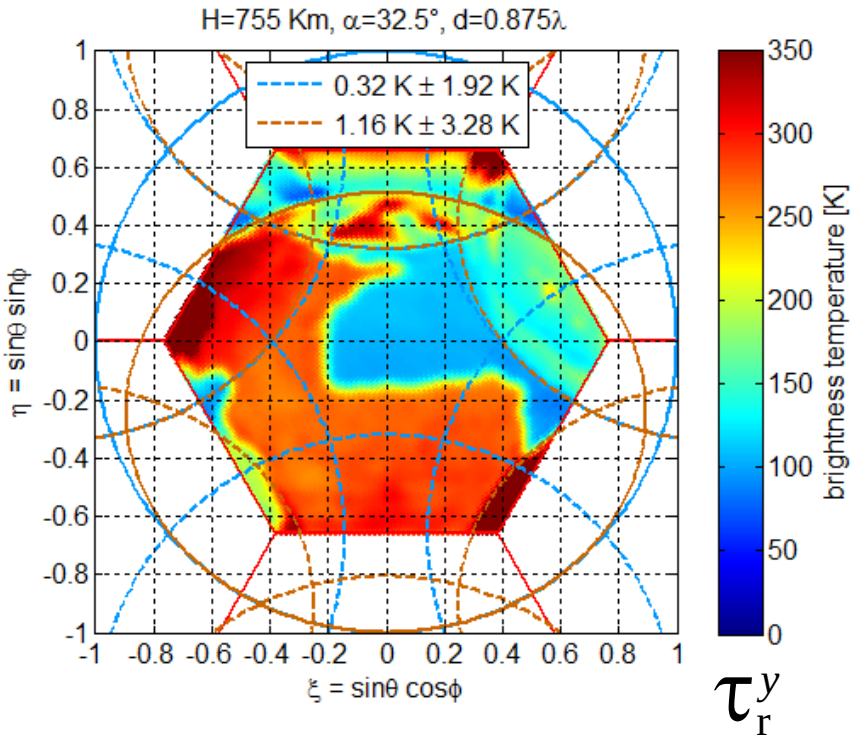

Illustrations & performances

❖ *Differential inversion with $\tilde{T}(t_{sky}, t_{earth})$*

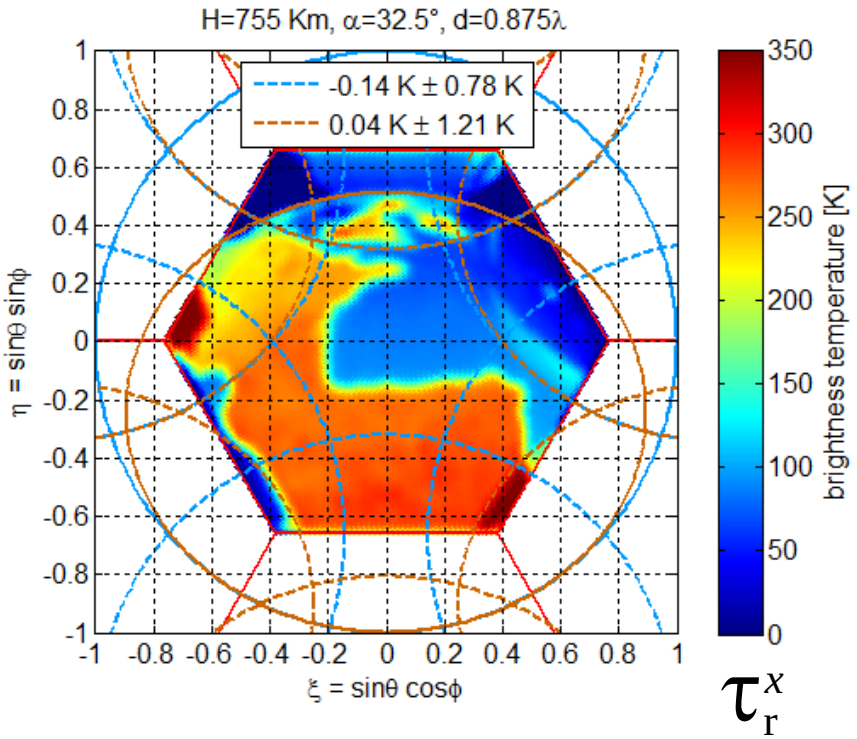

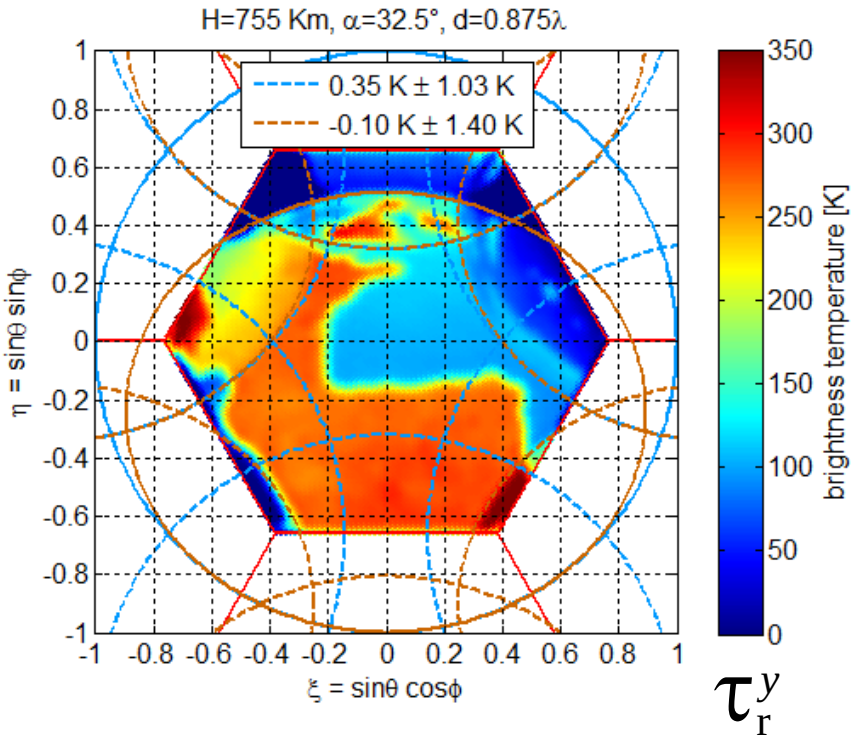

Illustrations & performances

❖ *Differential inversion with* $\tilde{T}(t_{sky}, t_{land}, t_{ocean})$

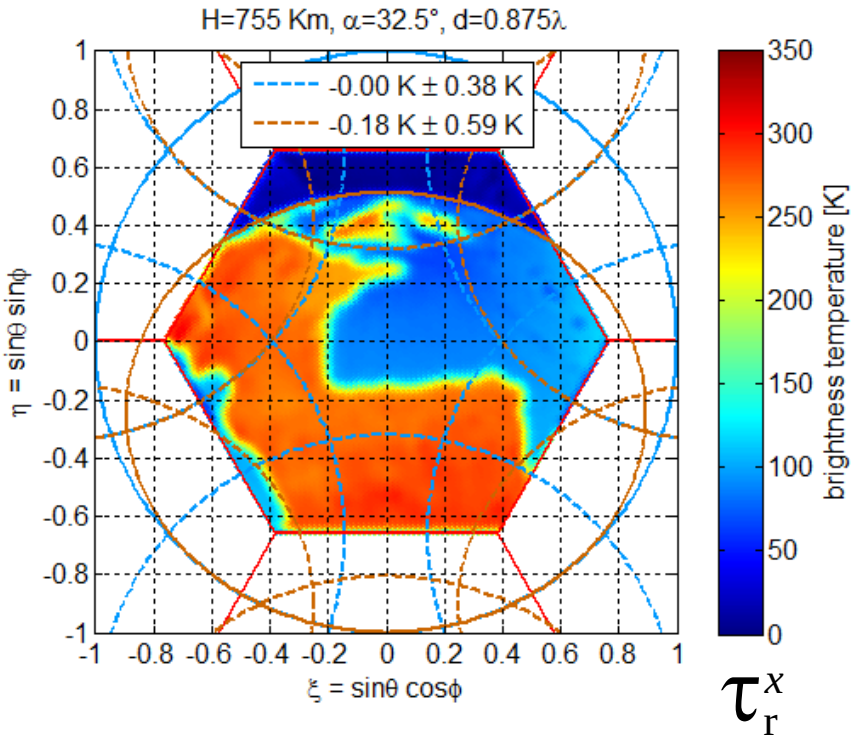

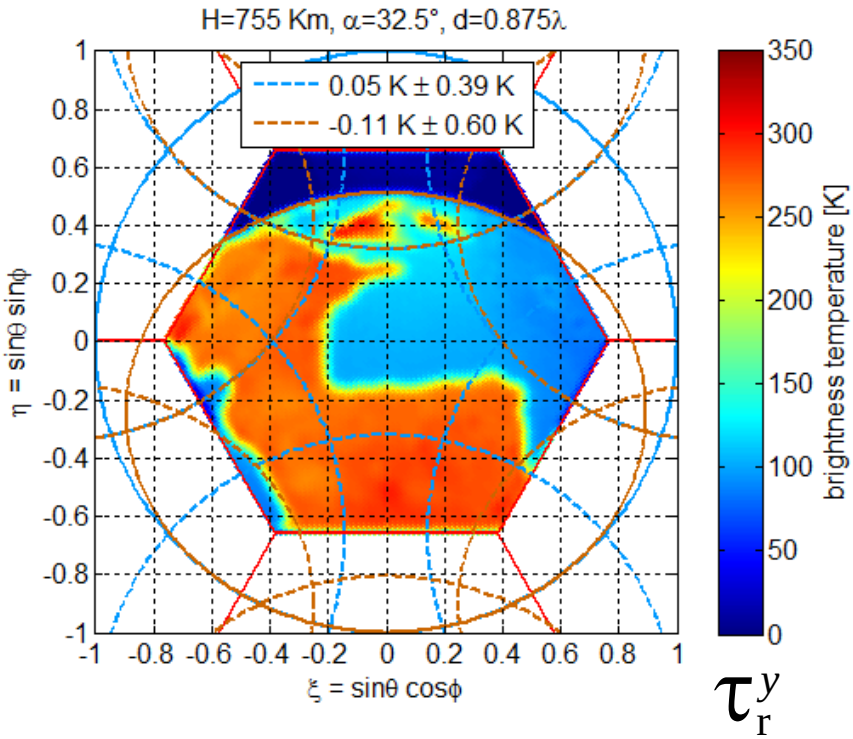

Illustrations & performances

❖ *Standard inversion*

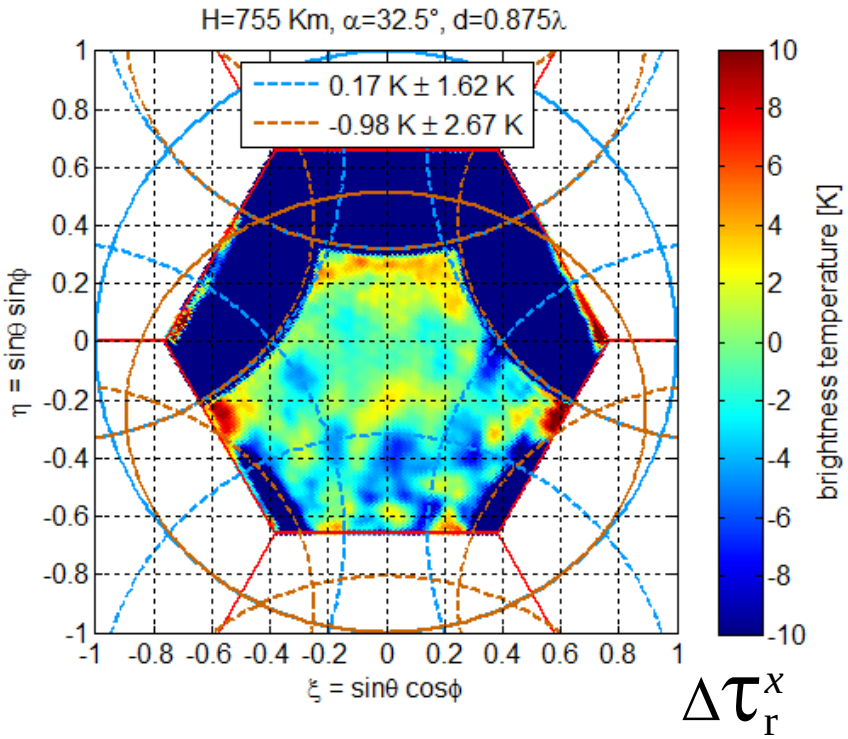

$\Delta\tau_r^x$

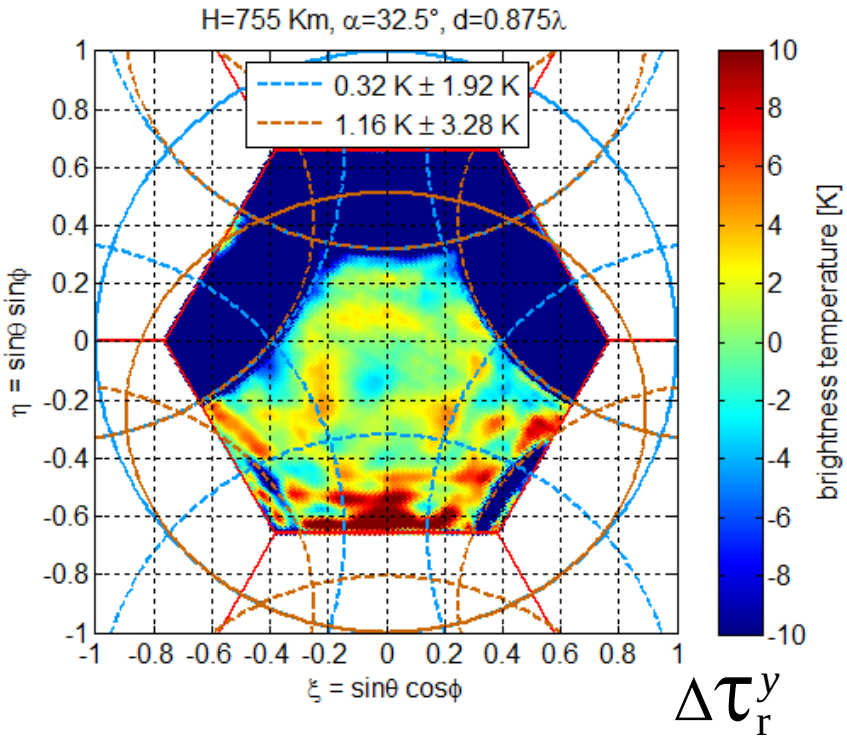

$\Delta\tau_r^y$

Illustrations & performances

❖ *Differential inversion with $\tilde{T}(t_{sky}, t_{earth})$*

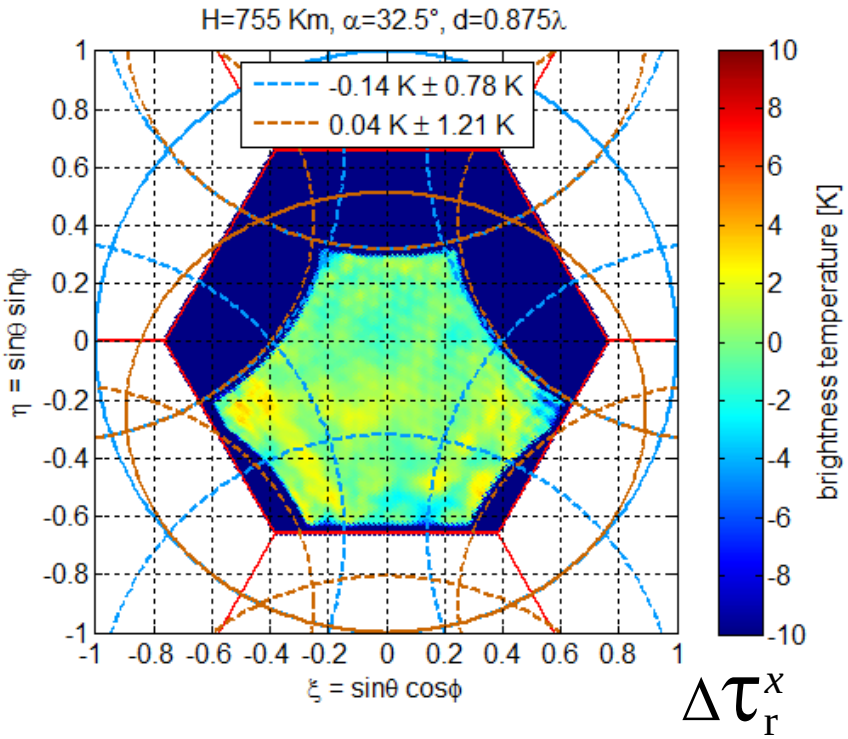

$\Delta\tau_r^x$

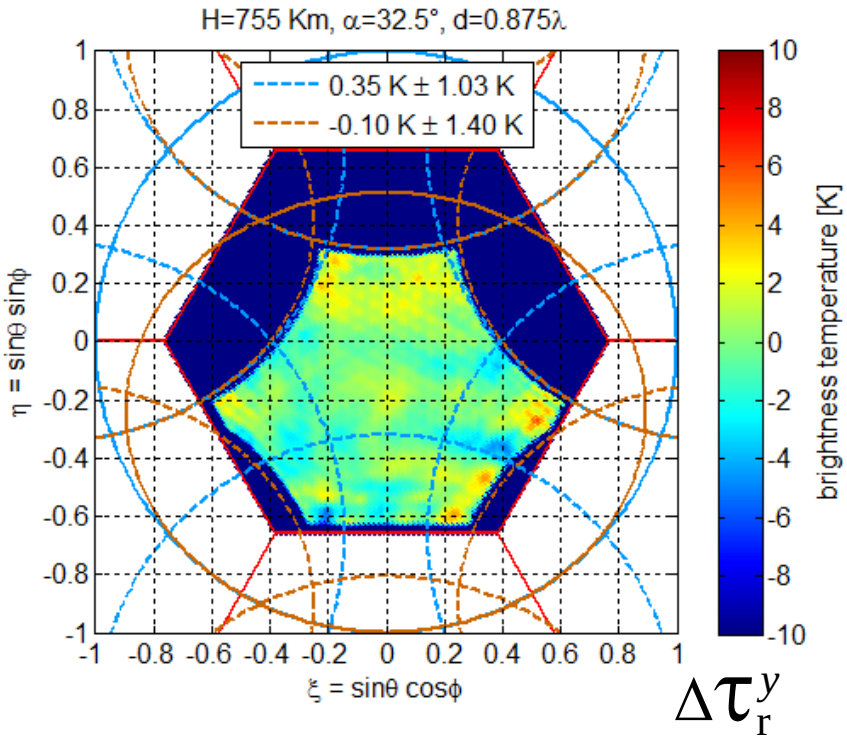

$\Delta\tau_r^y$

Illustrations & performances

- *Differential inversion with $\tilde{T}(t_{sky}, t_{land}, t_{ocean})$*

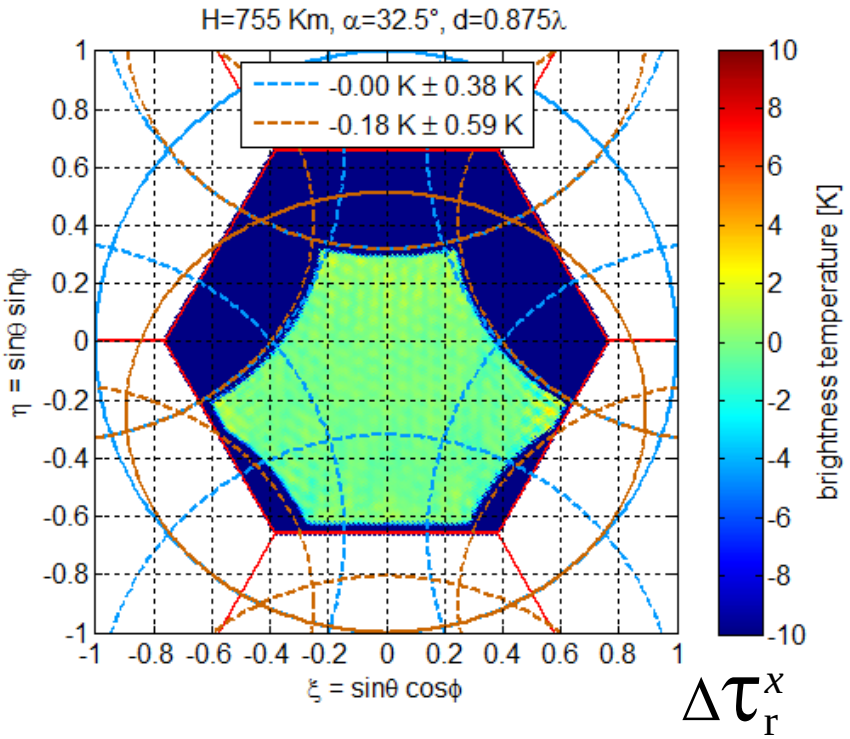

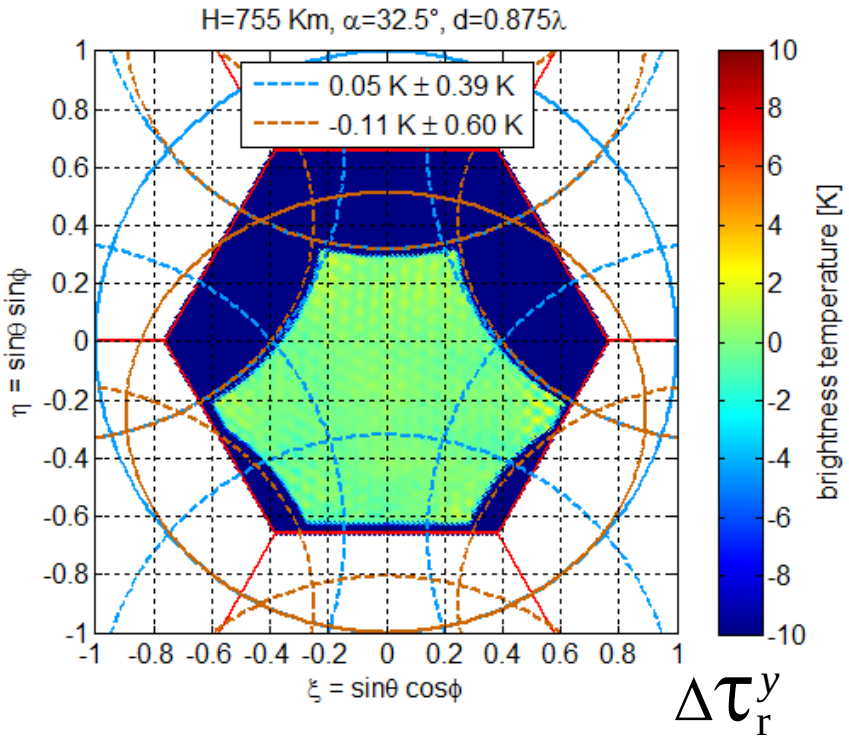

Retour d'expérience de la mission spatiale SMOS au service de la *co-conception* de la future mission SMOS*hr*

2nde partie: SMOS*hr*

The co-design approach

❖ *Participatory design (from Scandinavia)*

Co-design (or co-operative design) is an approach to design attempting to actively involve all stakeholders (e.g. employees, partners, customers, citizens, end-users) in the design process to help ensure the result meets their needs and is usable and marketable. All the participants are invited to cooperate during the several stages of an innovation process.

The co-design approach

❖ *Co-design (in scientific instrumention)*

Time consuming end-to-end simulations involving engineers, scientists and end-users actively collaborating are playing an ongoing role for assessing the sensitivity and the robustness of mission performances to driving parameters, to instrument errors and noises as well as to data processing and analysis.

The SMOS*hr* project

❖ *Synthetic Aperture Imaging Radiometer*

➢ protected L band: 1400-1427 MHz

❑ SMOS: launched Nov. 2009
full polarization: H&V not simultaneous
multi-angular: 0-60°
resolution: ~50 Km

❑ SMOShr
full polarization: H&V simultaneously
multi-angular: 0-60°
resolution: ~10 Km

The SMOS*hr* project

❖ *An end-to-end simulator for participatory design*

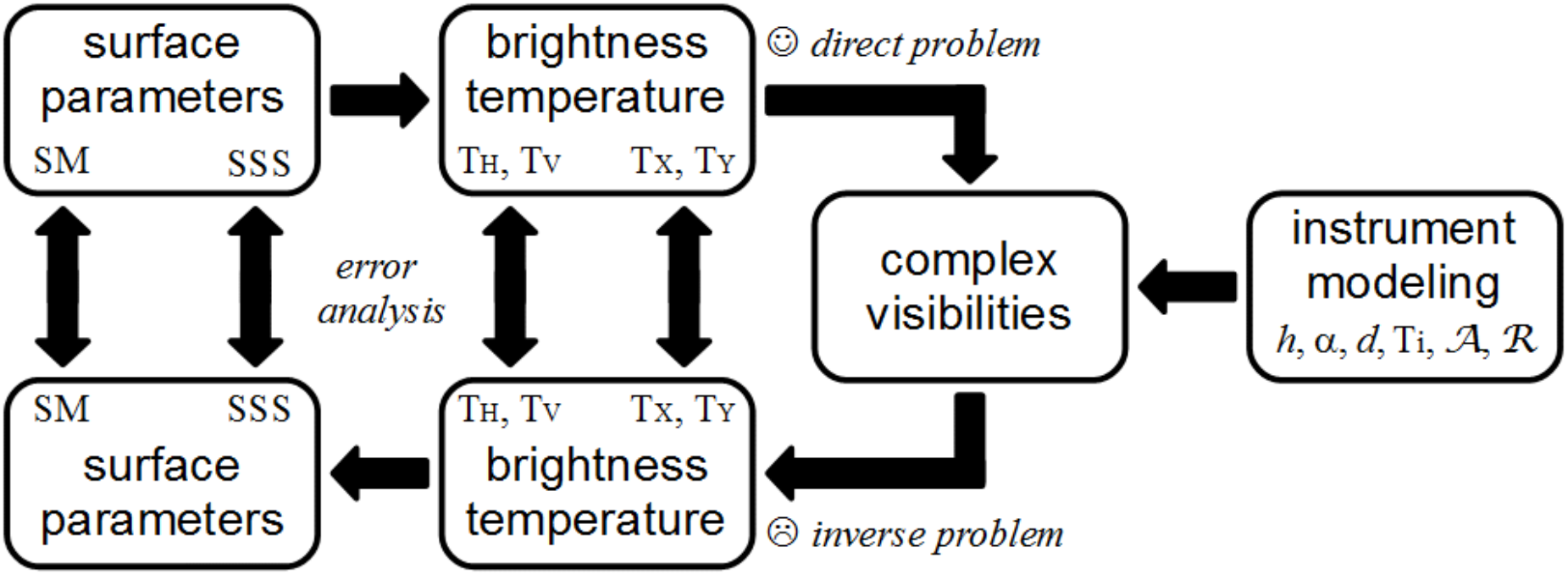

The SMOS*hr* project

❖ *Sampling grids:*

It is known from antiquity that the only regular sampling grids of the 2D Euclidean plane are:

Cartesian grid

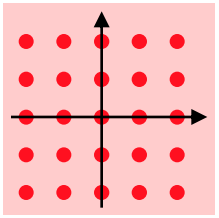

hexagonal grids

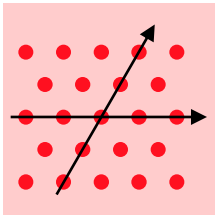

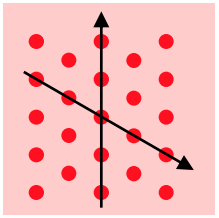

In aperture synthesis, these grids are derived from the (auto-correlation of the) spatial distribution of the antennas of an interferometric array.

The SMOS*hr* project

❖ *Antennas distribution:*

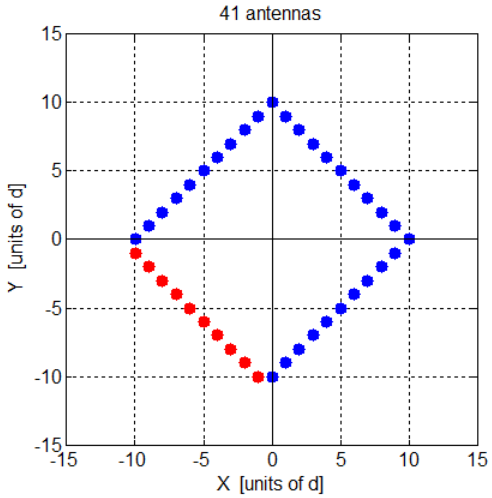

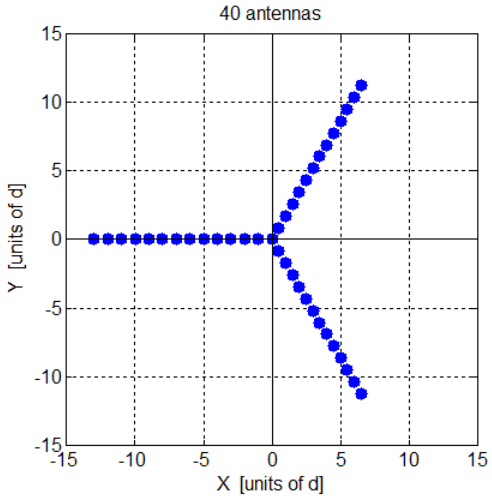

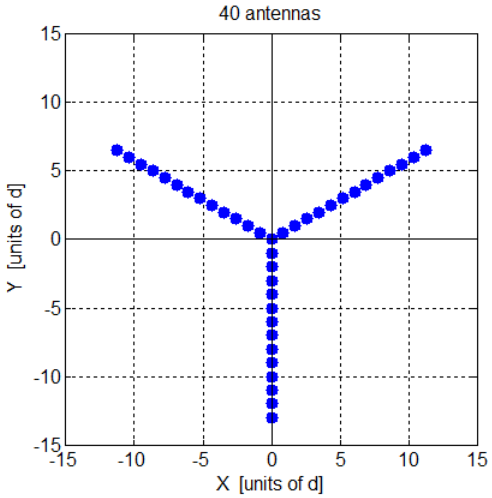

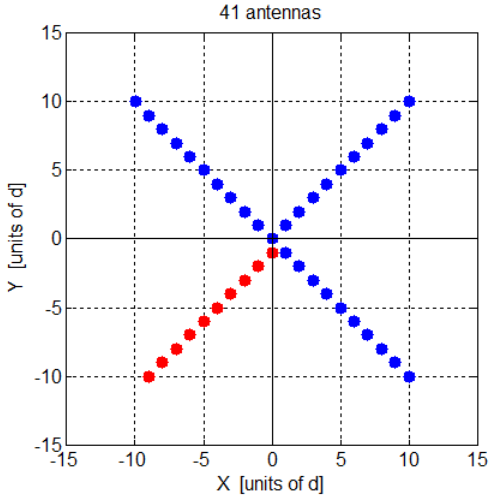

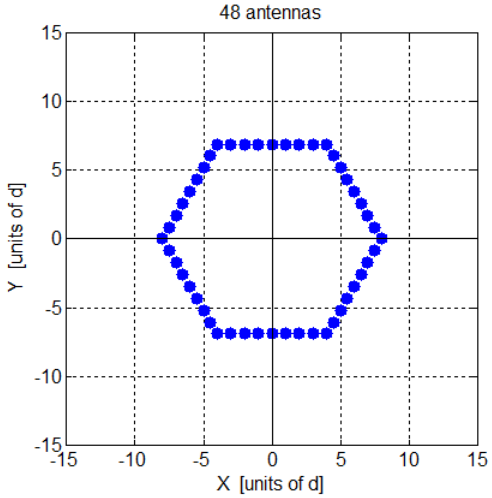

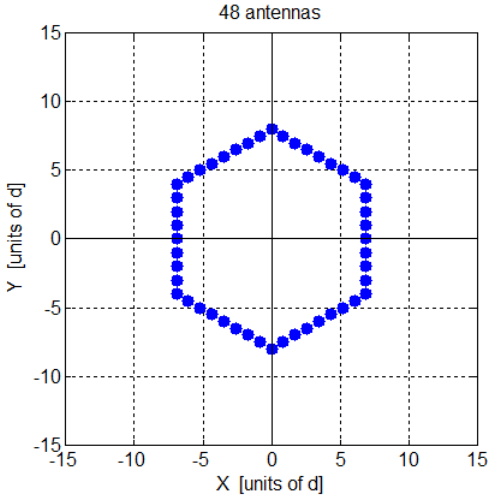

The SMOS*hr* project

- *Frequency coverage:*

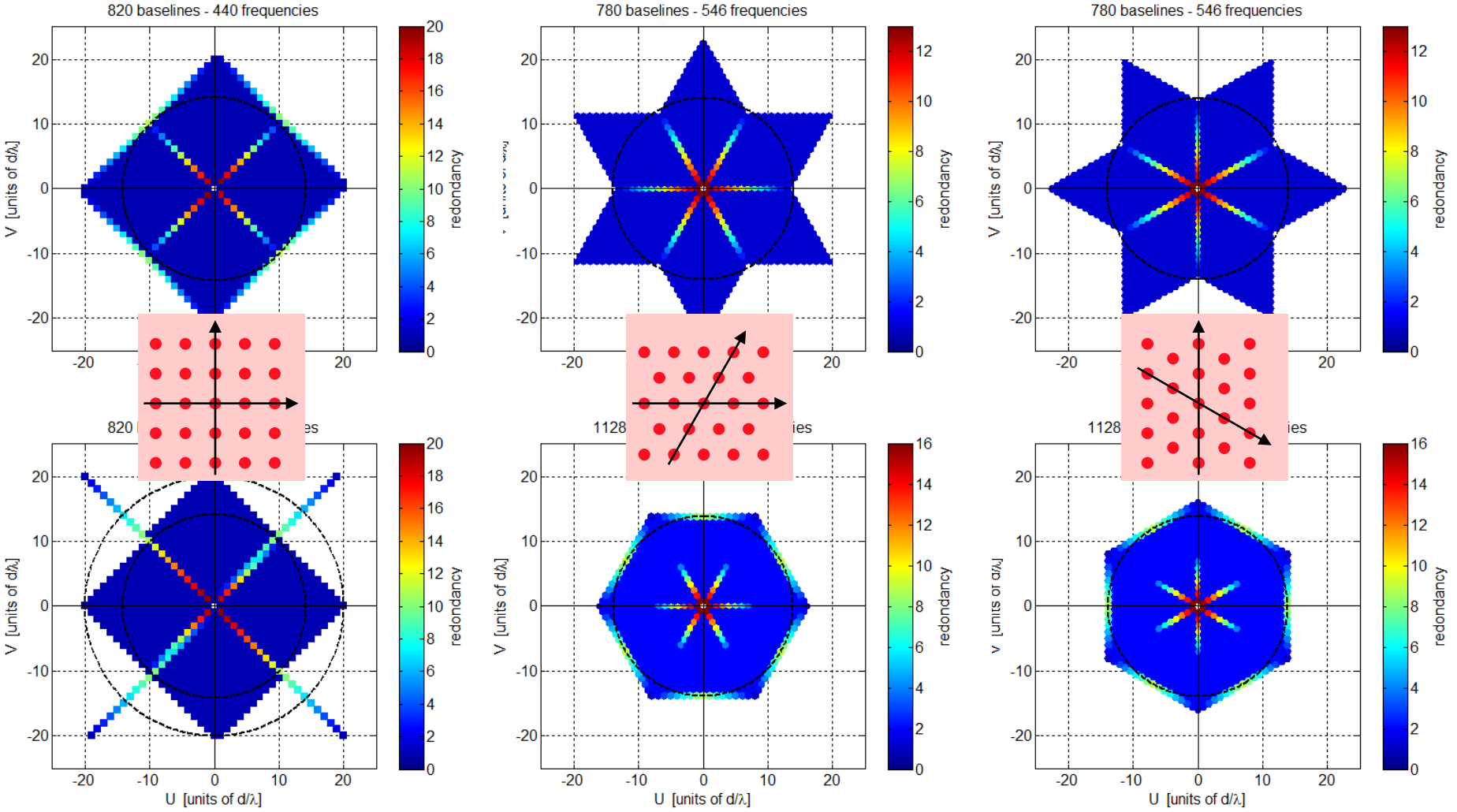

The SMOS*hr* project

- *RSC fails: additional antennas needed*

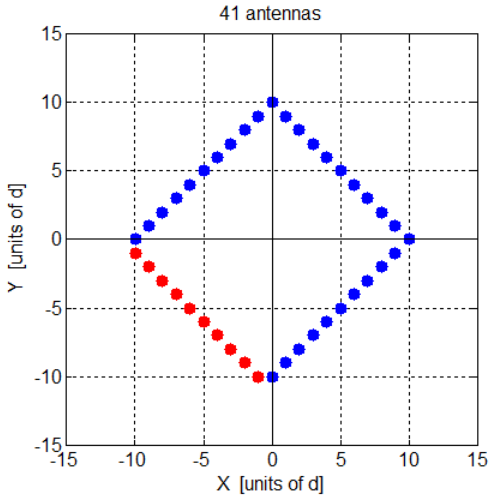

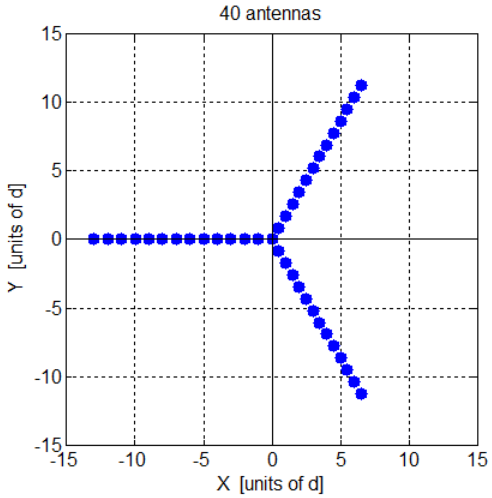

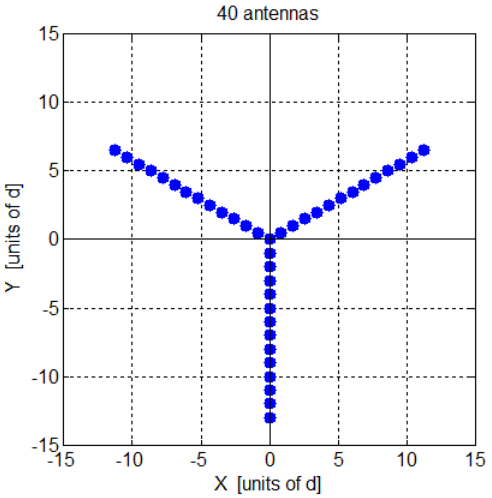

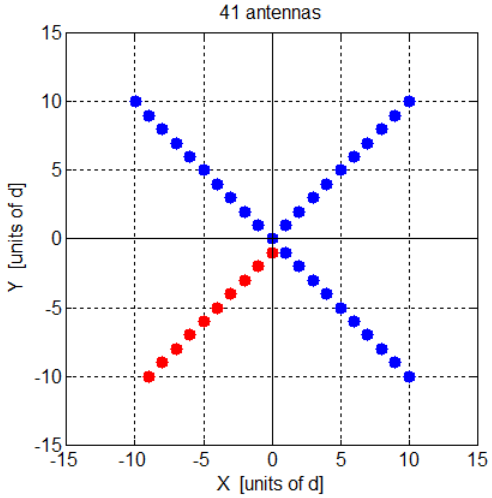

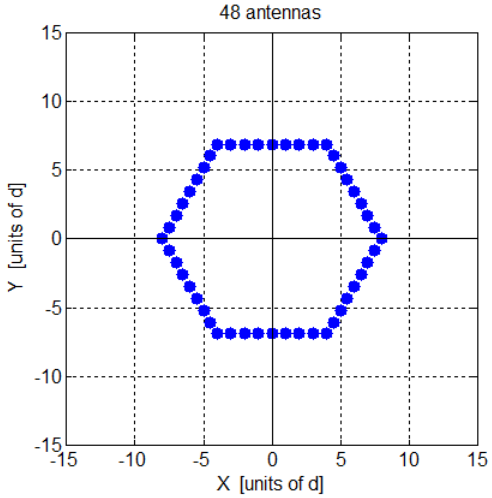

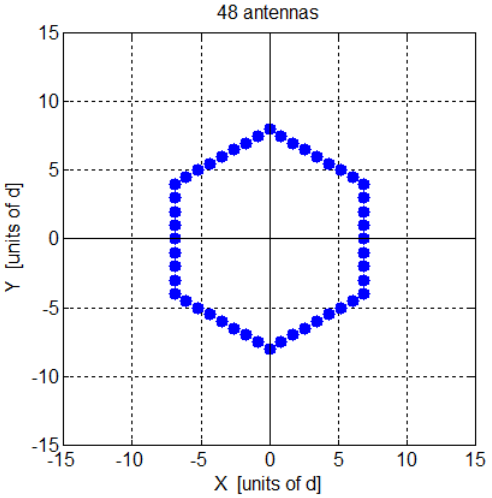

The SMOS*hr* project

- *RSC succeeds: full-phase arrays*

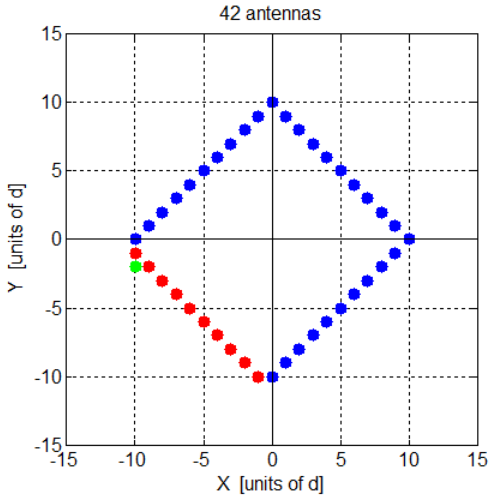

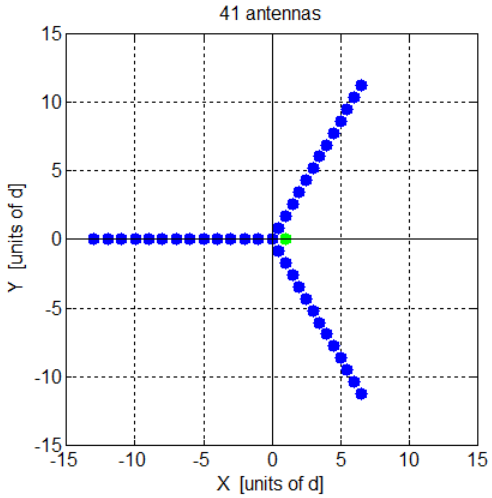

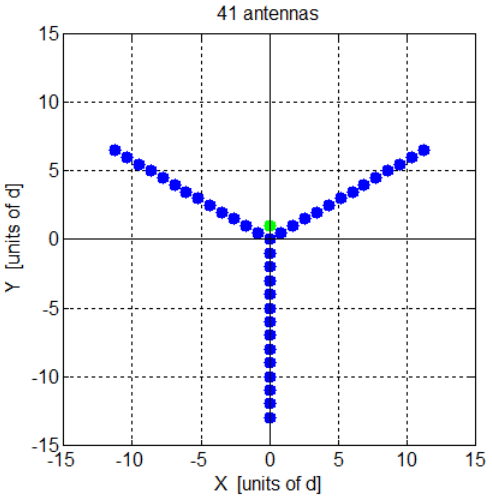

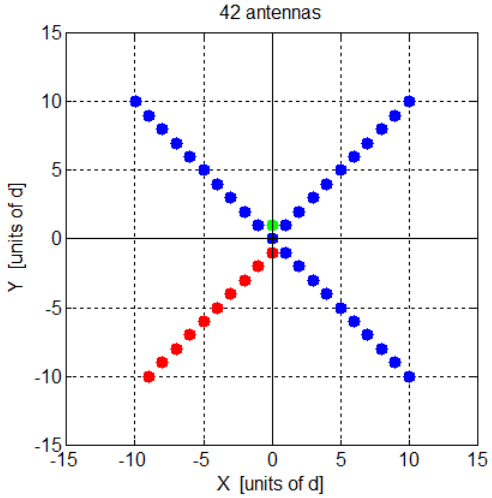

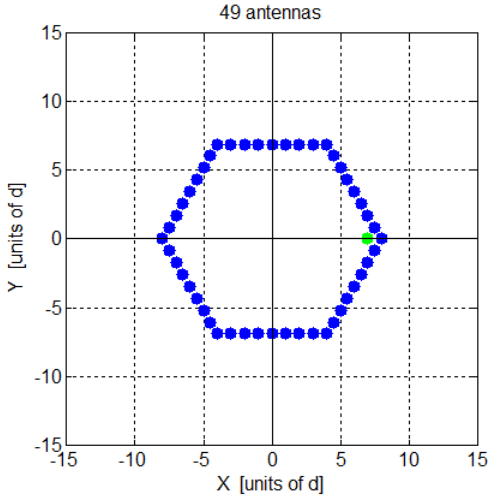

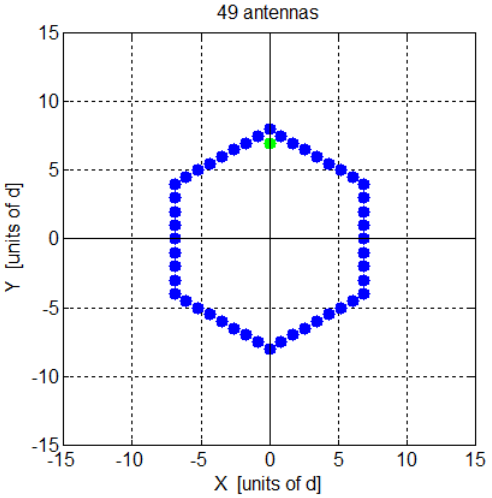

The SMOS*hr* project

- *RSC succeeds: robust full-phase arrays*

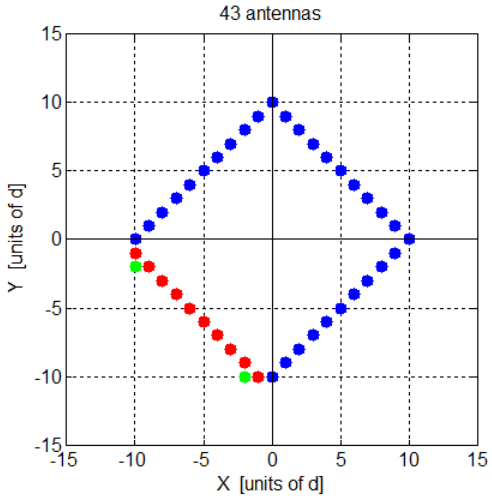

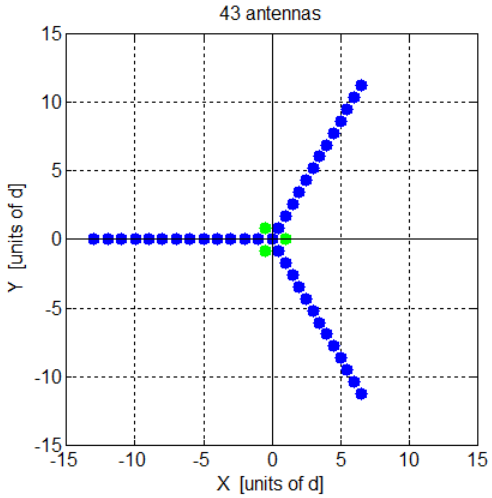

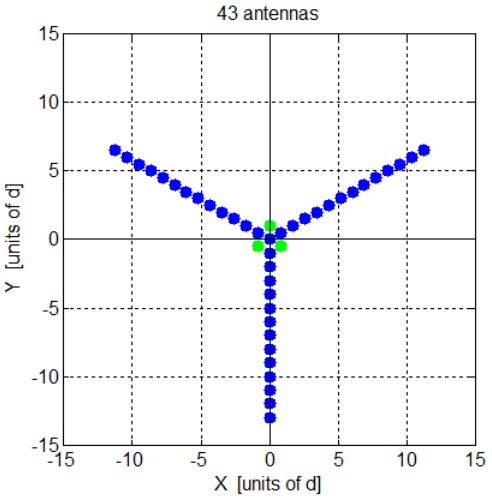

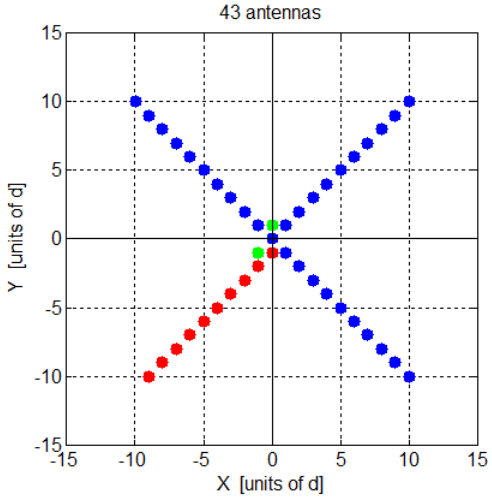

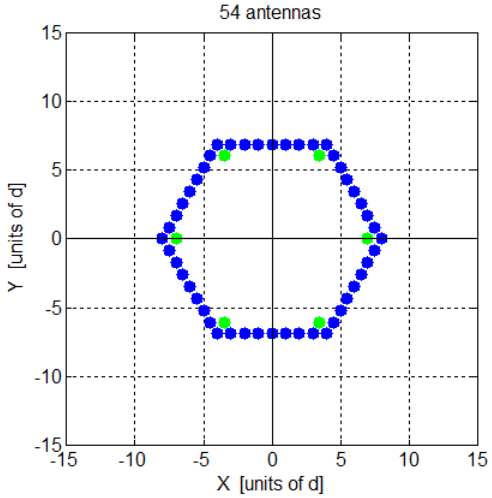

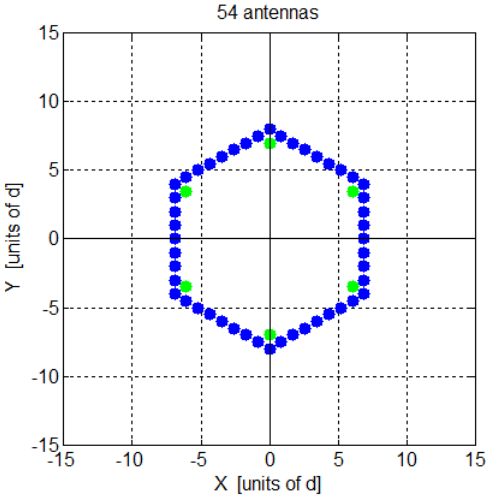

Parameters of the study

❖ *The role played by key parameters:*

- snapshot field of view depends on:
  - array geometry (i.e. sampling grids)
  - antenna spacing $\boldsymbol{d}$
  - plateform tilt α
- snapshot angular resolution is impacted by:
  - arms length $\mathcal{L} = \boldsymbol{P}\boldsymbol{d}$
- snapshot radiometric accuracy is impacted by:
  - collecting area $\mathcal{A} = \boldsymbol{N_a}\,\pi\boldsymbol{d}^2/4$
  - number of baselines $\boldsymbol{N_b} = \boldsymbol{N_a}(\boldsymbol{N_a}-1)/2$

Field of view

- *Earth/Sky aliases, alias-free field of view, swath:*

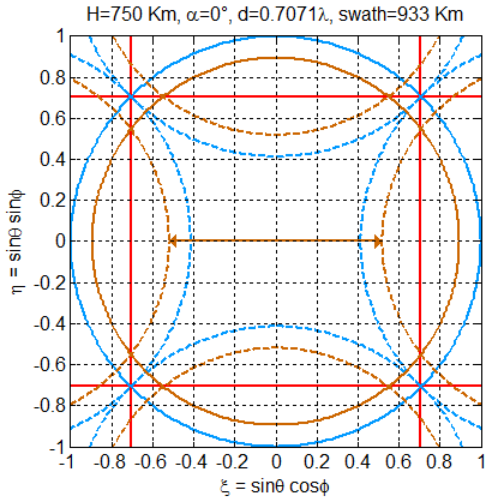

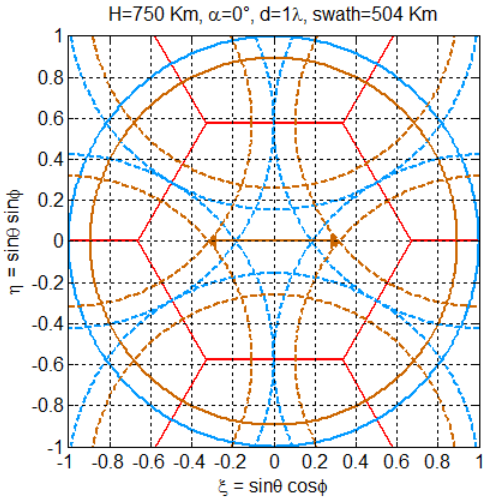

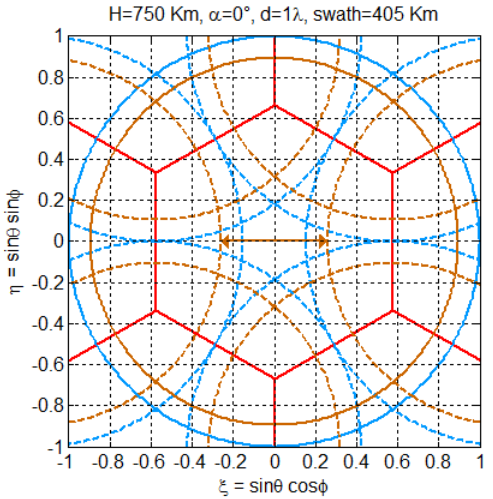

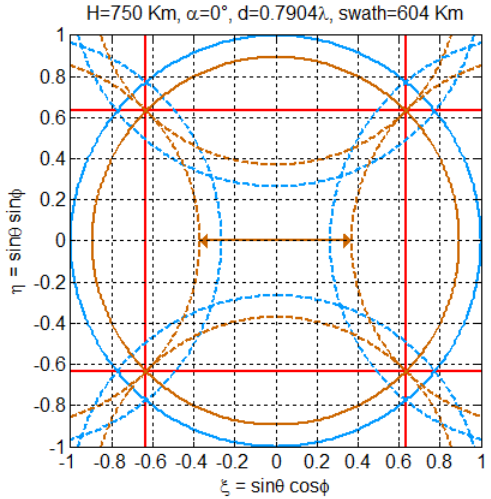

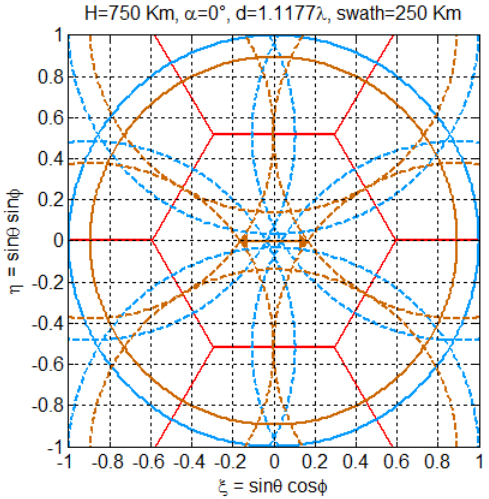

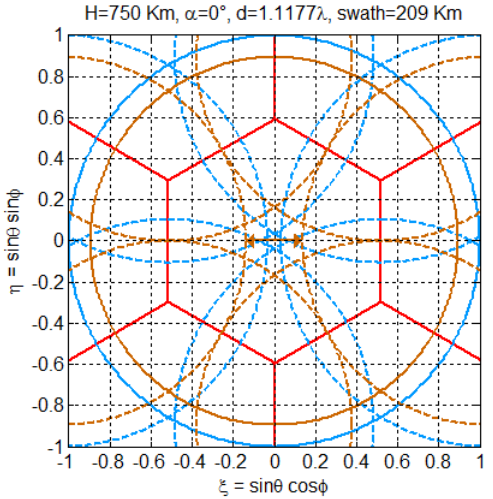

Field of view

- *The role played by array geometry and α:*

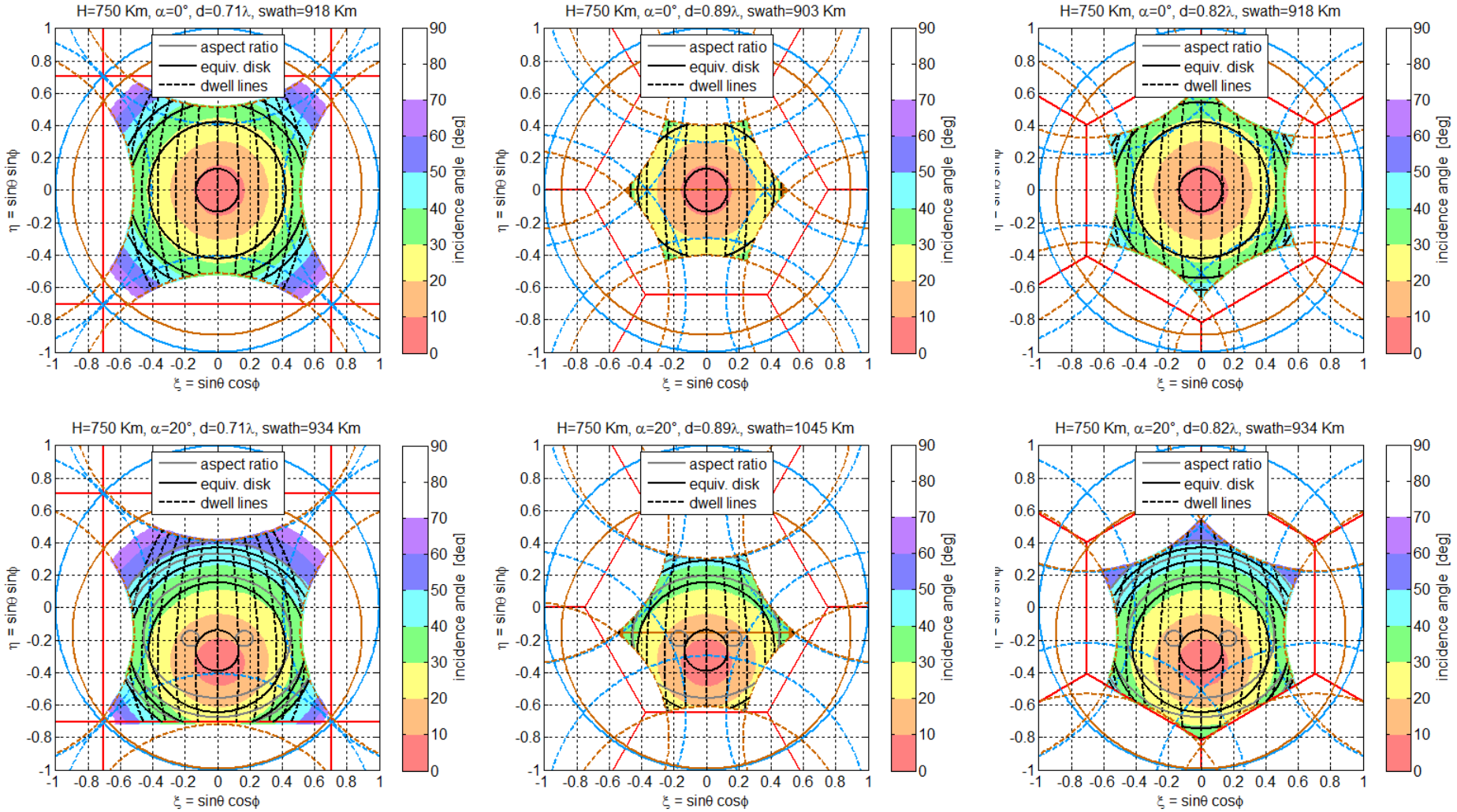

Field of view

- *The role played by array geometry and* ***d****:*

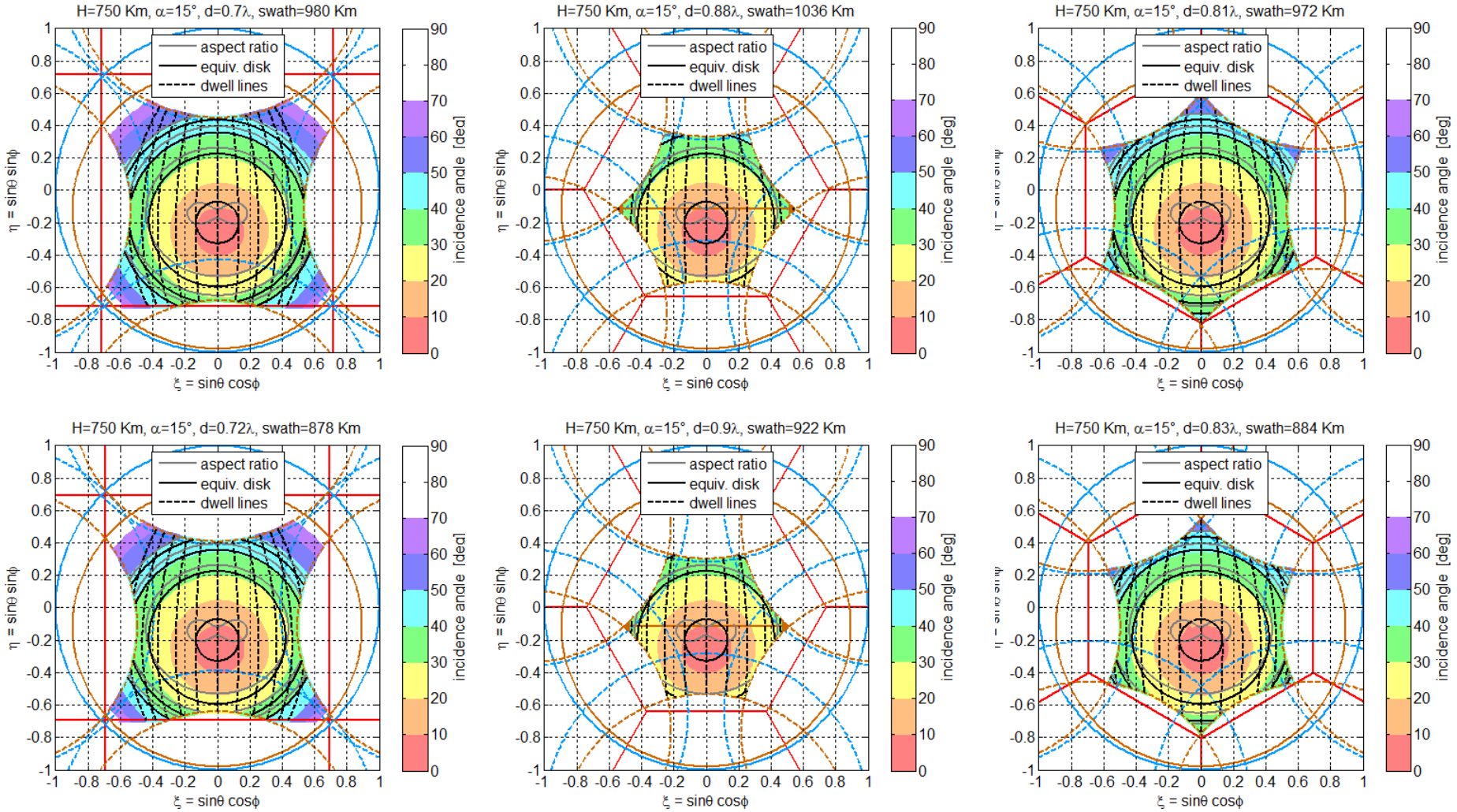

Field of view

- *The role played by array geometry, α and **d** on swath:*

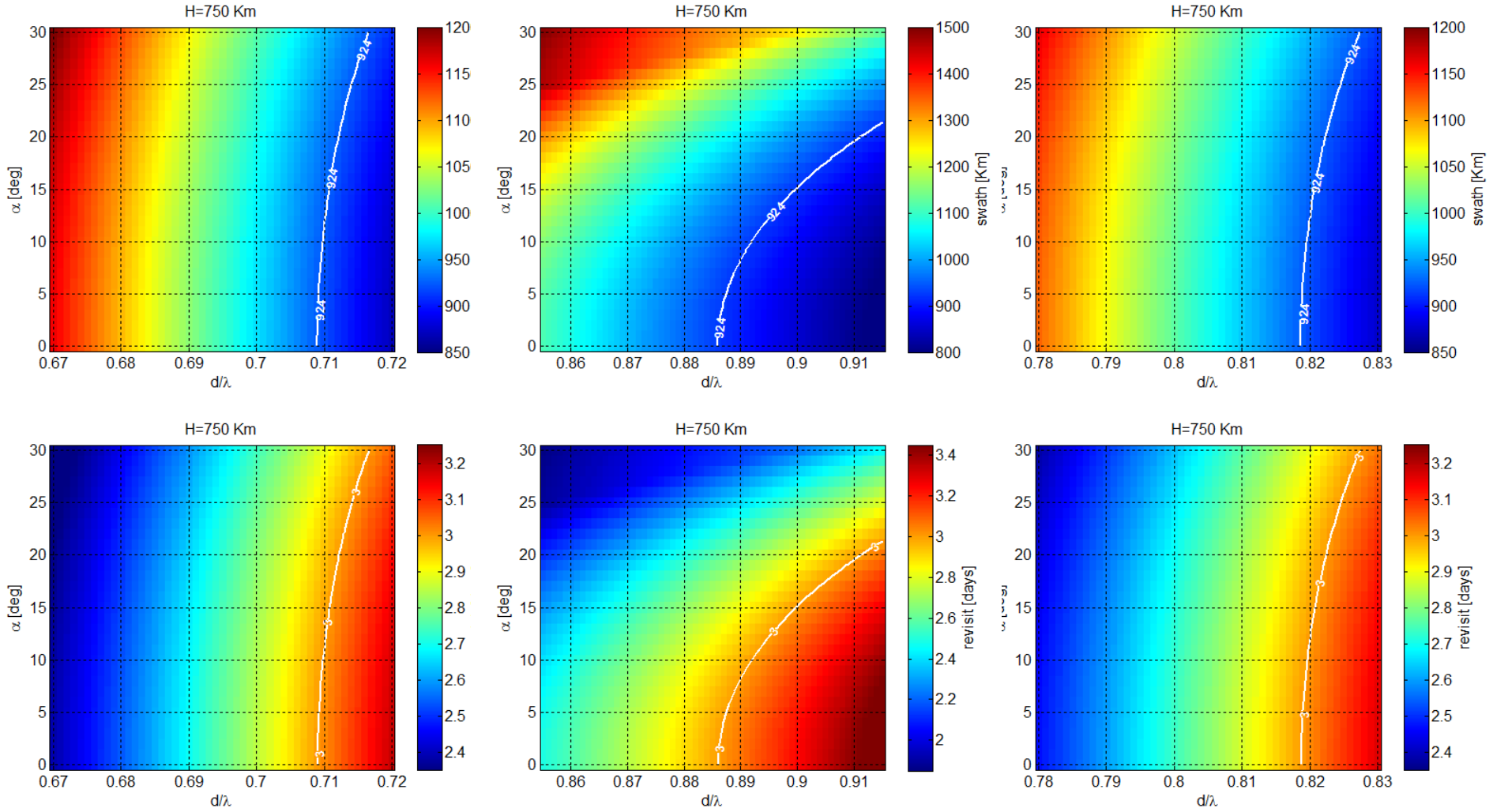

Field of view

❖ *The role played by array geometry, α and **d** on **i**:*

Nadir looking direction **x**
in Earth alias-free FOV

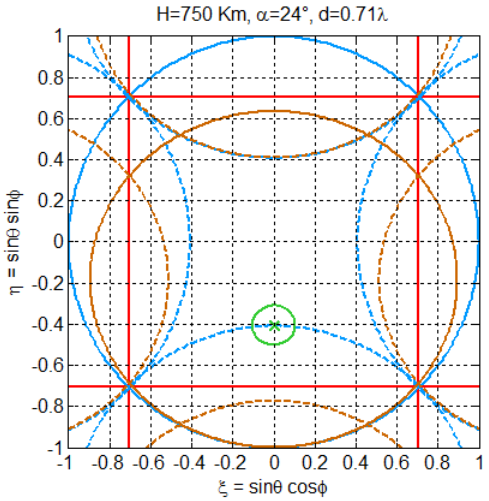

within O $i \leq 6°$

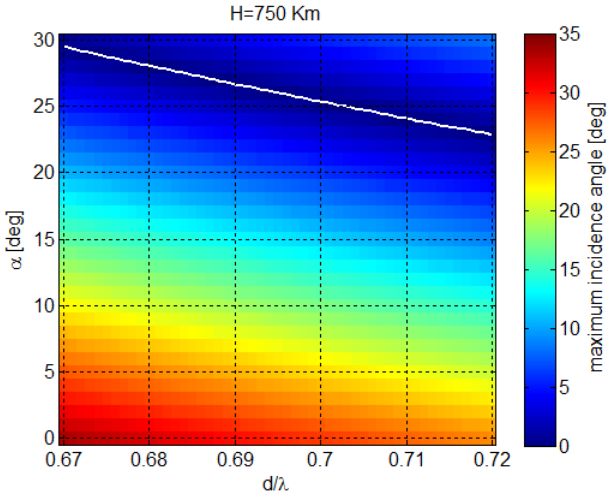

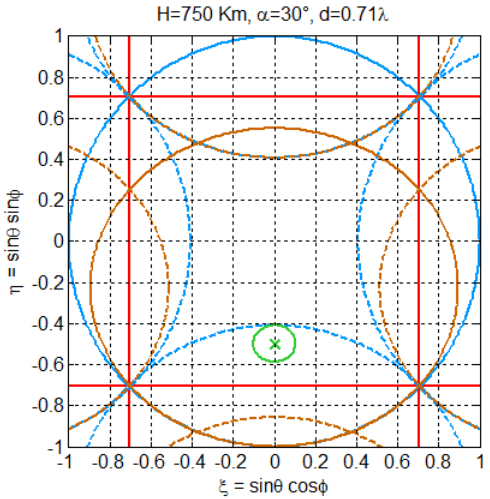

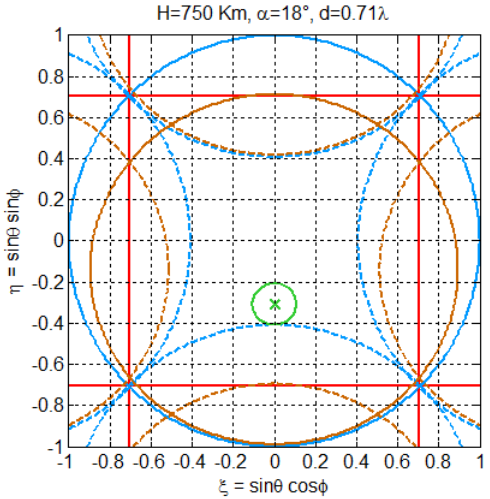

Nadir looking direction **x**
in alias-free FOV

Field of view

❖ *The role played by array geometry, α and **d** on **i**:*

Nadir looking direction **x**
in Earth alias-free FOV

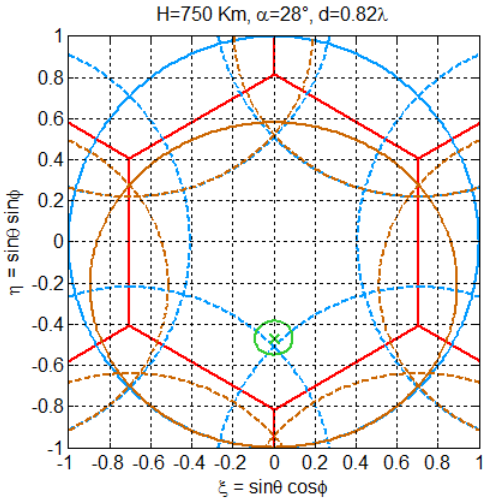

within O $i \leq 6°$

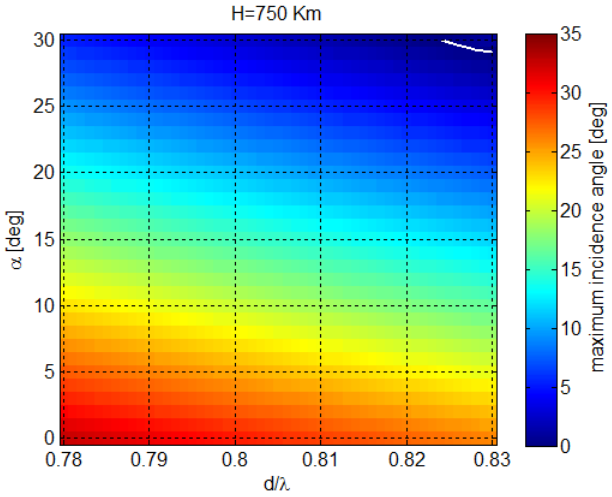

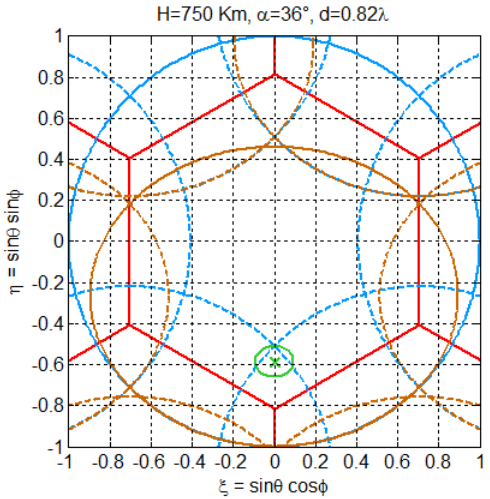

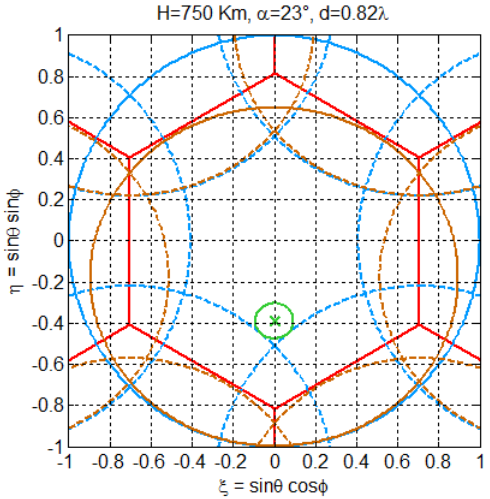

Nadir looking direction **x**
in alias-free FOV

Field of view

❖ *The role played by array geometry, α and **d** on **i**:*

Nadir looking direction **x**
in Earth alias-free FOV

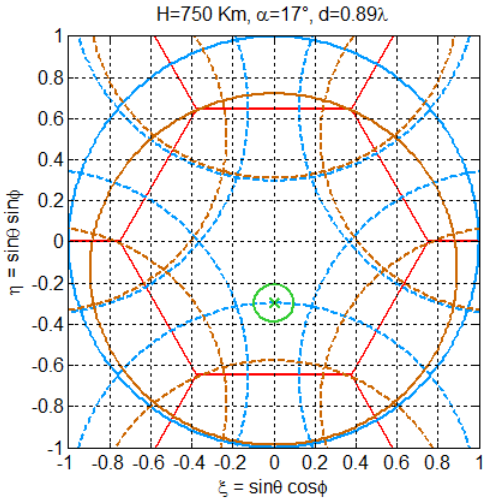

within O $i \leq 6°$

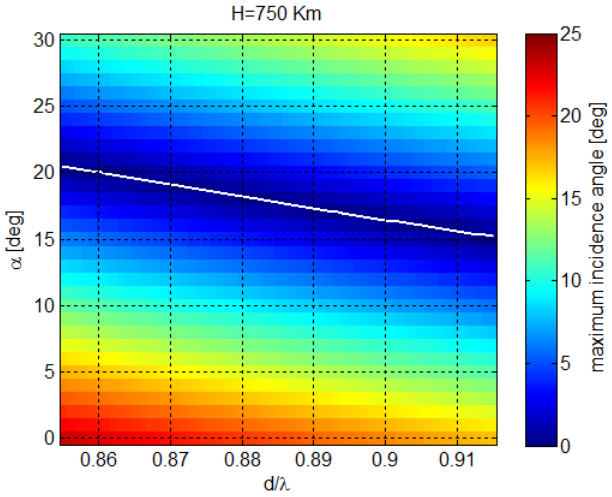

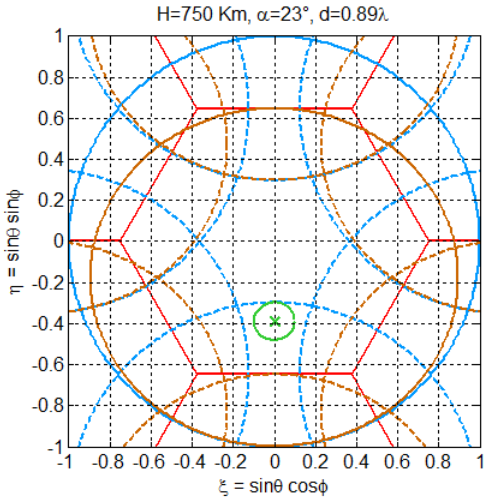

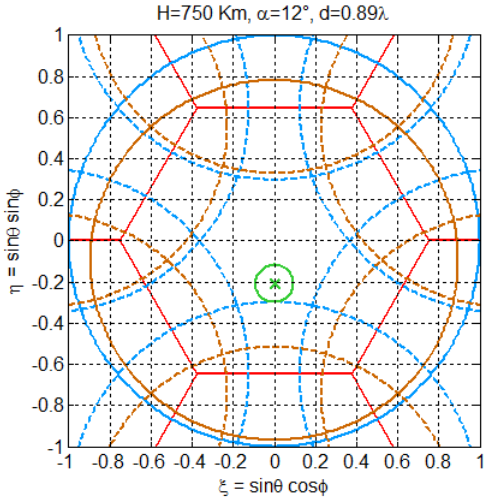

Nadir looking direction **x**
in alias-free FOV

Field of view

❖ *The role played by array geometry, α and **d** on **i**:*

Nadir looking direction **x**
in Earth alias-free FOV

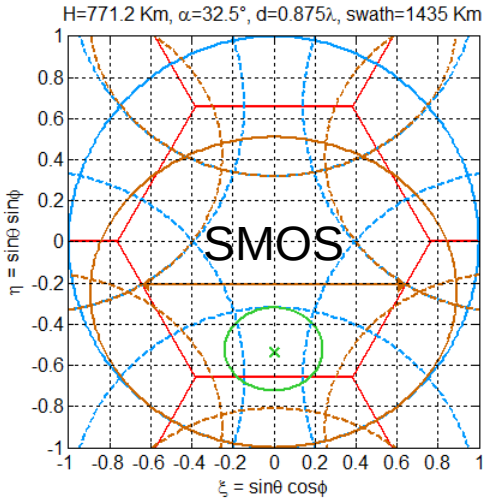

within O $i \leq 16°$

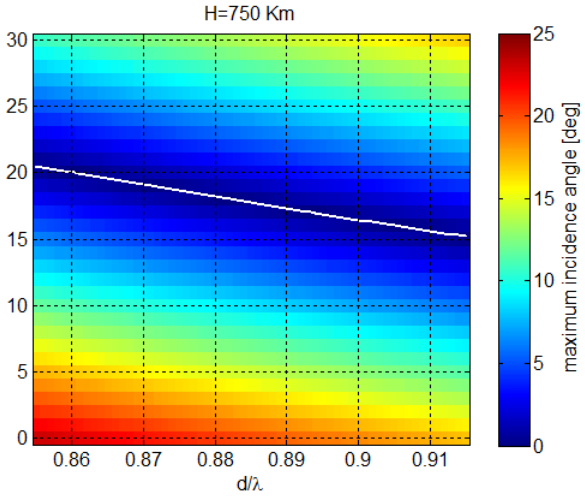

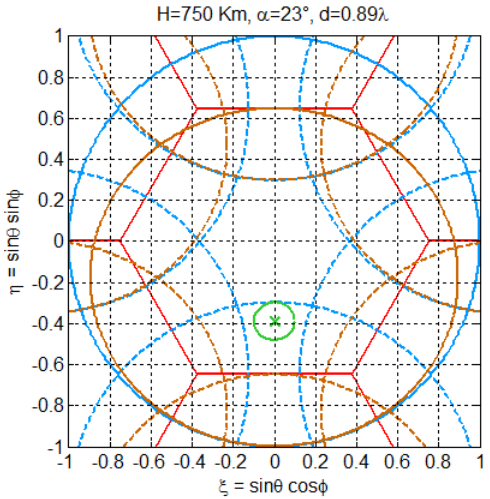

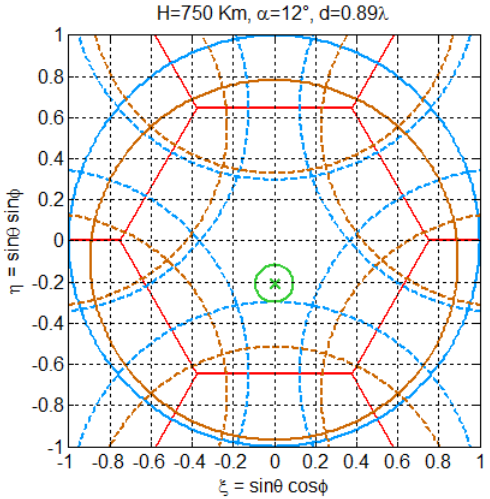

Nadir looking direction **x**
in alias-free FOV

Angular resolution

- *Collecting area prop. to **d** and to number of antennas*

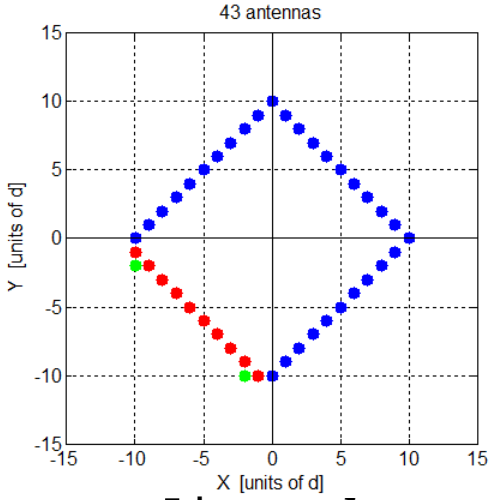

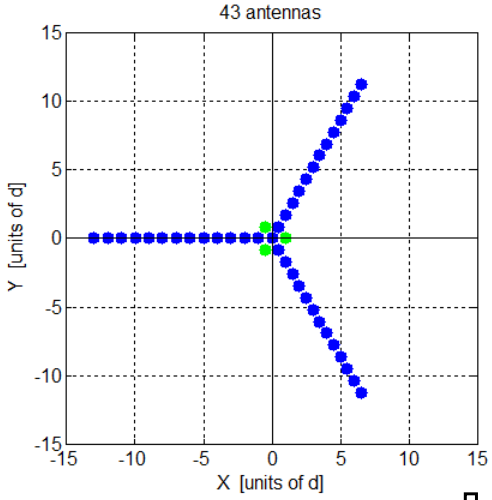

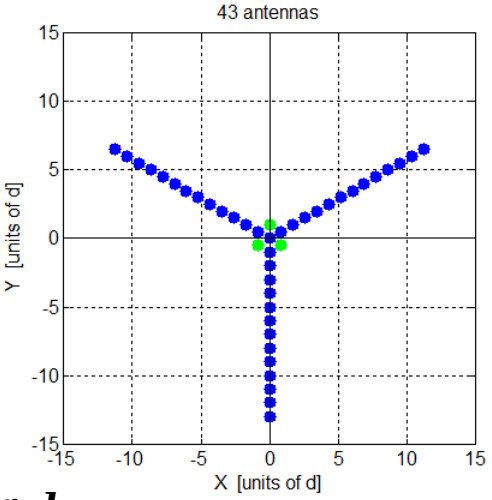

 larger ***d***

 smaller ***d***

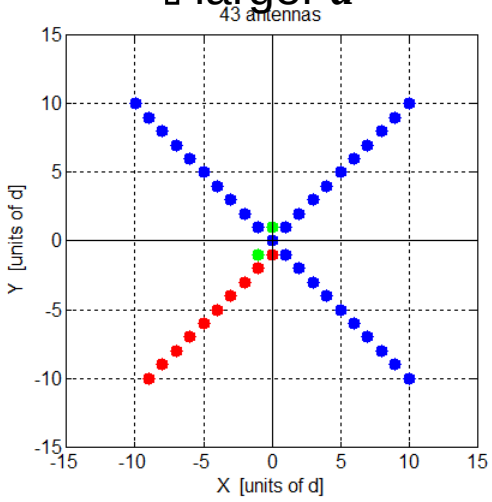

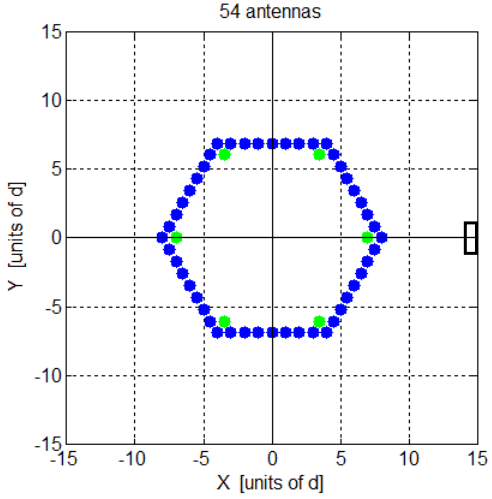

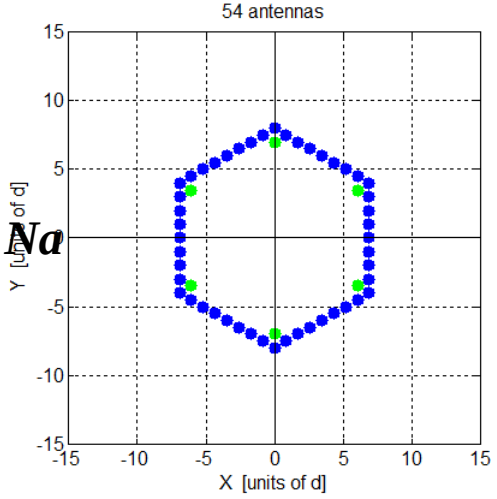

 larger ***Na***

Angular resolution

- *Angular resolution prop. to frequency coverage*

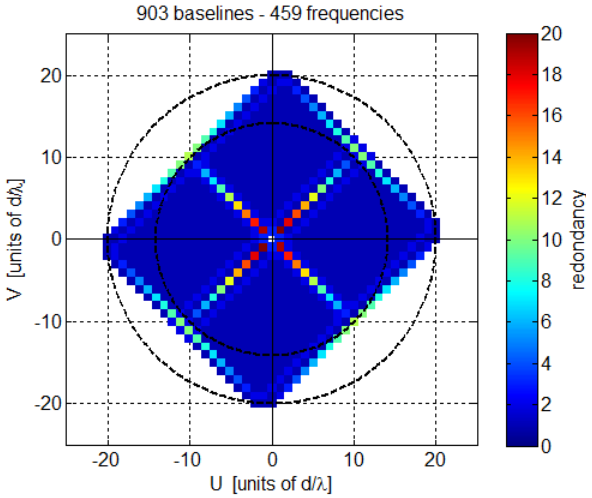

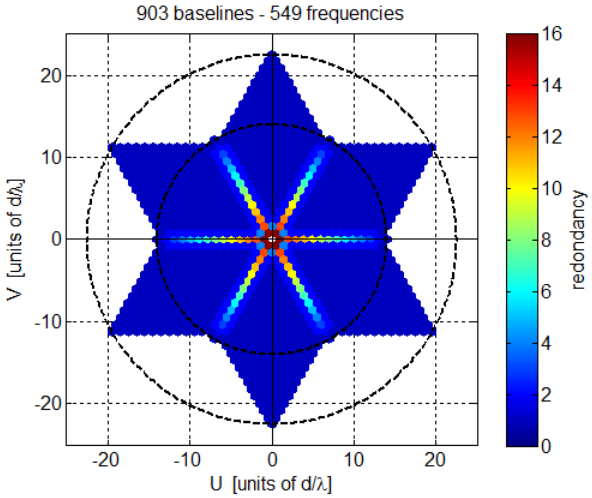

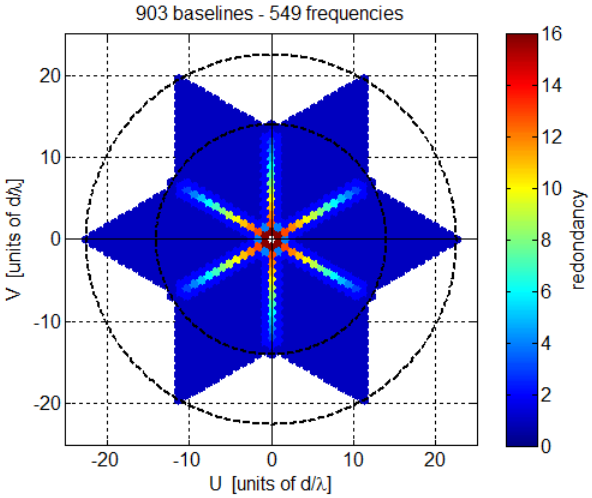

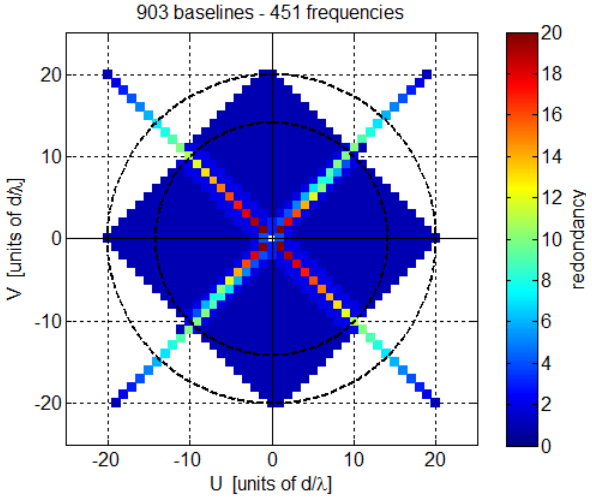

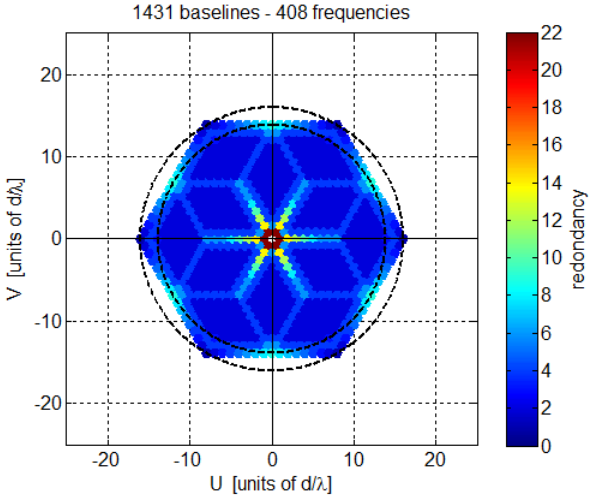

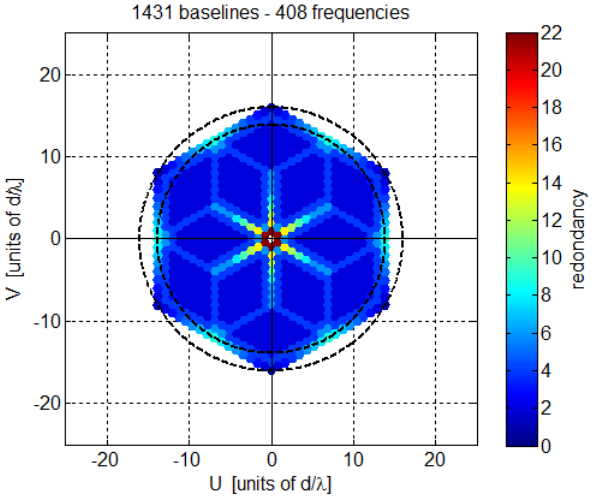

Ground resolution

- *10 Km is not a dream:*

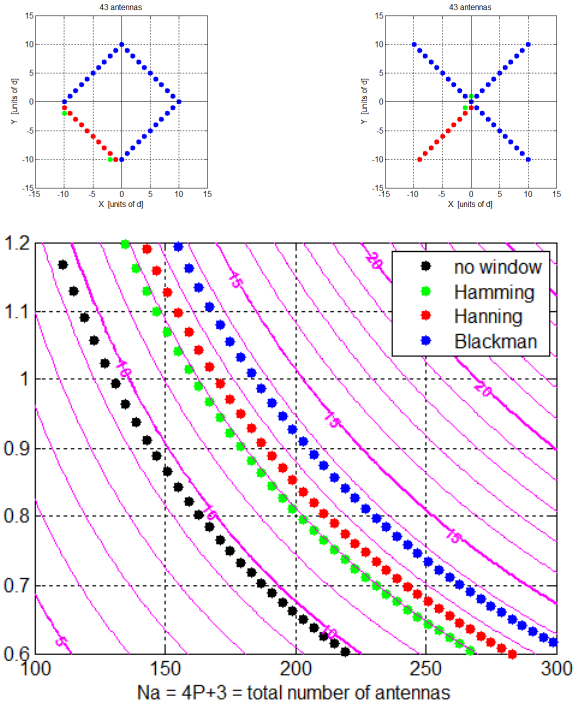

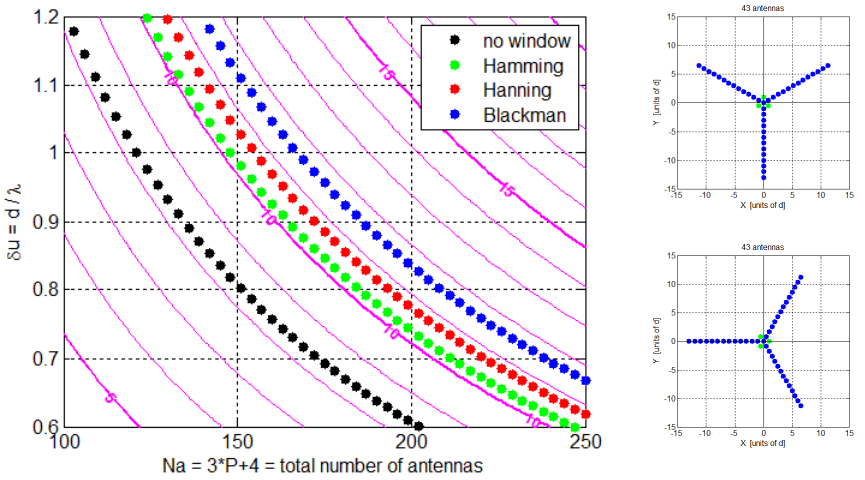

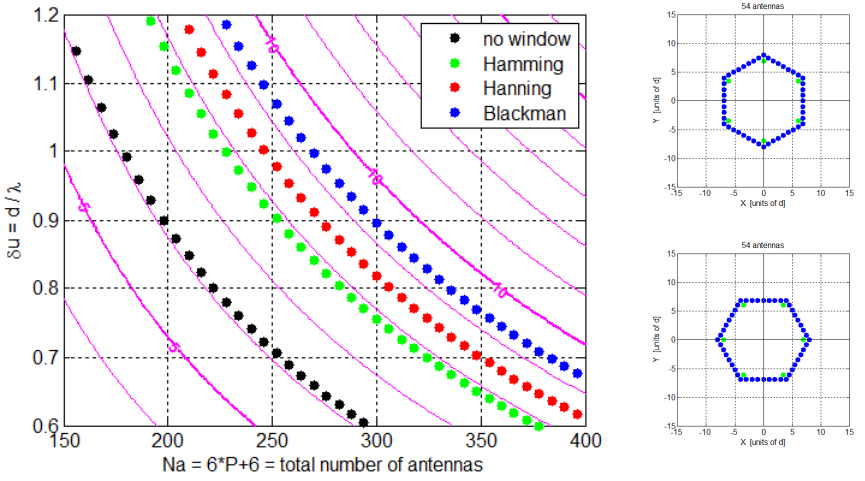

Candidate arrays

- *Two arrays with 231 antennas spaced every λ*

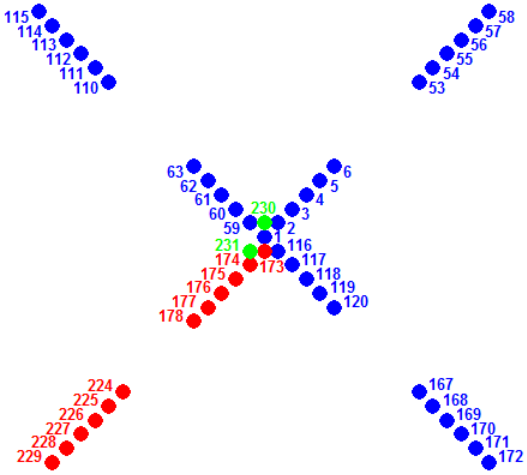

arms length
57×λ ≈ 12 m

swath
≥ 924 Km ∀ tilt

resolution
0.0133 rad (Hamming)
10 Km @ 750 Km

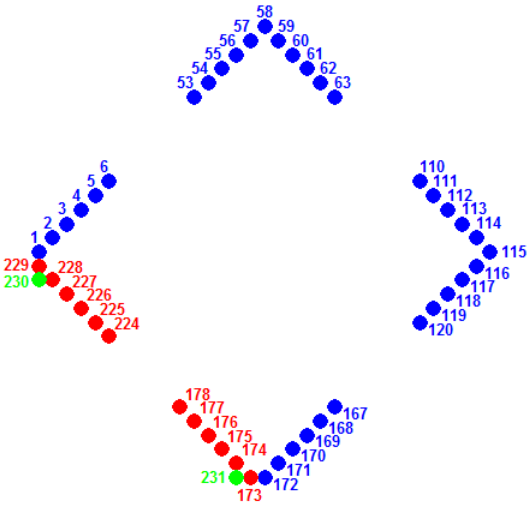

26565	baselines	26565
13282	frequencies	13337
53361x65536	**G** matrix	53361x65536
53361x26565	**J** matrix	53361x26675

Modeling matrices

❖ *Conditioning of* **G** *and* **J**: *invertible*

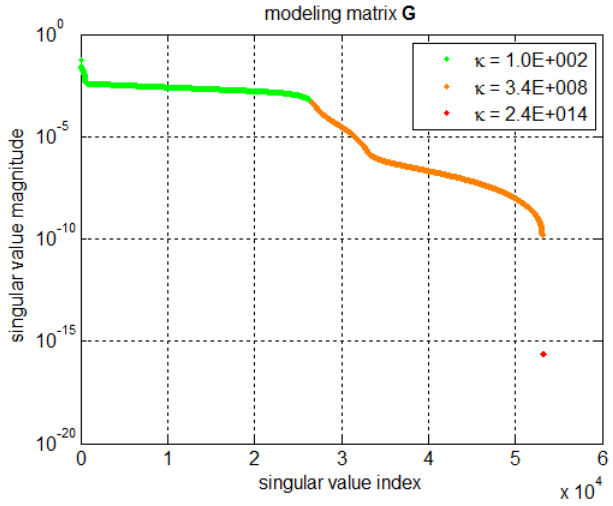

G

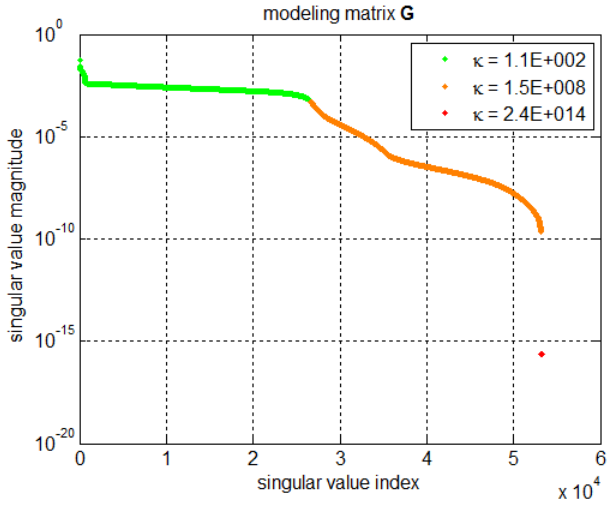

singular values

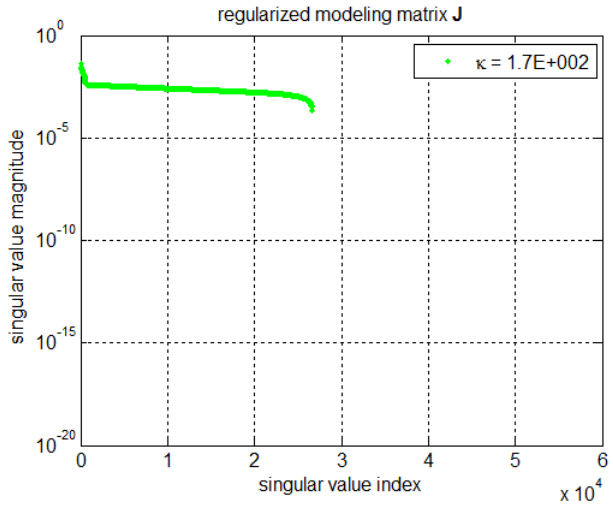

J

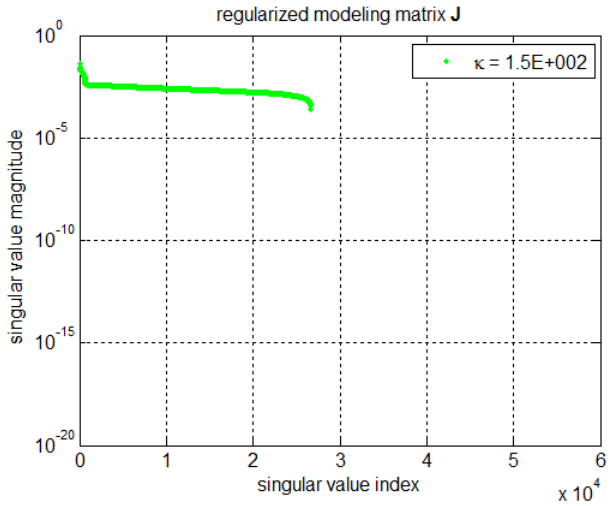

Modeling matrices

❖ *Propagation of round off errors for* $\mathbf{J}^+$*: under control*

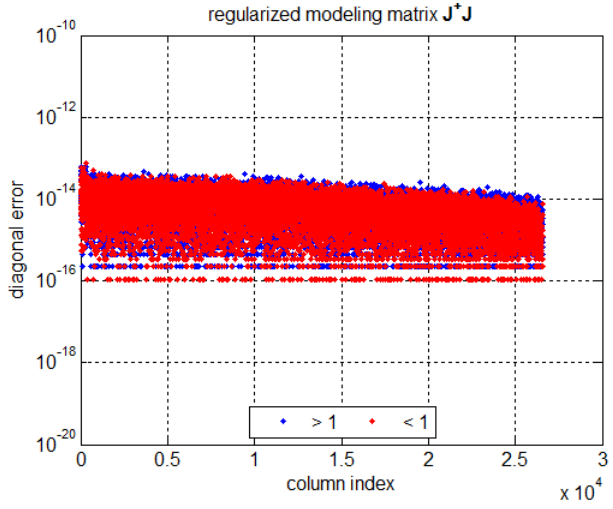

diagonal *vs*. 1

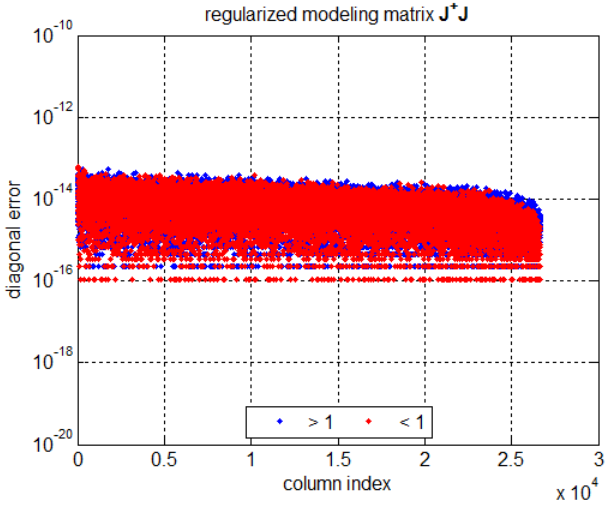

$J^+J = I$

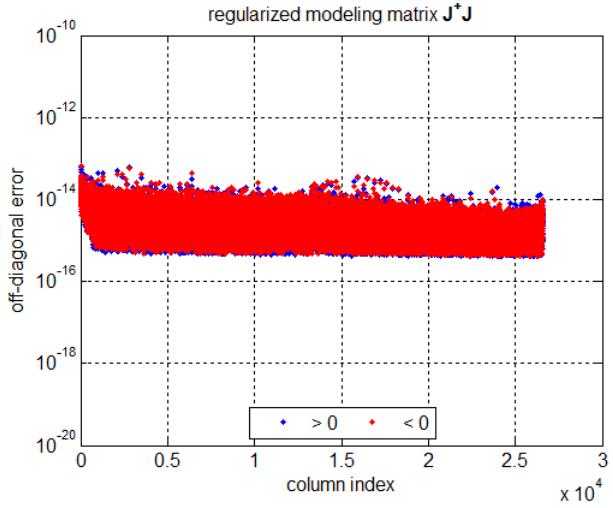

off diagonal *vs*. 0

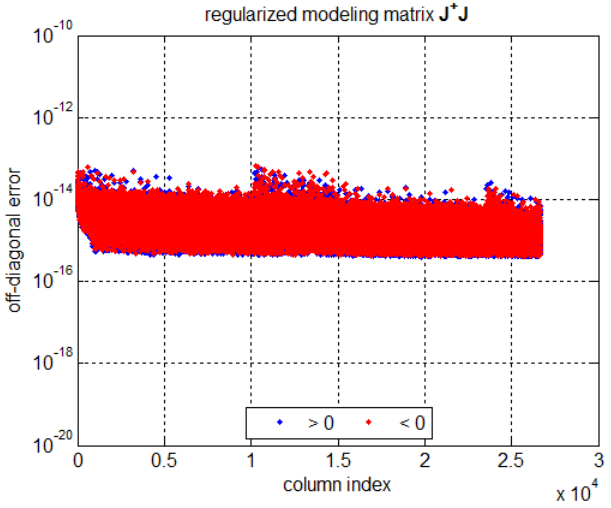

Inversion of noisy visibilities

❖ *Reconstruction schemes:*

G is the modeling operator of the instrument:

- standard approach: $V = \mathbf{G}T$ is solved for T
- differential approach: $\delta V = \mathbf{G}\delta T$ is solved for δT

with $\delta V = V - V'$ and $\delta T = T - T'$

where $V' = \mathbf{G}T'$ and T' is an artificial scene

Inversion of noisy visibilities

- *Flat scene, single pol: floor error map*

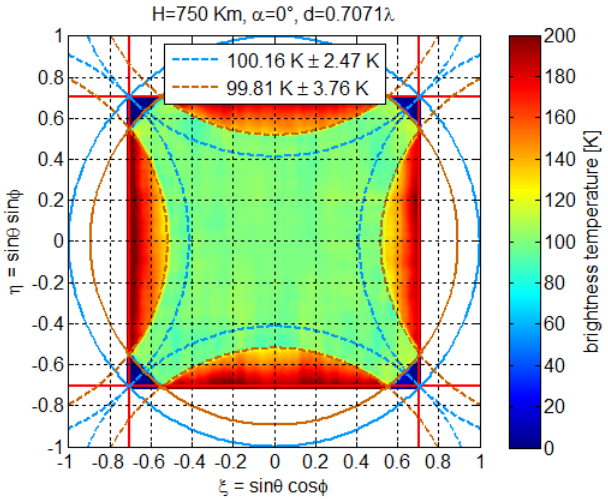

$$V = V + \Delta V$$

$$\sigma_{\Delta V} = 0.01\ K$$

$$\Downarrow$$

1000 rand

$$\Downarrow$$

$$\langle T \rangle$$

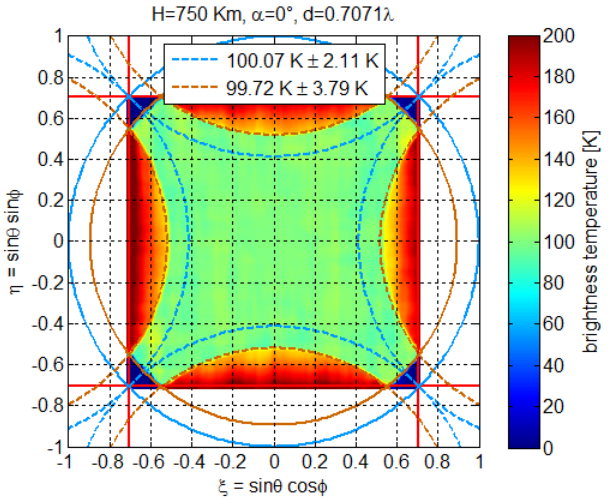

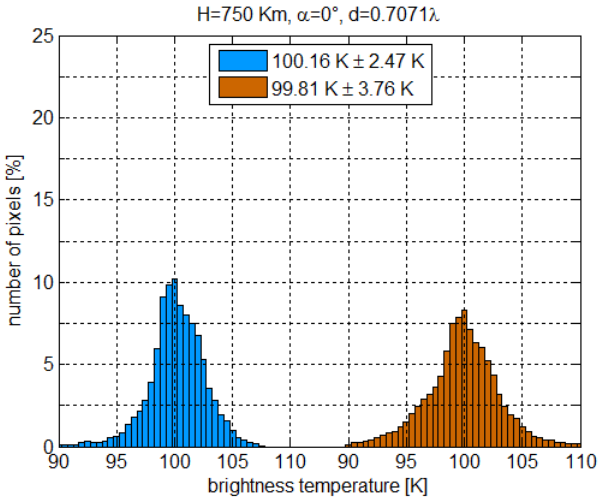

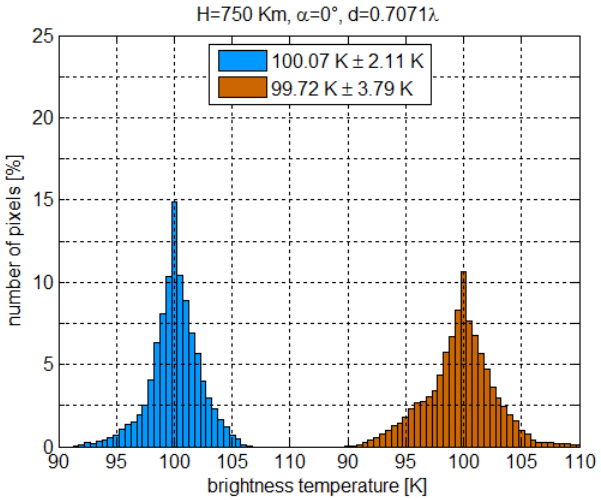

Inversion of noisy visibilities

❖ *Flat scene, single pol: rms error map*

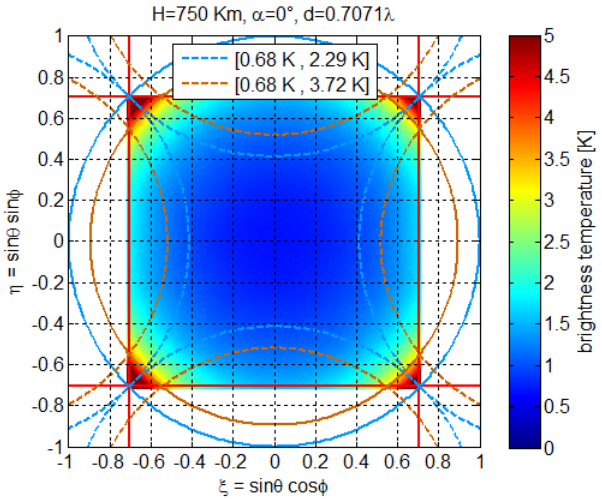

$$V = V + \Delta V$$

$$\sigma_{\Delta V} = 0.01\ K$$

$$\Downarrow$$

1000 rand

$$\Downarrow$$

$$\sigma_{\Delta T}$$

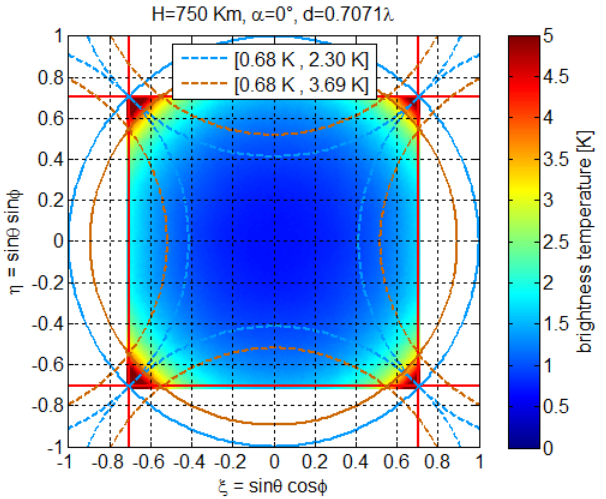

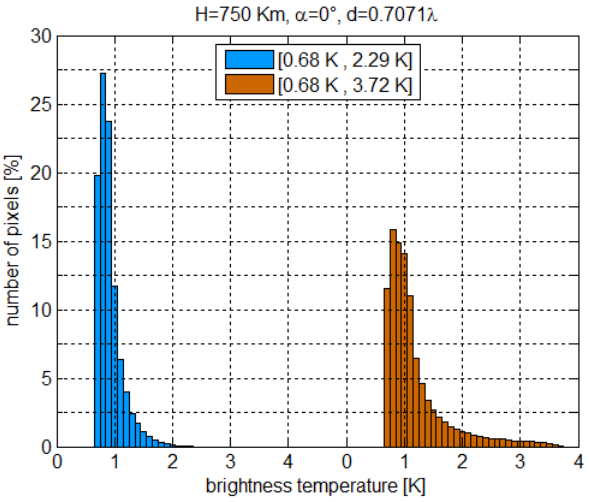

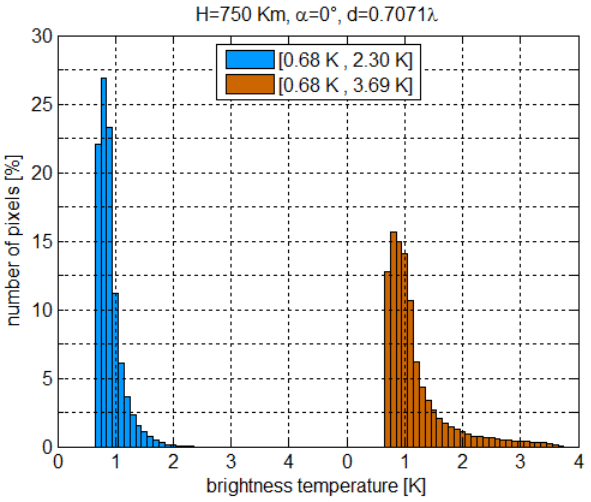

Inversion of noisy visibilities

❖ *Radiometric sensitivity per snapshot at boresight*

SMOShr

$V = V + \Delta V$

$\sigma_{\Delta V} = 0.01$ K

⇓

1000 rand

⇓

$\sigma_{\Delta T} = 0.68$ K

BUT

$T_{int} = 3.60$ sec

4 bits corr (÷ 1.4)

simultaneous H&V

$T_{eff} = 2.57$ sec

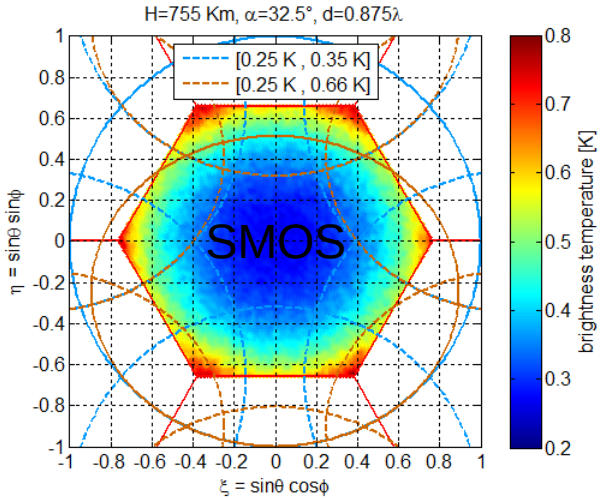

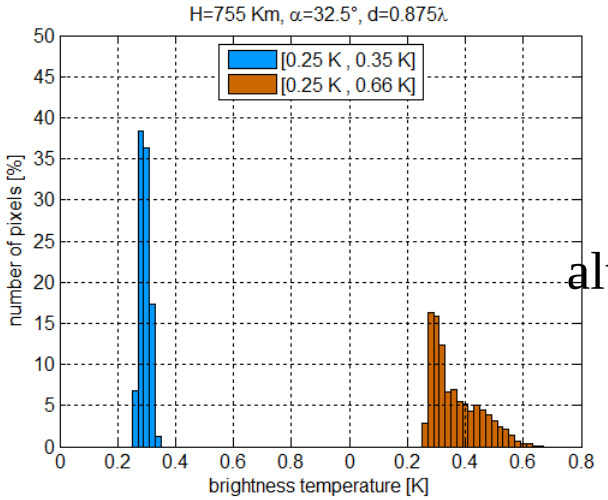

SMOS

$V = V + \Delta V$

$\sigma_{\Delta V} = 0.01$ K

⇓

1000 rand

⇓

$\sigma_{\Delta T} = 0.25$ K

BUT

$T_{int} = 3.60$ sec

1 bit corr (÷ 1.8)

alternate H&V (÷ 3)

$T_{eff} = 0.66$ sec

Inversion of noisy visibilities

- *Fresnel scene, dual pol: standard approach*

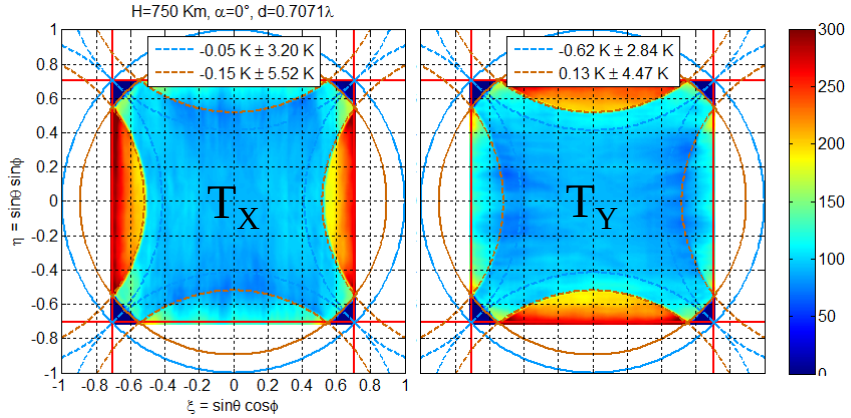

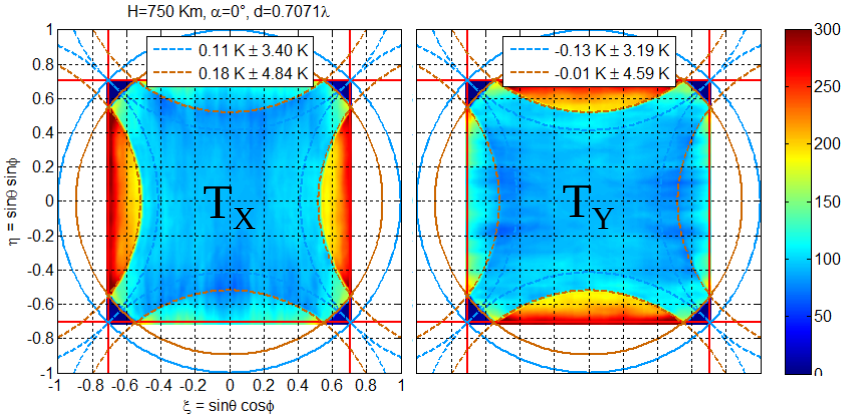

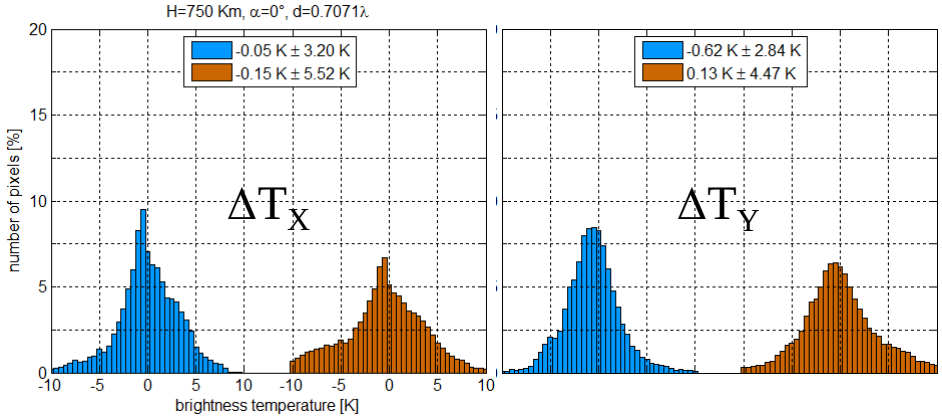

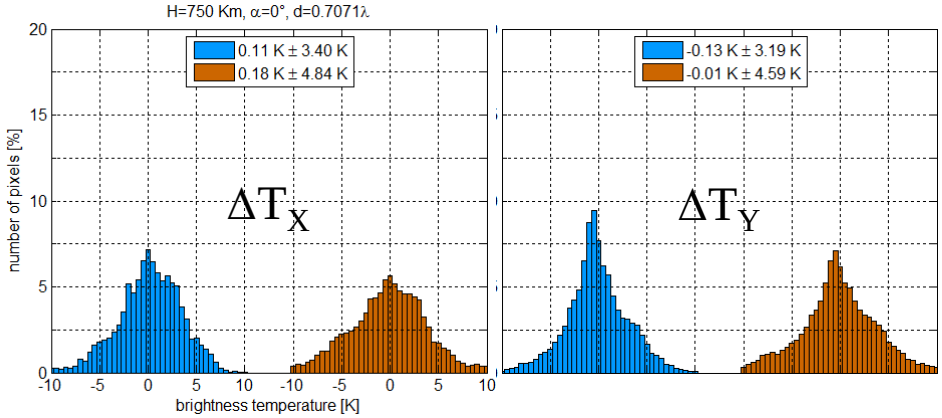

Inversion of noisy visibilities

- *Fresnel scene, dual pol: differential approach*

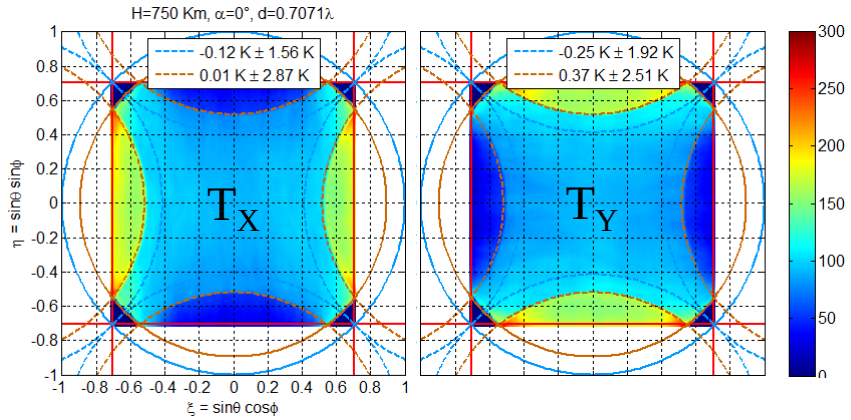

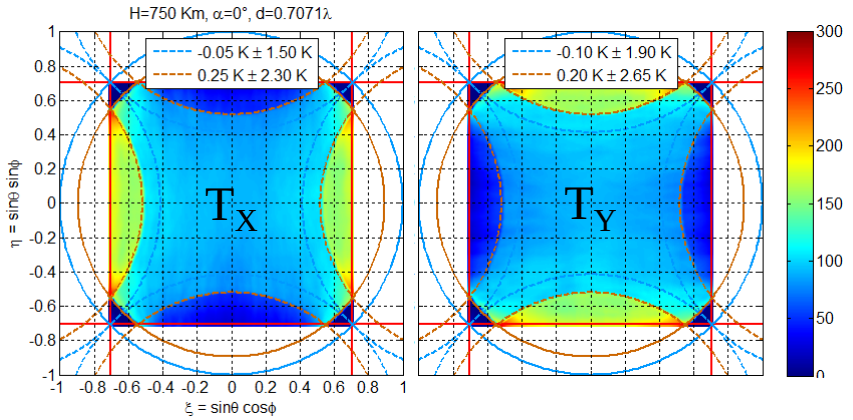

Differential approach behaves exactly like expected!

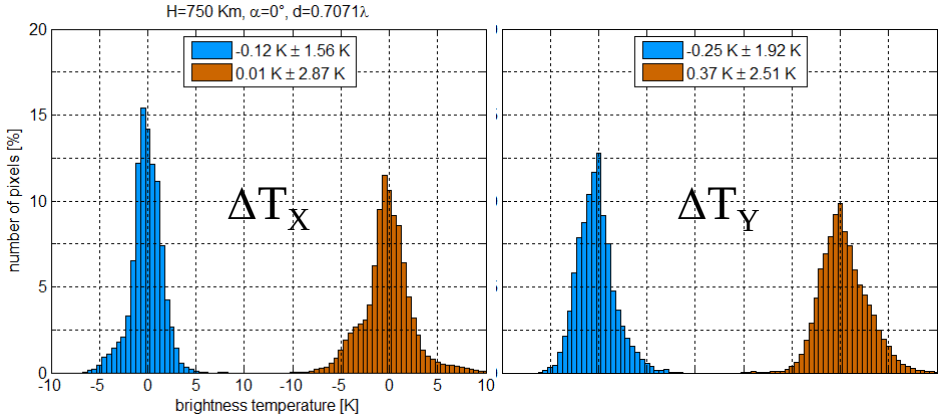

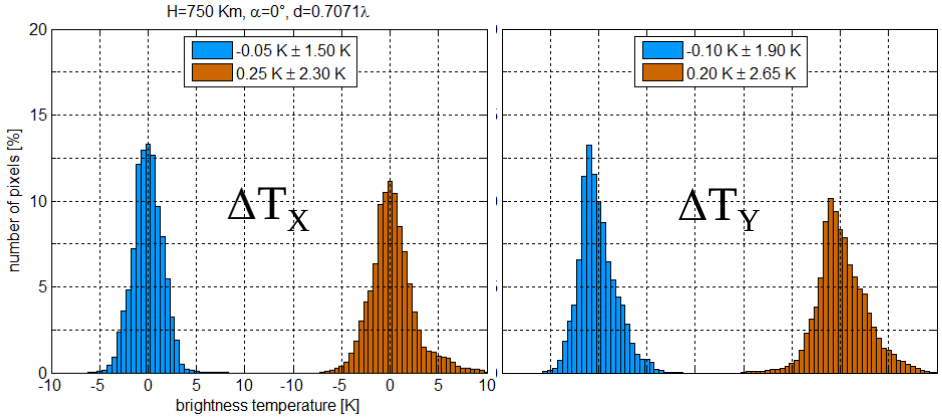

Inversion of noisy visibilities

❖ *Fresnel scene, dual pol: standard approach*

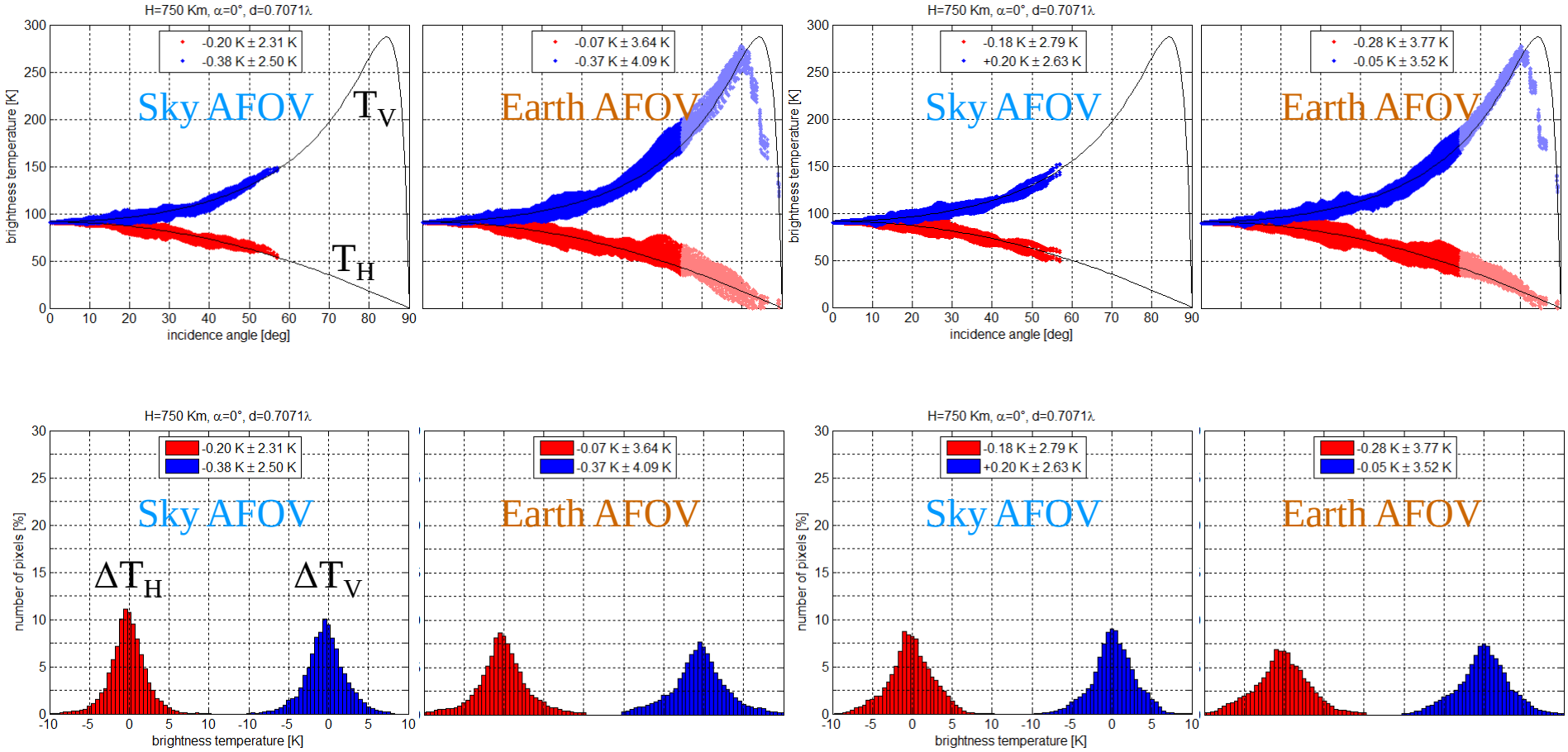

Inversion of noisy visibilities

❖ *Fresnel scene, dual pol: differential approach*

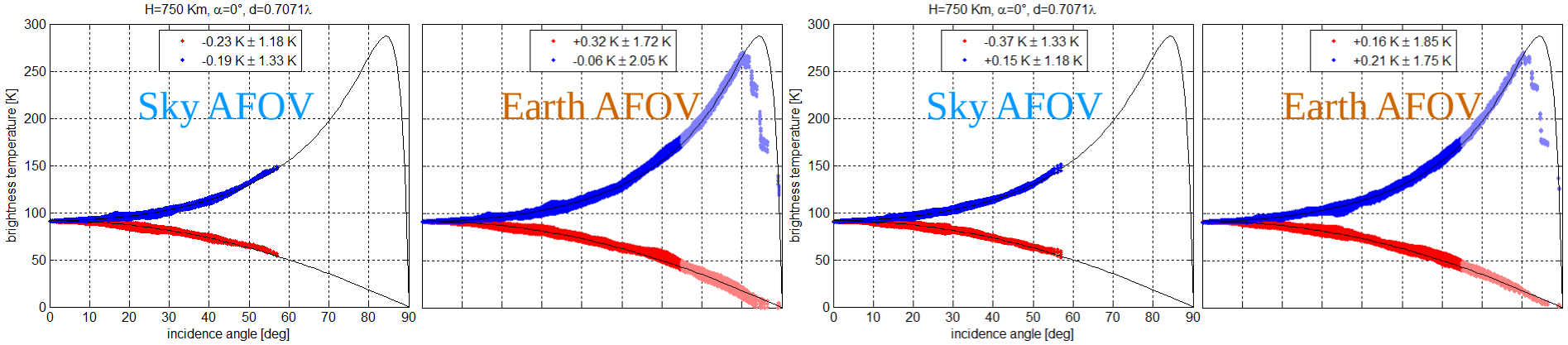

Differential approach behaves exactly like it is actually implemented in SMOS!

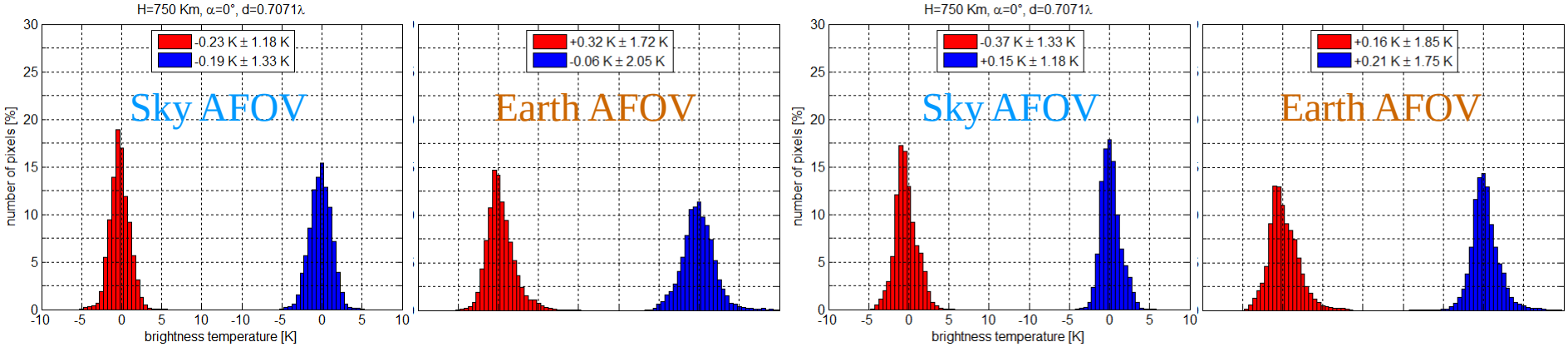

Impact of antennas disparity

- *Disparity of SMOS antennas patterns:* central hub

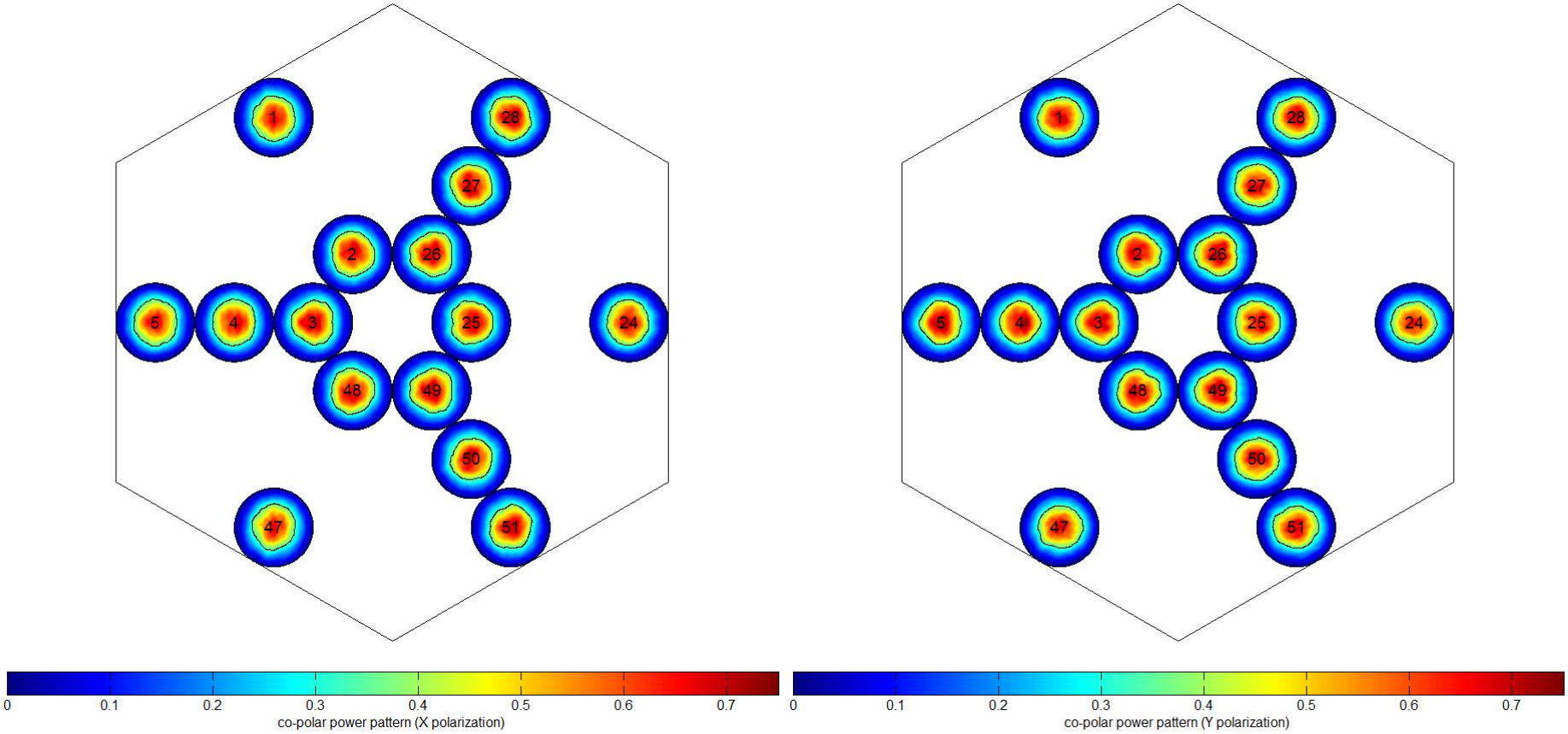

Impact of antennas disparity

- *Disparity of SMOS antennas patterns:* arm A

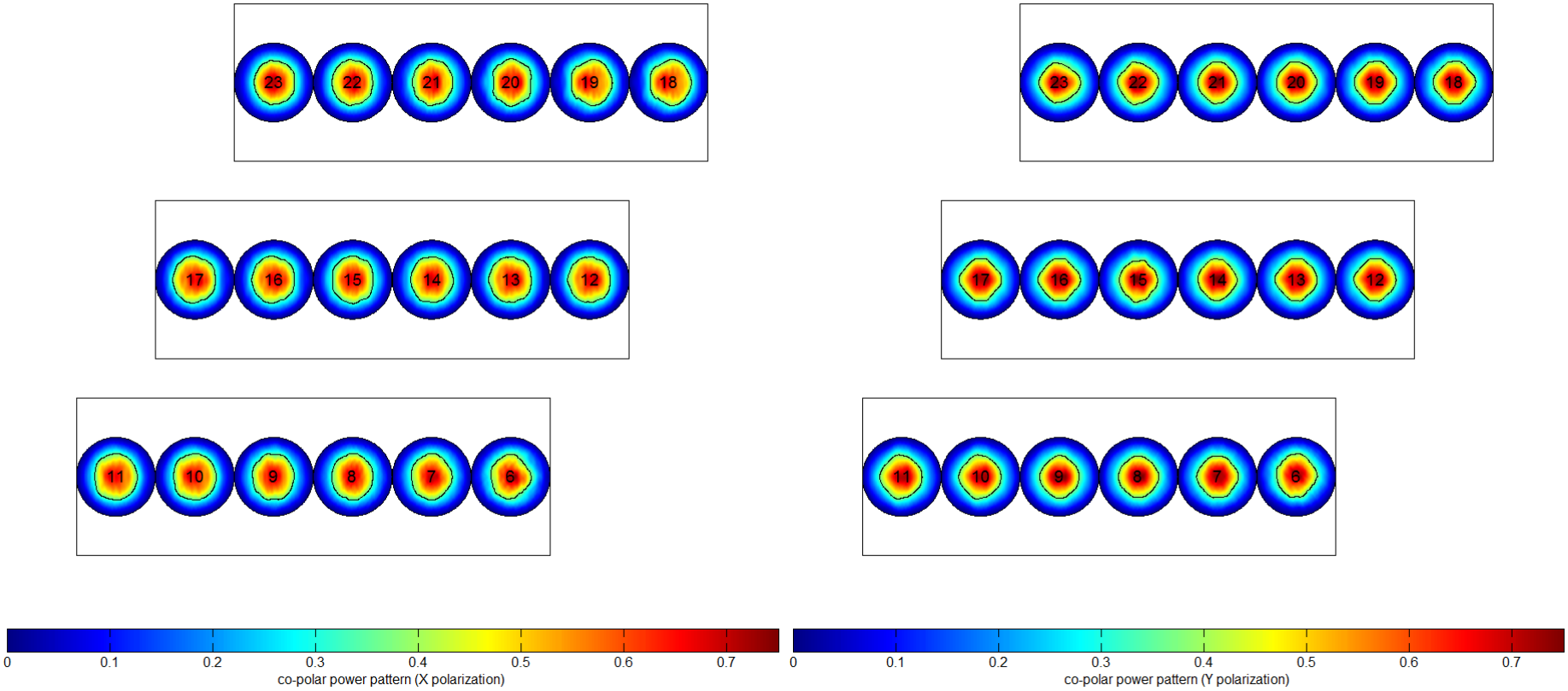

Impact of antennas disparity

❖ *Disparity of SMOS antennas patterns:* arm B

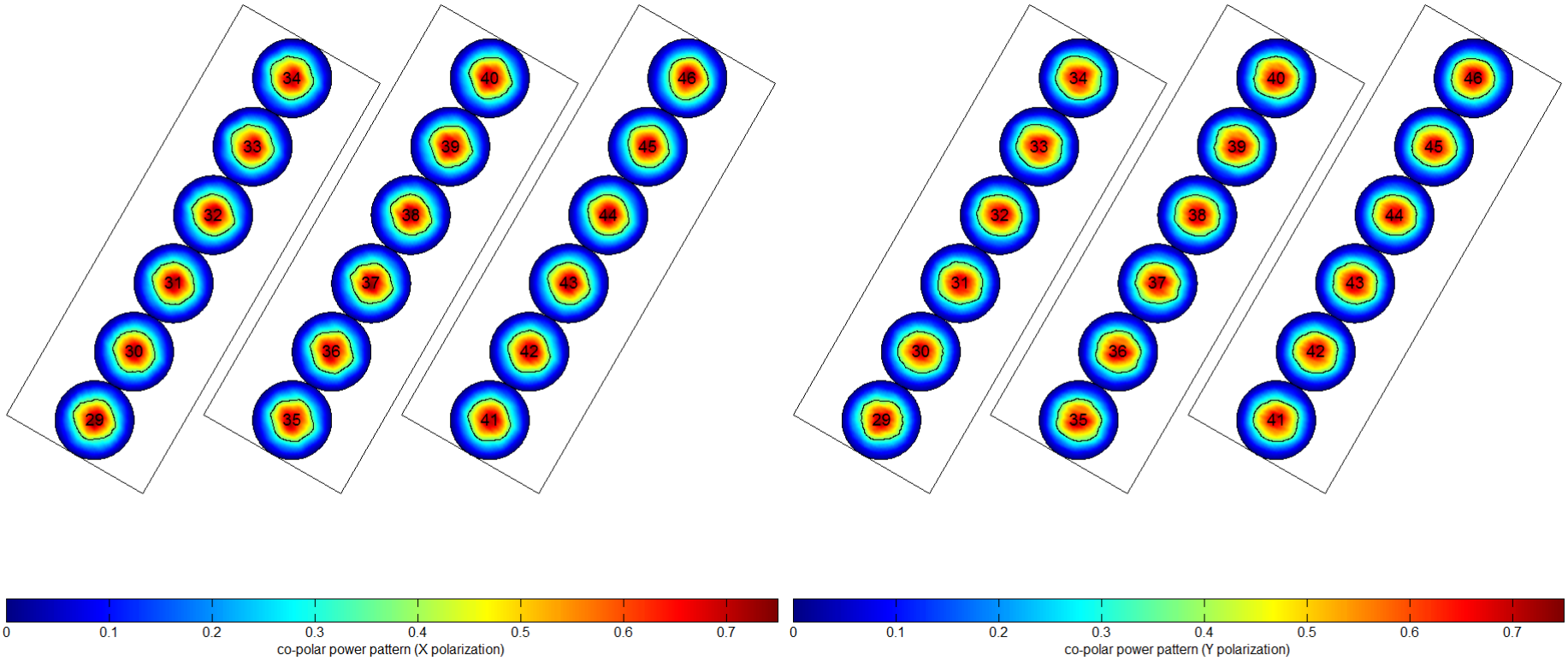

Impact of antennas disparity

- *Disparity of SMOS antennas patterns:* arm C

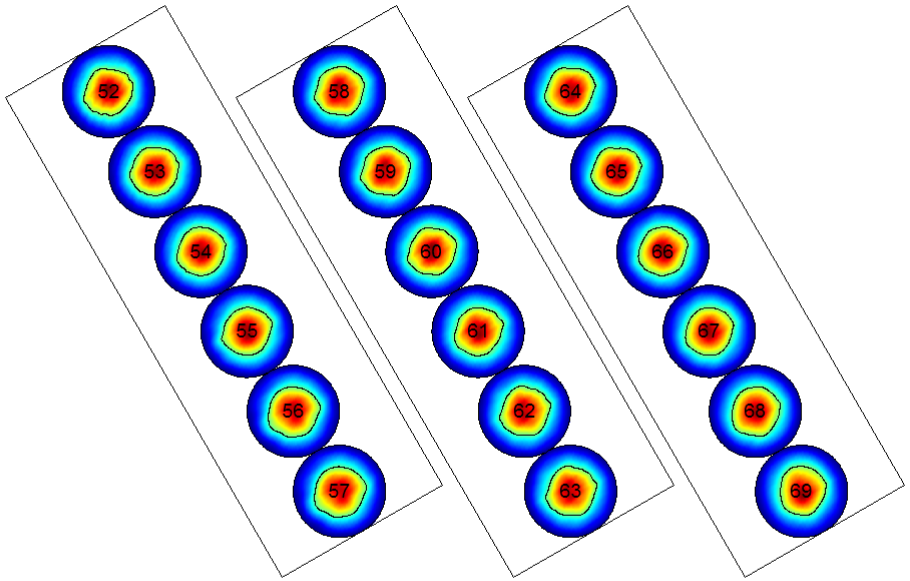

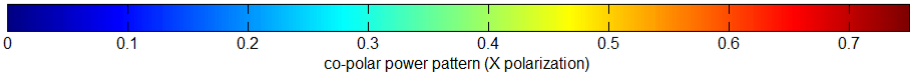

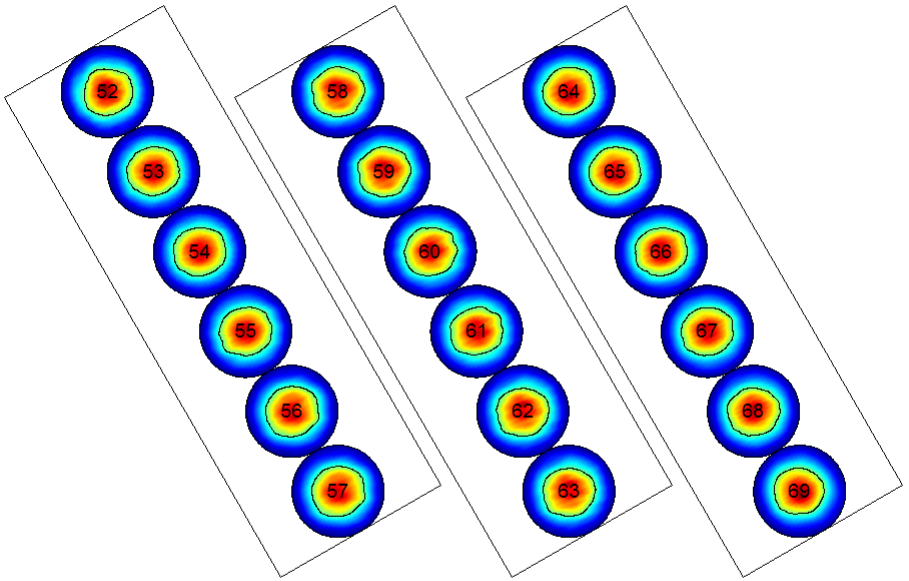

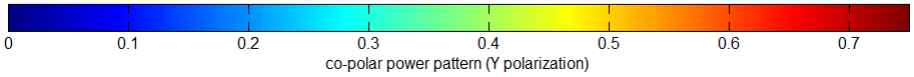

Impact of antennas disparity

❖ *Estimating / Controlling the disparity*

There is no satisfying metric to measure quantitatively the difference between radiation patterns. However, there is one pseudo-metric that can be easily used without any ambiguity: the comparison to the diversity of these radiations pattern without estimating the diversity itself:

$$\boldsymbol{\mathcal{F}}_{a} = \langle \boldsymbol{\mathcal{F}}_{a'} \rangle_{a'=1}^{231} + \gamma\left(\boldsymbol{\mathcal{F}}_{a} - \langle \boldsymbol{\mathcal{F}}_{a'} \rangle_{a'=1}^{231} \right) \text{ with } 0 \leq \gamma \leq 1.$$

The case $\gamma = 1$ corresponds to the current situation, whereas for $\gamma = 0$ the instrument is equipped with identical patterns (equal to the average of the actual ones). Between these two extreme cases, the disparity between the radiation patterns is reduced compared to the actual one.

Impact of antennas disparity

❖ *Conditioning of* **G** *and* **J**: $\gamma = 1$

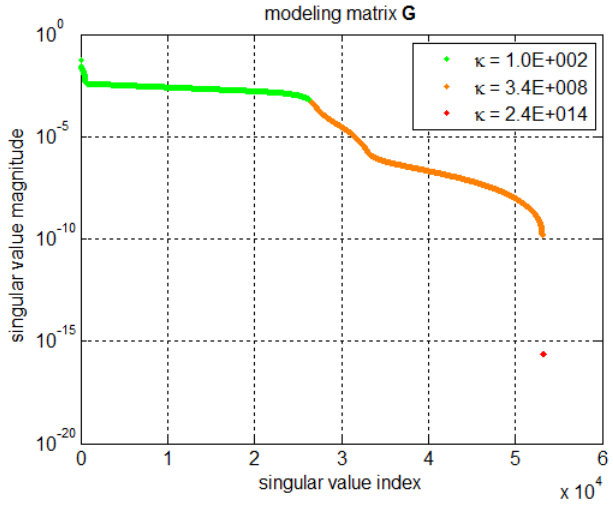

G

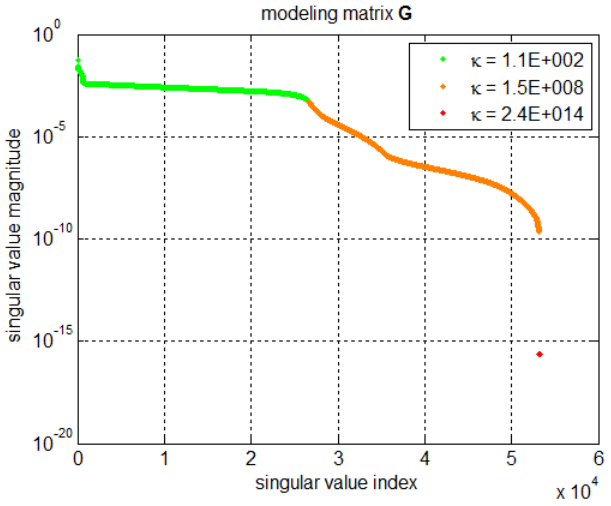

singular values

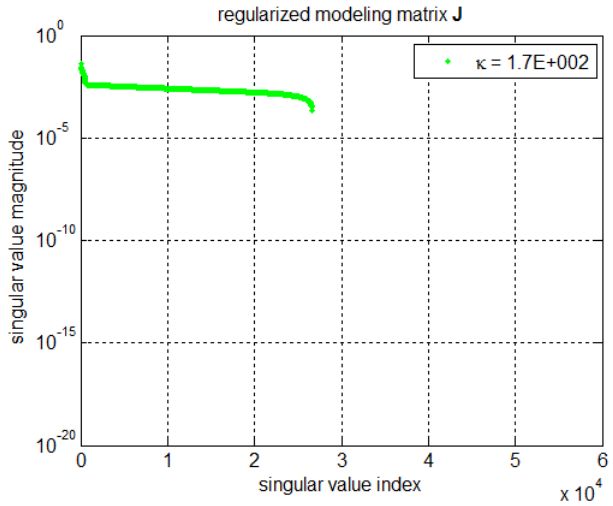

J

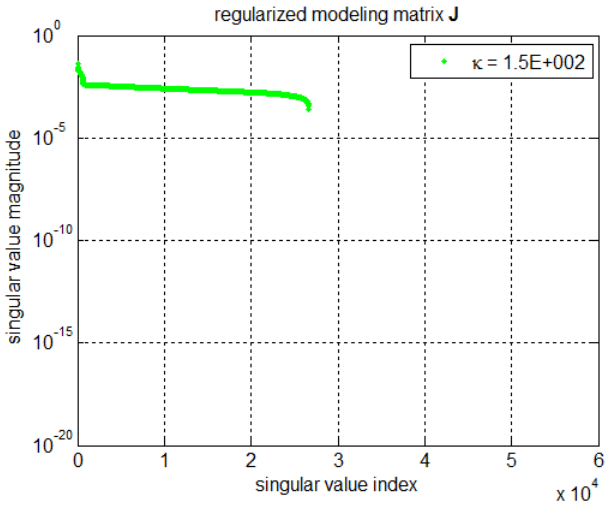

Impact of antennas disparity

❖ *Conditioning of* **G** *and* **J**: $\gamma = 0$

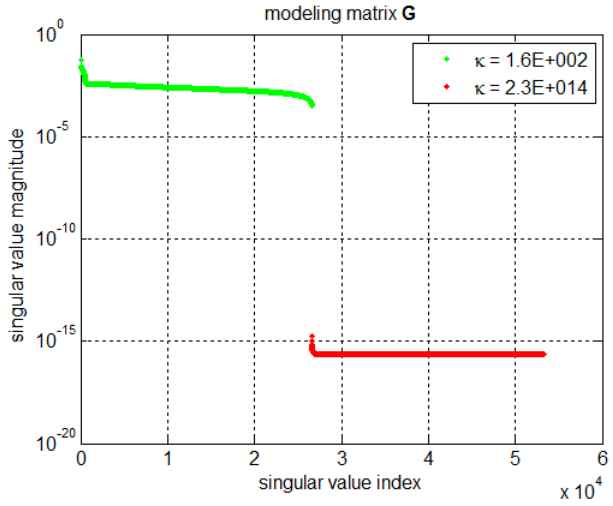

G

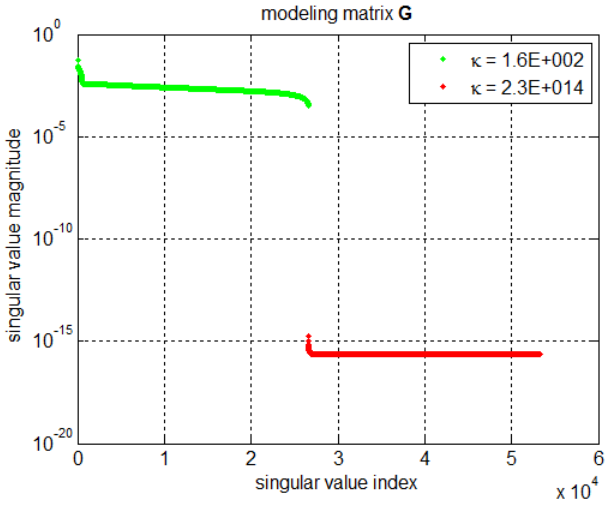

singular values

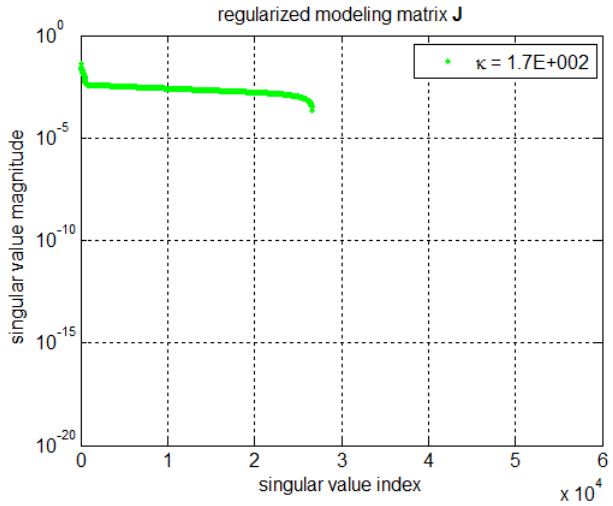

J

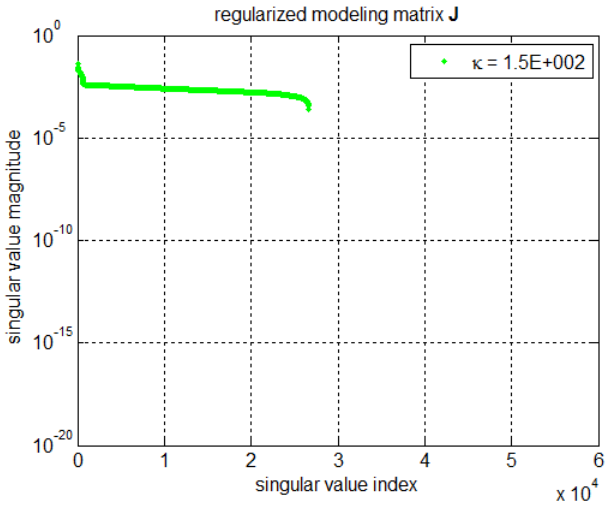

Impact of antennas disparity

❖ *Conditioning of* **G** *and* **J**: $\gamma = 0.5$

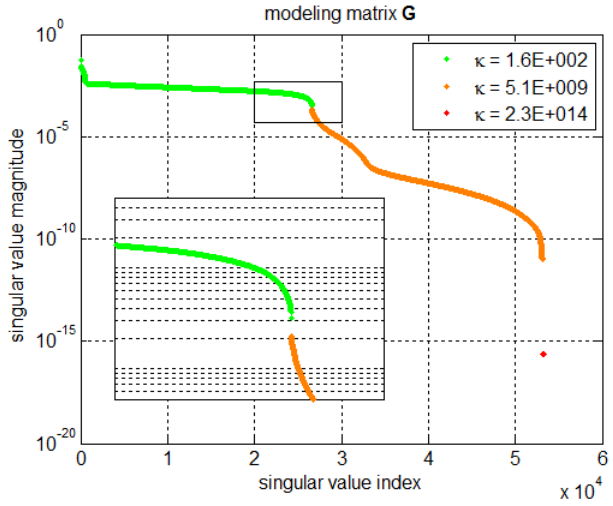

G

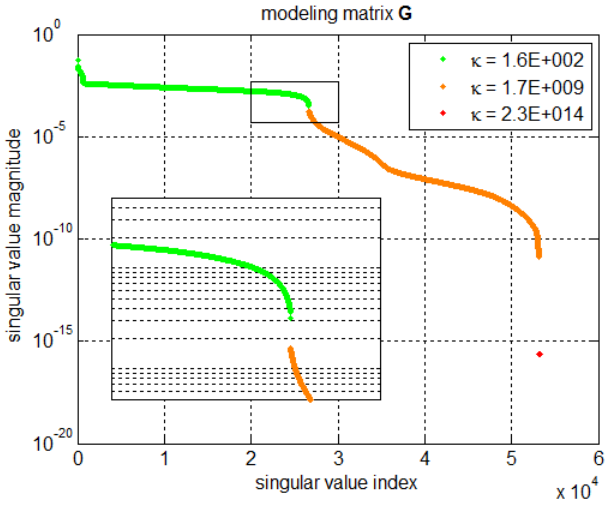

singular values

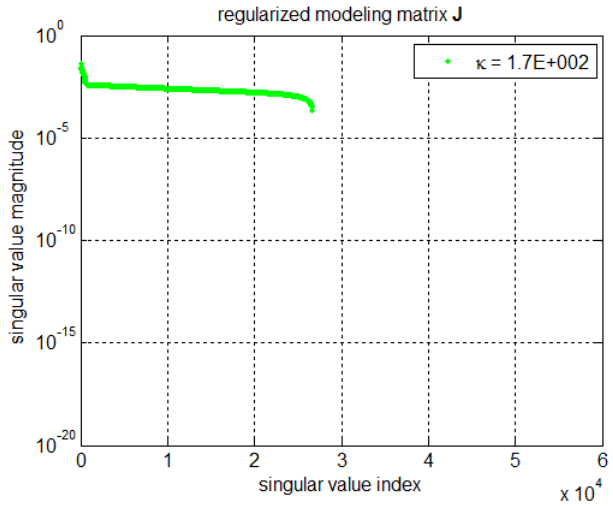

J

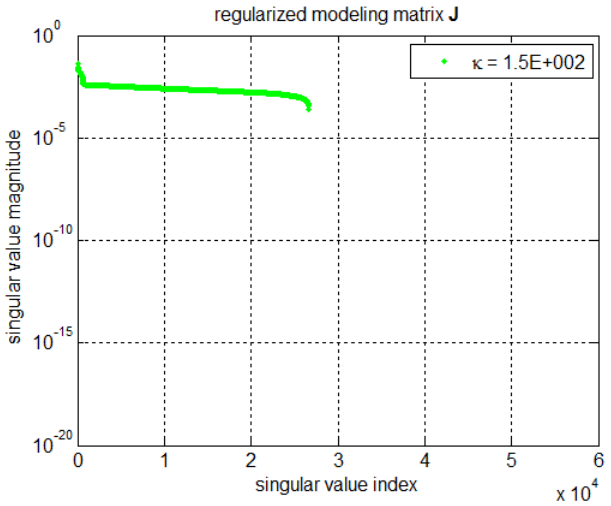

Impact of antennas disparity

❖ *Fresnel scene, dual pol: γ = 1*

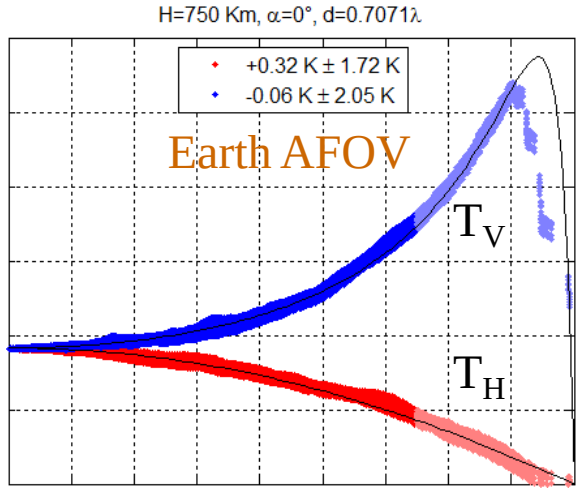

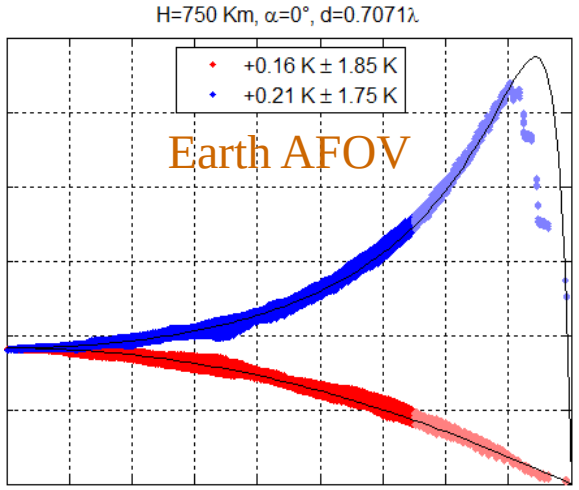

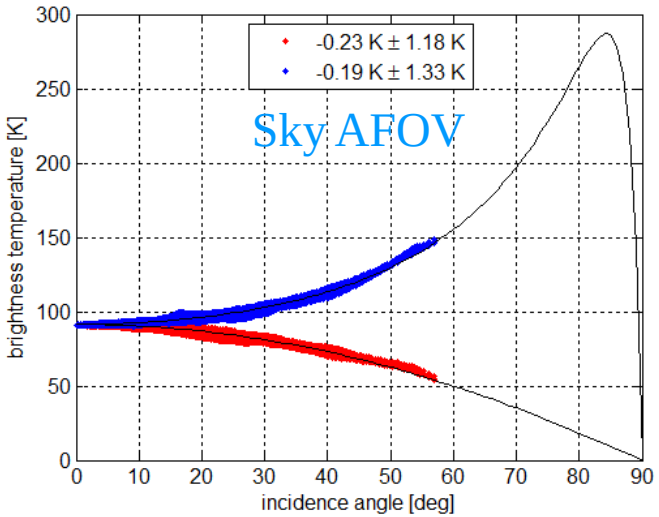

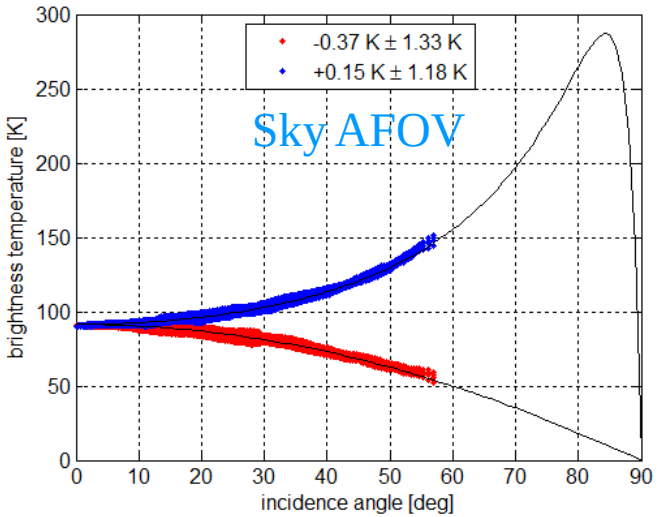

Impact of antennas disparity

❖ *Fresnel scene, dual pol: γ = 0.5*

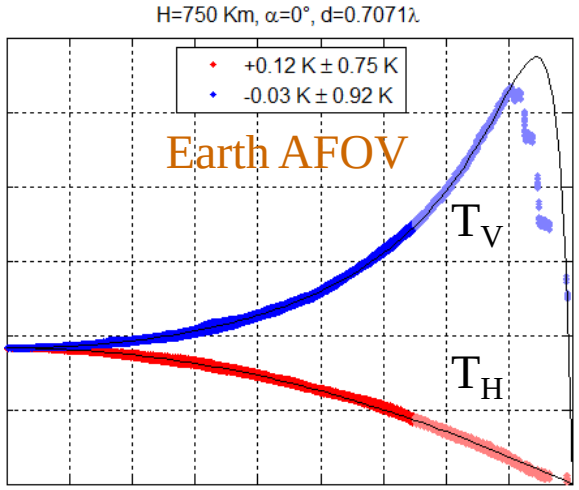

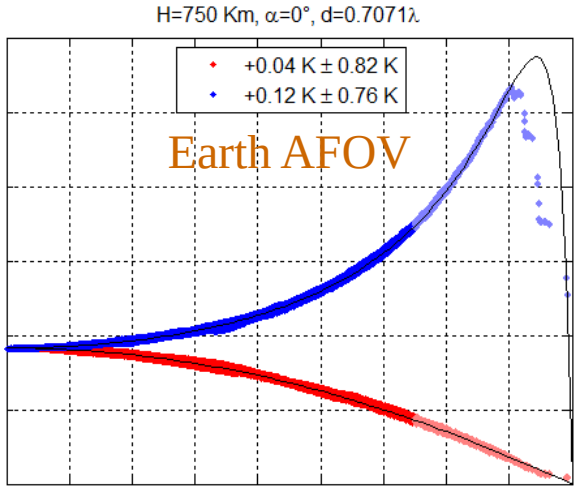

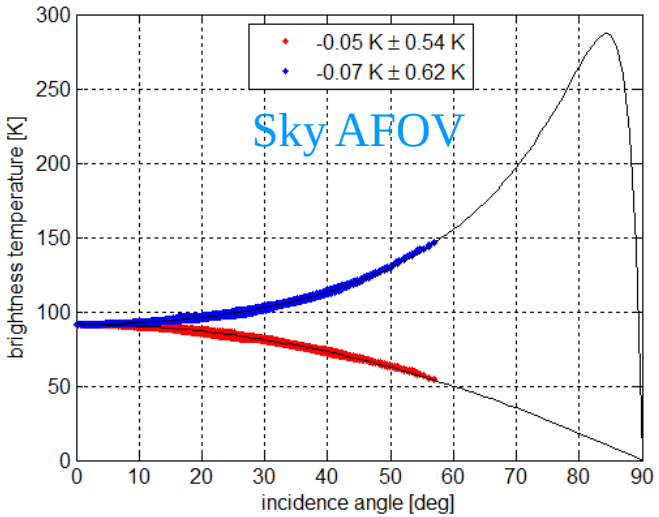

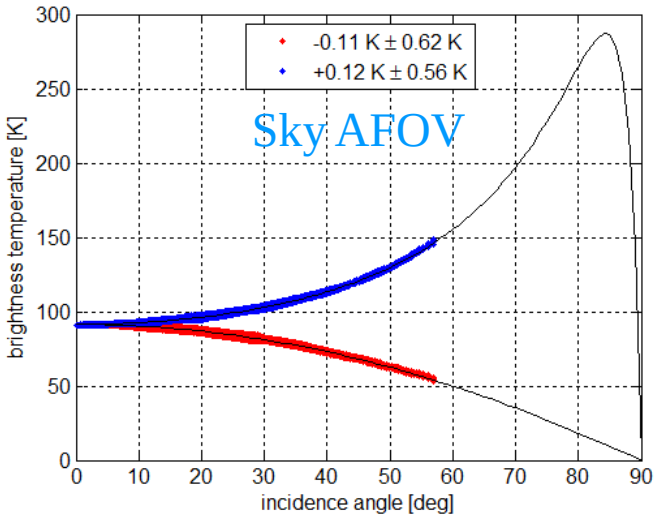

Impact of antennas disparity

❖ *Estimating / Controlling the disparity*

A new metric for estimating the distance between antennas patterns has been recently proposed. It is based on the notion of equivalent solid angle Ω of an antenna power pattern:

$$\Omega = \iint_{\|\xi\| \le 1} \frac{|\mathcal{F}(\xi)|^2}{\sqrt{1-\|\xi\|^2}} d\xi = \iint_{\|\xi\| \le 1} \frac{\mathcal{F}(\xi)\,\mathcal{F}^*(\xi)}{\sqrt{1-\|\xi\|^2}} d\xi$$

This definition has been extended to complex values to introduce the notion of cross solid angle between a pair of antennas voltage patterns:

$$\Omega_{pq} = \iint_{\|\xi\| \le 1} \frac{\mathcal{F}_p(\xi)\,\mathcal{F}_q^*(\xi)}{\sqrt{1-\|\xi\|^2}} d\xi$$

Impact of antennas disparity

❖ *Estimating / Controlling the disparity*

This definition has been extended to complex values to introduce the notion of cross solid angle between a pair of antennas voltage patterns:

$$\Omega_{pq} = \iint_{\|\xi\| \le 1} \frac{\mathcal{F}_p(\xi)\,\mathcal{F}_q^*(\xi)}{\sqrt{1-\|\xi\|^2}}\,d\xi$$

and the inner product between them:

$$\langle \mathcal{F}_p | \mathcal{F}_q \rangle \equiv \frac{\Omega_{pq}}{\sqrt{\Omega_p \Omega_q}}$$

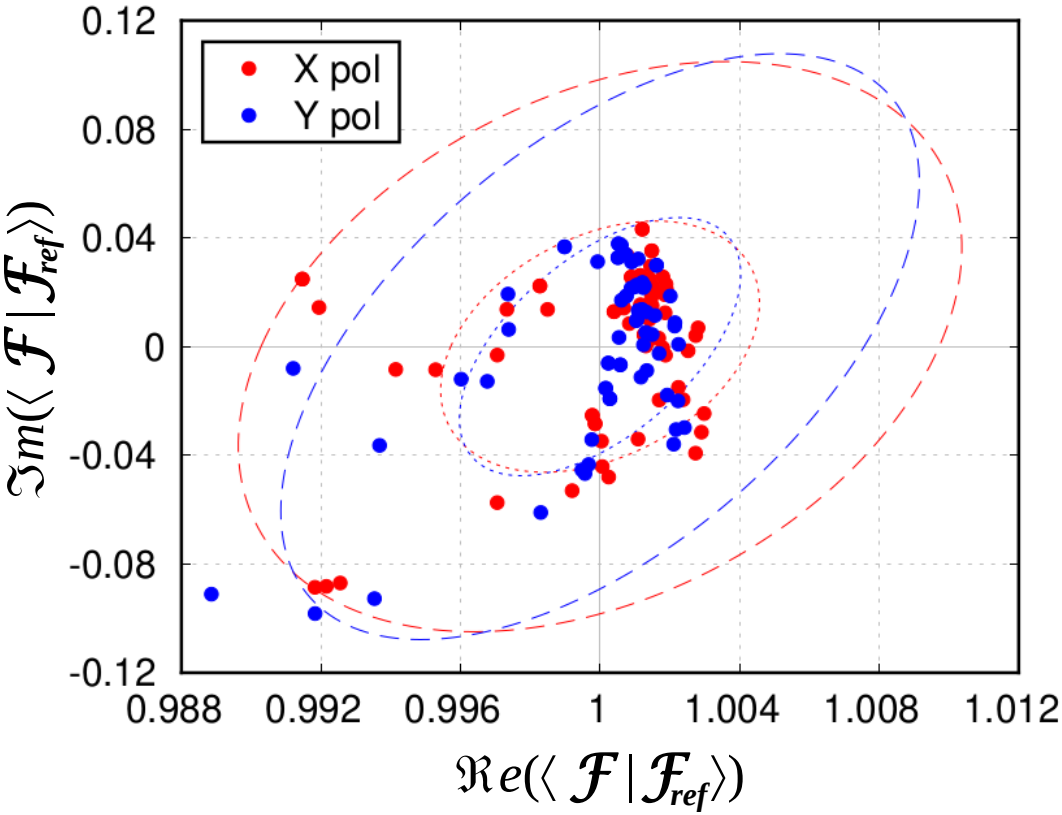

Impact of antennas disparity

- *Estimating / Controlling the disparity*

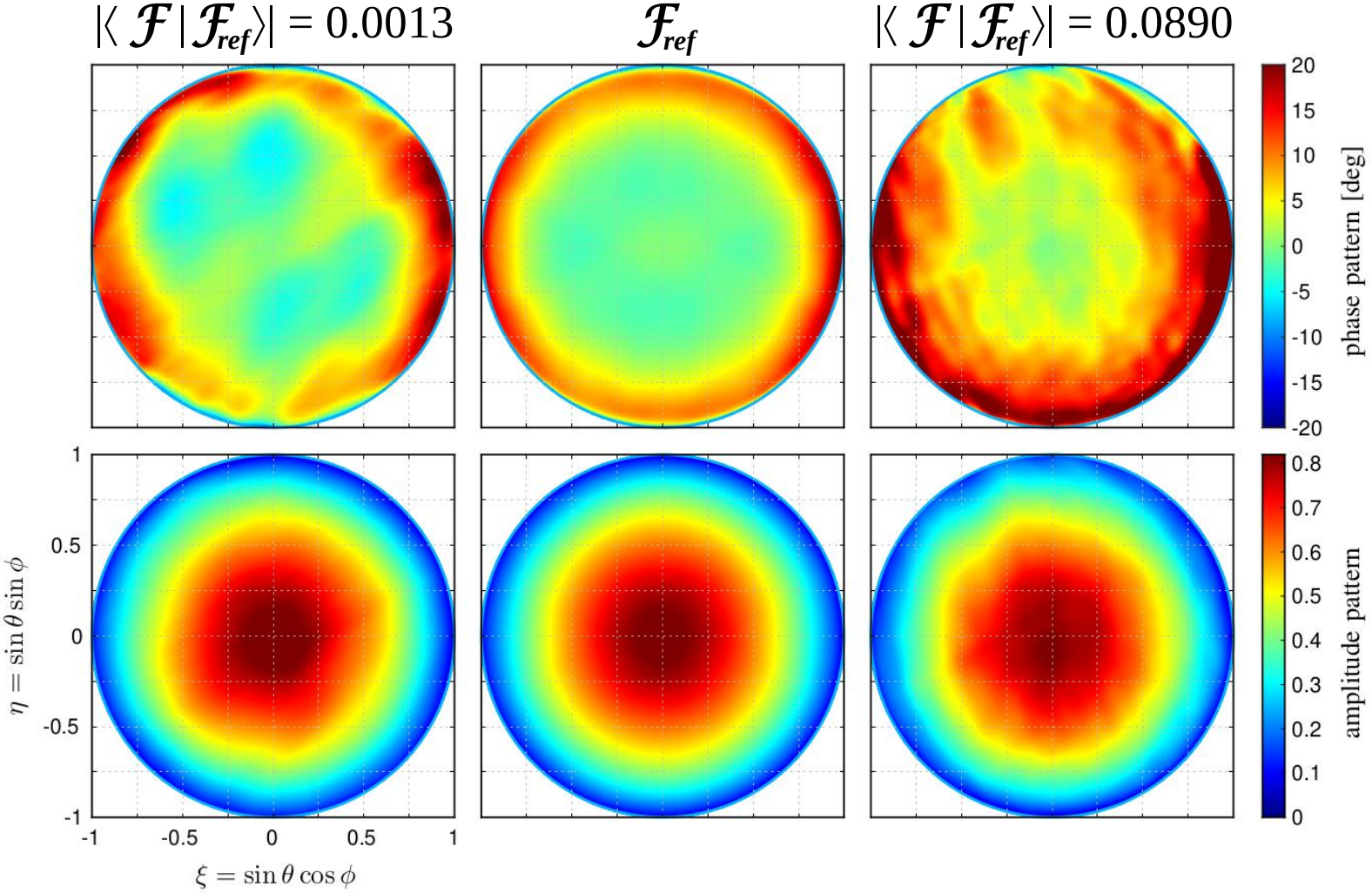

Impact of antennas disparity

❖ *Estimating / Controlling the disparity*

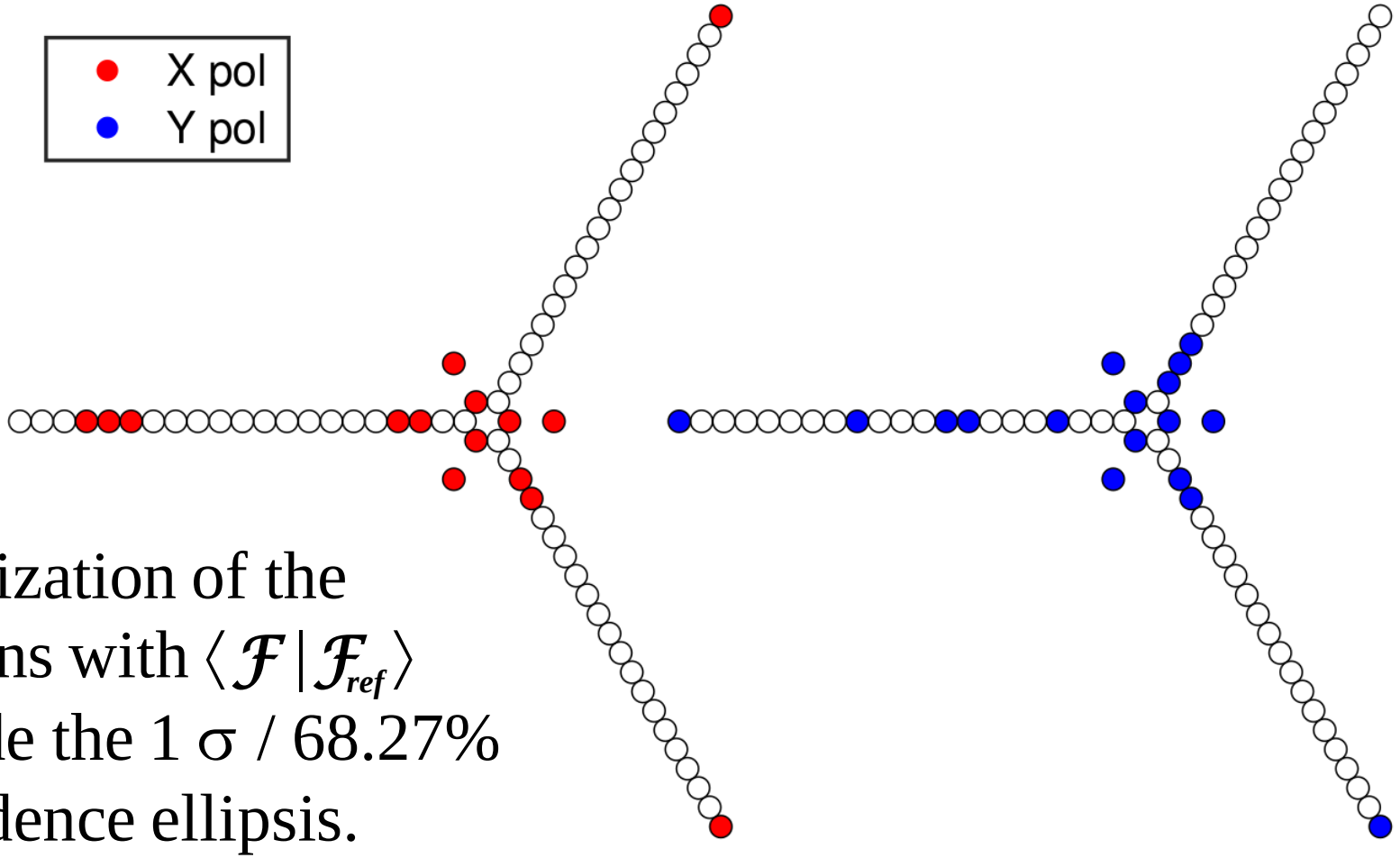

Localization of the patterns with $\langle \mathcal{F} | \mathcal{F}_{ref} \rangle$ outside the 1 σ / 68.27% confidence ellipsis.

Impact of antennas disparity

❖ *Conclusion of the co-study*

➢ A recommendation…

➢ "Whatever the reconstruction operator, the level of the reconstruction floor error of both arrays candidate for SMOS*hr* can be reduced down to that of SMOS provided the disparity between the 231 radiation patterns with respect to the average antenna pattern is almost twice smaller than that of the 69 antennas of SMOS."

Impact of thermoelastic

- *Modeling the effect*

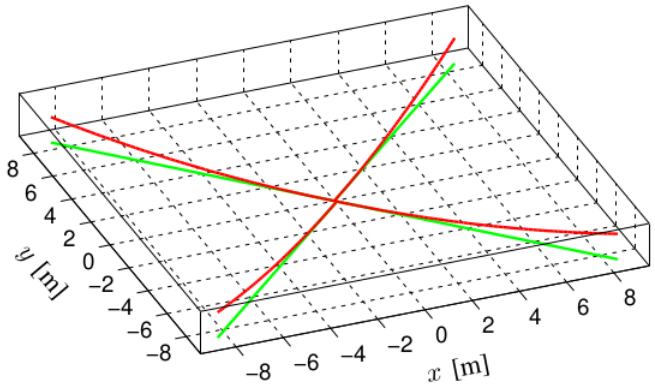

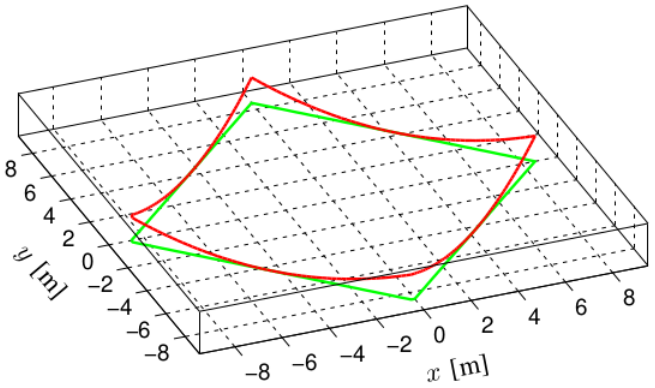

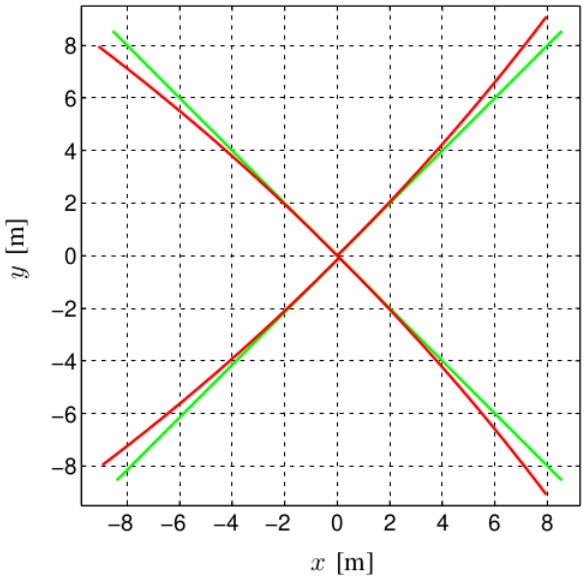

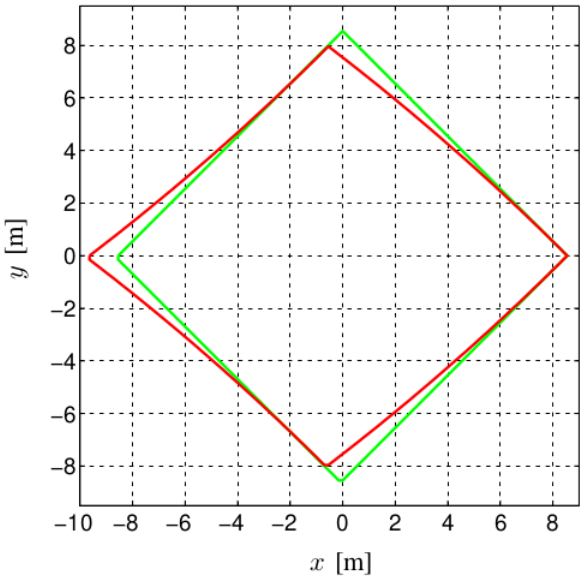

Impact of thermoelastic

❖ *Quantifying the effect on the **G** operator*

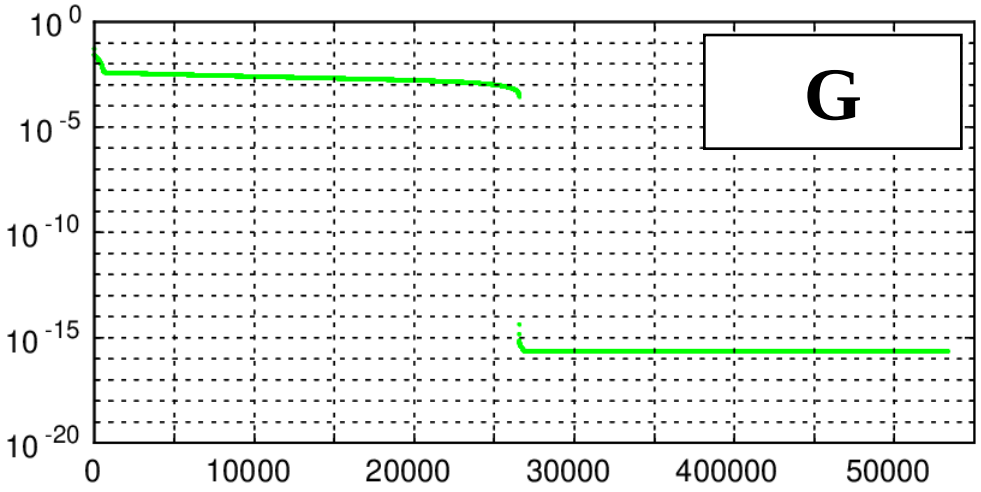

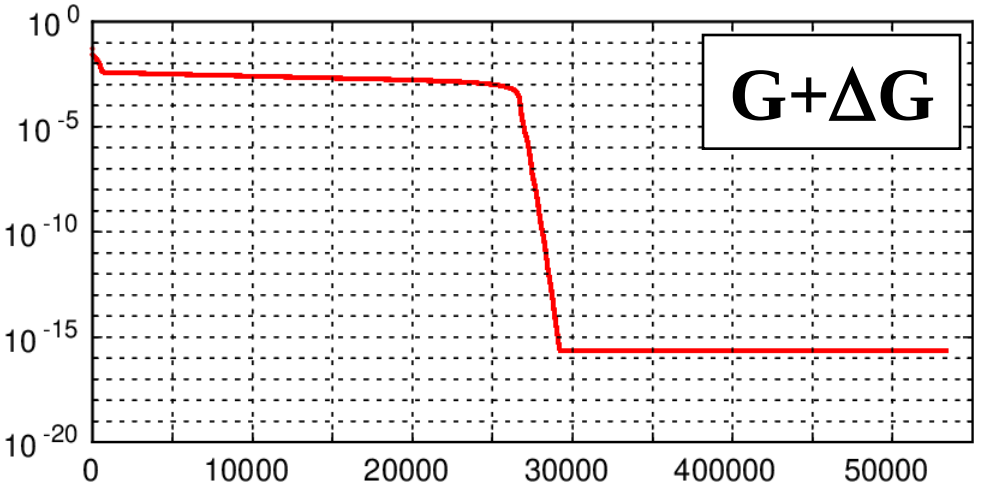

Impact of thermoelastic

❖ *Quantifying the effect on the baselines*

cross

square

out-of plane

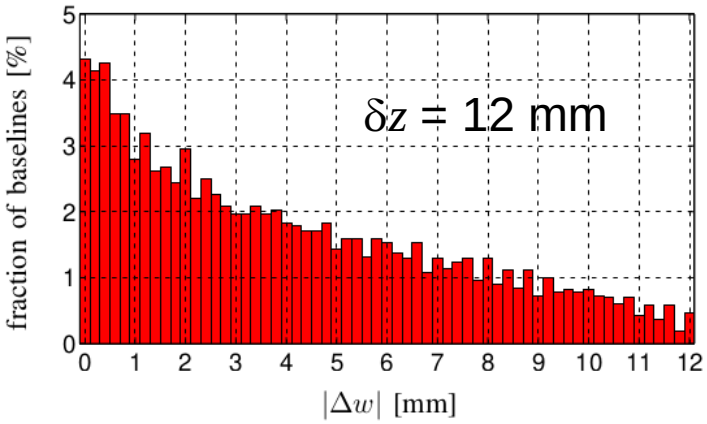

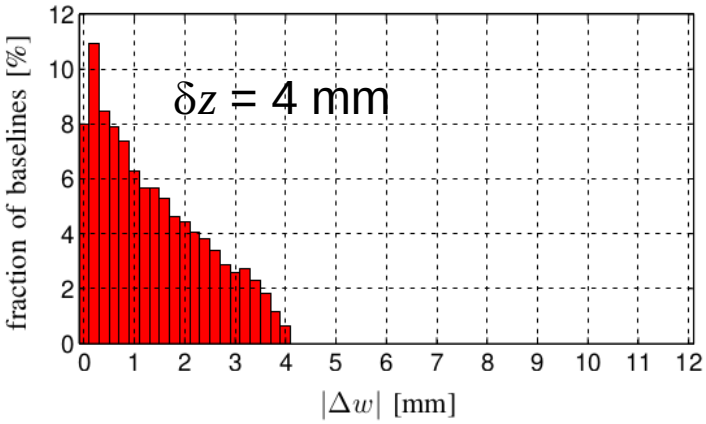

in-plane

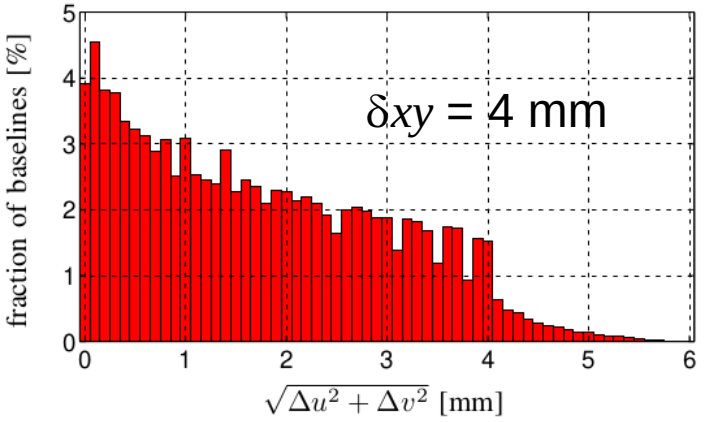

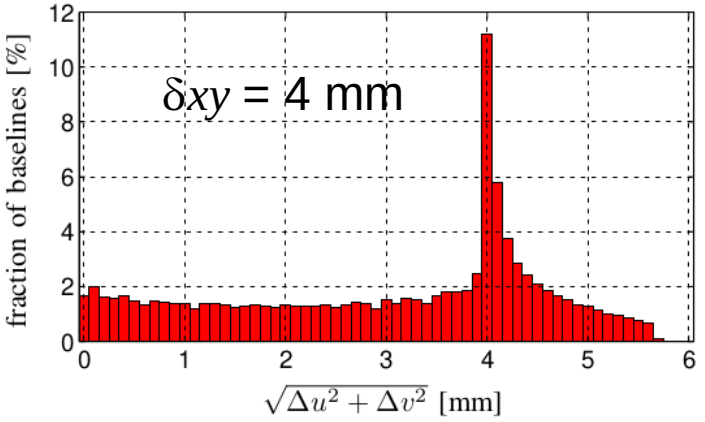

Impact of thermoelastic

❖ *Estimating the impact of ΔV on the floor error*

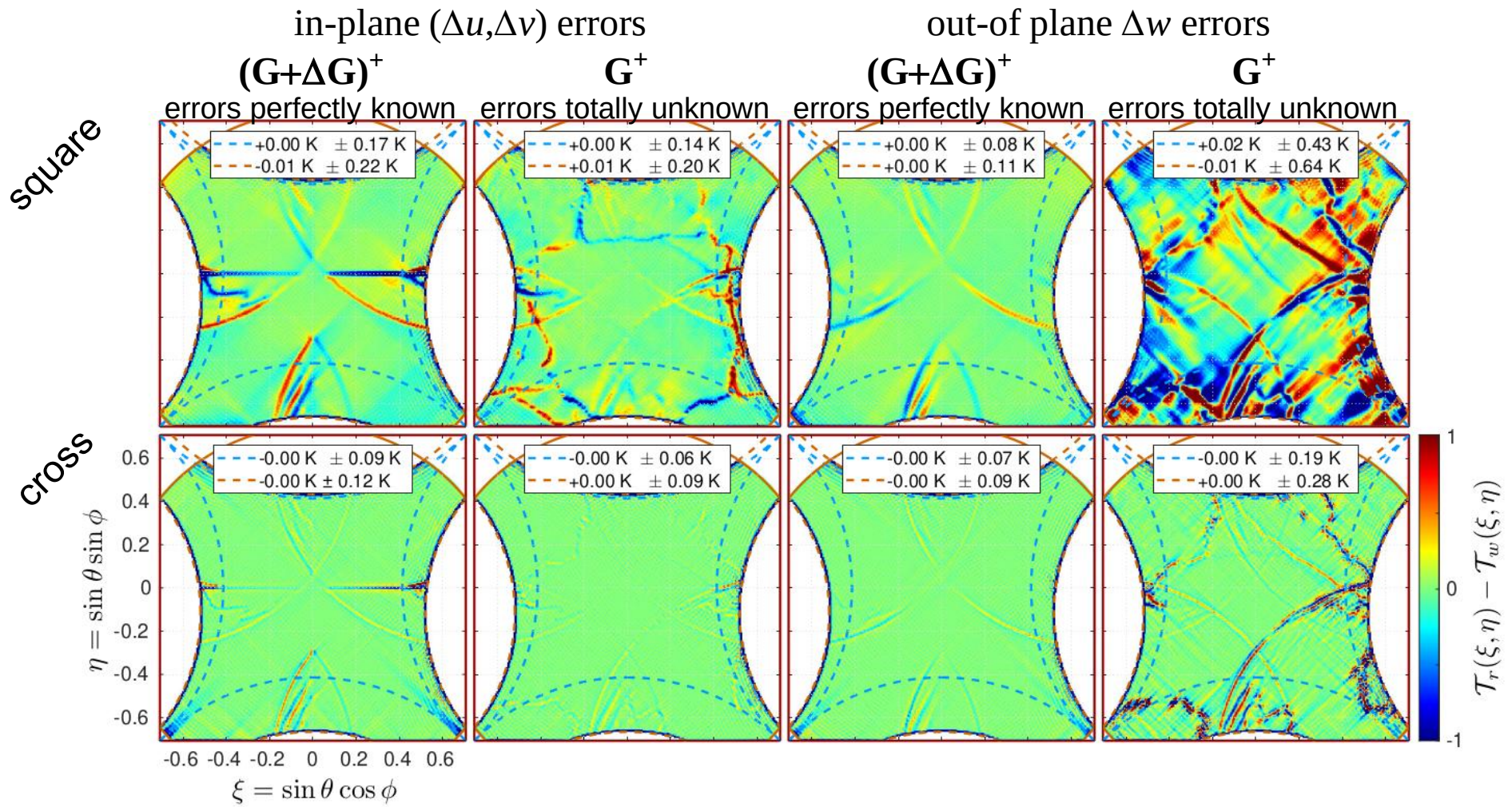

Impact of thermoelastic

❖ *Estimating the impact of ΔV on the floor error*

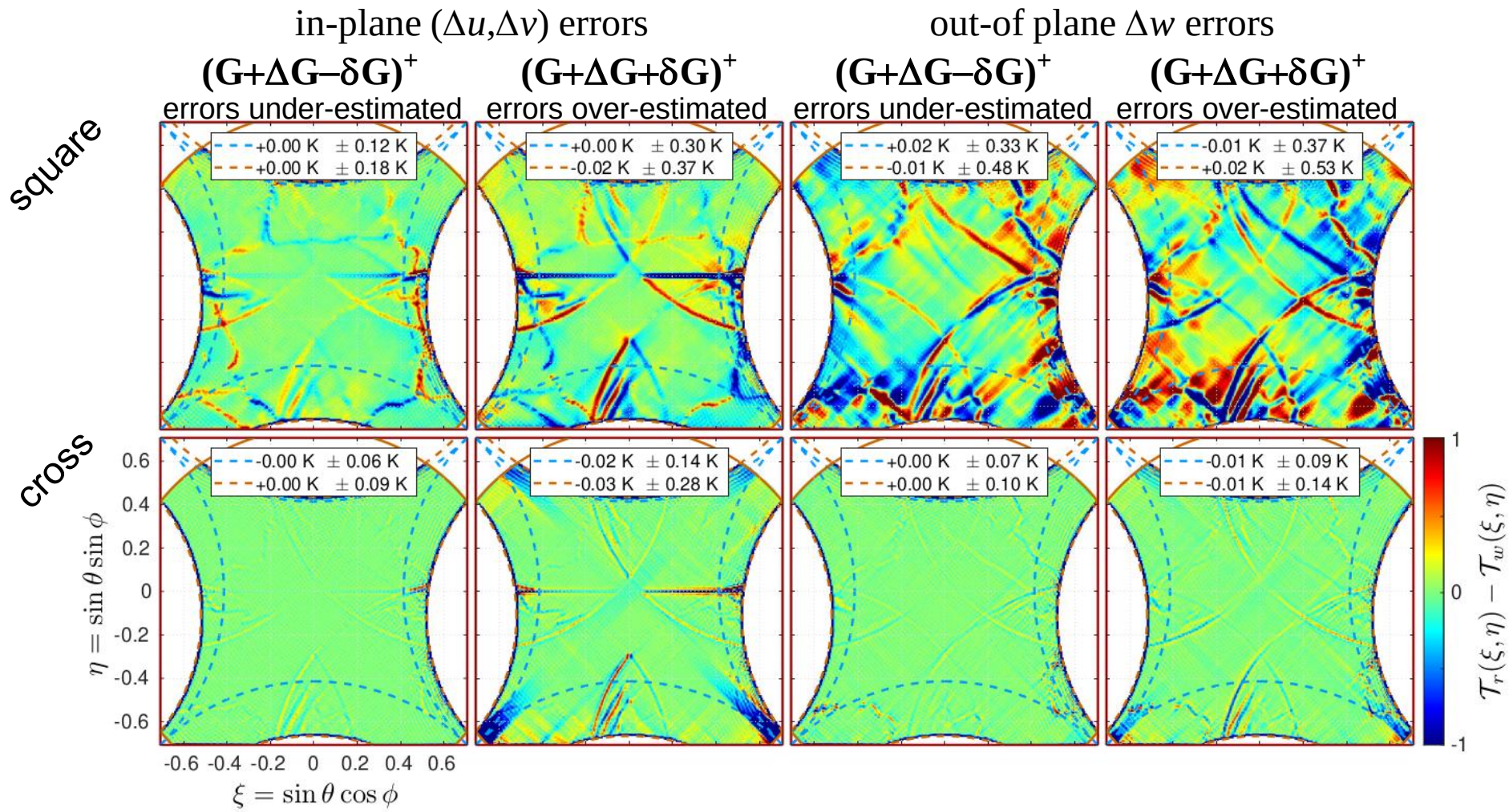

Impact of thermoelastic

❖ *Conclusion of the co-study*

The cross-shaped array has shown a smaller impact of any distortion of the arms compared to that observed with the square-shaped array.

However, when reducing the analysis to the geometry of the two arrays and to the outputs of a thermal study, at first glance, the square-shaped array might be more robust to deformations than the cross-shaped one.

As the final conclusion is the opposite, the interest of conducting studies at industrial and research levels within the frame of a co-design approach is clearly illustrated here.

Retour d'expérience de la mission spatiale SMOS au service de la *co-conception* de la future mission SMOS*hr*

conclusion

Conclusion

- End-to-end simulations are used for:
  - quantifying the sensitivity of mission performances to driving parameters, to instrument errors and noises, and to data processing…
  - estimating the robustness to failures…

- Co-design is the new paradigm…
  …end-to-end simulations with engineers, scientists and end-users actively involved are playing an ongoing role in the development of future sensors (using aperture synthesis).